Mémoire

Auteur : Baijot, Cedric
Promoteur(s) : De Becker, Michaël
Faculté : Faculté des Sciences
Diplôme : Master en sciences spatiales, à finalité approfondie
Année académique : 2023-2024
URI/URL : http://hdl.handle.net/2268.2/19772

Department of Astrophysics, Geophysics and Oceanography

Impacts of different shock types on astrochemistry in molecular clouds

Master thesis presented for the purpose of the obtention of
the academic grade of master in space sciences

Academic Year: 2023 - 2024

Author: Baijot Cedric
Supervisor: M. De Becker

Reading Committee: M. De Becker
V. Van Grootel
MA. Dupret
B. Hubert

Abstract

The study of the interstellar medium (ISM) is one of the main interests of astrophysicists given the importance of this environment. One has to cite the number of physical processes taking place in this medium and the fundamental place it takes in the stellar origin or in the galactic evolution. Nevertheless, many topics are still unclear due to the many physical laws governing it and, more than that, the influence of the chemical compounds forming a big part of the ISM – The molecular clouds.

Beneficiating from the most recent progress in this discipline, this master thesis studies and analyzes one of the most impressive physical events in the ISM: The interstellar shocks. But these shocks are also a complex subject in their own right, and there are different types of shock, depending on whether they exhibit jumping "J-type shock", continuous "C-type shock" behavior, or alternative types such as "C-J-type shock". For this purpose, we principally take the point of view of an astrochemist by computationally predicting the impacts of the shock type on the different reactions and thus on the molecular abundances in diffuse molecular clouds.

In this field, our master's thesis is structured around two main research questions: "How can we make use of astrochemistry to characterize interstellar shocks?" and "How do shocks influence the overall chemistry of the interstellar medium?". The goal is double. We want to increase our understanding of the chemical dynamics happening in shocks and we want to evaluate molecular tracers to determine, from our telescopes, the properties of an observed shocked region. To do so, we will simulate a complete set of shock models focusing on the dynamics and the chemical evolution of the shock. With our results in hand, two discussions will be made (one for each question). In the first one (Chap. 4), we will identify a method to use astrochemistry on shocked regions such as L1157 B2 while the second discussion (Chap. 5) analyzes through graphs the behavior of our main molecular tracer.

This master's thesis registers in the current desire to adopt astrochemistry to achieve a new point of view to see and describe astrophysical processes. Here, the famous interstellar shocks.

Acknowledgements

Dans les quelques prochaines pages qui suivent se trouve mon mémoire. Bien qu'il soit le fruit d'une année de travail et de découvertes dans les sciences spatiales, il est aussi le résultat d'une aventure humaine que j'aurai bien du mal à oublier. Car derrière un travail de fin d'étude se cachent les études en elles-mêmes. Et derrière ses études se trouve un panel de personnes qui m'ont aidé, directement ou pas, mais qui ont dans tous les cas laissé une trace indélébile dans mon apprentissage. Voici donc mes remerciements – non seulement pour le mémoire – mais aussi pour tous ceux qui le précèdent.

Je commencerai par remercier mon promoteur – Pr. Michaël De Becker – pour les conseils qu'il m'a prodigués tout au long du mémoire, pour l'aide incroyable apportée dans mes projets de doctorat, pour les cours Interstellar Medium et Astrochemistry qui ont été à la base de ce mémoire, ainsi que pour la grande autonomie qu'il m'a octroyée au cours de mes recherches. Pour tout cela, un grand merci !

Je remercierai aussi mon comité de lecture composé de Pr. Michaël De Becker, Pr. Valérie Van Grootel, Pr. Marc-Antoine Dupret, et Pr. Benoît Hubert. Je suis tout à fait reconnaissant de la lecture que vous ferez de mon mémoire et je ne peux qu'espérer que vous apprécierez les conclusions obtenues. Pour l'intérêt apporté, un grand merci !

Je continuerai par les étudiants du master en sciences spatiales qui ont particulièrement bien enjolivé ce voyage parmi les étoiles. Que ce soit les futurs Dr. Sacha Peters et Dr. Guillaume Timmermans ainsi que tous les autres que je ne citerai malheureusement pas par manque de place. On est très forts ! Et pour tout cela, un grand merci !

Un petit peu plus loin se profilent les étudiants qui m'ont accompagné durant mon bachelier à l'ULB. Se reconnaîtront Téo Miglionico, Bruno Vilaseca Vanoekel, et Raphaël Amiri. Il y a des hommes qui vous tirent vers le haut à grand coup de discussions ou d'activités, ceux-ci vous projettent. Pour toutes nos années et toutes les prochaines, un grand merci !

S'égarant plus dans le passé viendront ceux qui m'auront connu durant mes années secondaires tels que Jacky Tissot, Tijl Van den Brugghen, Hervé Frys ou encore Adrien Giot qui ont véritablement marqué mon développement. Je remercie également les professeurs Maxime De Buyser et Christophe Derenne pour avoir été présents au début de ma passion pour les sciences. Pour ces beaux débuts, un grand merci !

Une gratitude absolue est aussi dirigée vers ma famille. Pour avoir financé mes études, oui. Mais aussi pour le soutien. Pour ce qu'ils m'ont appris. Pour tout ce qu'ils m'ont donné depuis plus de vingt ans et, d'avance, pour toute l'aide que je leur quémanderai encore pendant les vingt prochaines. Merci à une mère incroyable – Patricia Jadot. Merci à un père phénoménal – Alain Baijot. Merci à deux sœurs fantasques – Aurélie et Nathalie Baijot. Merci à tous les autres. Pour cette famille magnifique, un grand merci !

Je passerai désormais aux inclassables qui sont pourtant tout aussi nécessaires à mon parcours académique. Maria Groyne – Merci pour l'astrochimie et nos futures recherches ! Géraud Frys – Merci pour nos soirées Minecraft ! Maïa Albert – Merci pour m'avoir laissé squatter bien trop souvent ! Alexia Tissot – Merci de me rappeler que l'amitié est essentielle ! JP – Merci d'être JP ! Pour tous ces amis, un grand merci !

Enfin, un Merci qui ne pourra jamais être assez grand à ma compagne Laure Degives pour toutes les conversations scientifiques – parfois subies – mais toujours écoutées. Pour tellement, un grand merci !

À tous, que la vie nous porte ! Un tout grand merci !

"Est-ce que Monsieur est Fou ?" me dit-elle
Je fis un signe affirmatif.
"Et il vous emmène avec lui ?"
Même affirmation.
"Où cela ? dit-elle."
J'indiquai du doigt le centre de la terre.
"À la cave ? s'écria la vieille servante.
- Non, dis-je enfin, plus bas !"

Voyage au centre de la Terre de Jules Verne

"À notre point de vue, toute la vie est une suite d'accidents auxquels nous parons par des solutions improvisées. À leurs yeux, l'existence est un enchainement logique qui doit être déterminé par des calculs précis."

Seconde Fondation de Isaac Asimov

"Dans l'Univers, les sillages de propulsion par courbure pouvaient donc à la fois marquer le danger ou la sécurité. Si les sillages apparaissaient à proximité d'un monde, celui-ci apparaissait menaçant ; s'ils enveloppaient le monde, il apparaissait inoffensif. C'était une corde de potence : dans une main, elle était annonciatrice de danger ; autour d'un cou, elle était un gage de sûreté."

La Mort immortelle de Liu Cixin

"Les sciences, dont chacune tend dans une direction particulière, ne nous ont pas fait trop de mal jusqu'à présent ; mais un jour viendra où la synthèse de ces connaissances dissociées nous ouvrira des perspectives terrifiantes sur la réalité et la place effroyable que nous y occupons : alors cette révélation nous rendra fous, à moins que nous fuyions cette clarté funeste pour nous réfugier dans la paix et la sécurité d'un nouvel âge des ténèbres."

L'appel de Cthulhu de H.P. Lovecraft

"À travers ma lentille, c'est la lumière qui scintille. Des milliards d'étoiles qui dansent dans un ballet endiablé. Certaines naissent. D'autres meurent. Un grand nombre clignotent – Une fois bleues puis une fois rouges – Et ce sont mes paupières qui clignent. Elles ne se voient pas – Enfin pas dans les temps – Mais dansent toutes ensemble dans un mouvement cohérent. Elles se devinent peut-être ?"

Contents

Chapter 1

The scientific context

This first chapter marks the beginning of my master's thesis studying shocks in molecular clouds focusing on the astrochemical aspects. As required in any scientific endeavor, we have to define the environment – or the subject – and the scientific field in which my master's thesis is registered. This is the purpose of this section. Beginning with a broad overview of the interstellar medium, its material, and energetic components including the famous molecular clouds, we will continue with an introduction to the scientific field which is astrochemistry. In doing so, the basic concepts needed to understand the main work of this thesis will be presented and explained in such a way that it will be possible for each person with an interest in astrophysics to enjoy the results of my work. At the end of the chapter, the main objectives are described with a clear overview of the organization and the research questions that will be used as a red thread during the following chapters.

1.1 An overview of the interstellar medium

Space is vast and contains many scientific curiosities. From solar-type stars to black holes, passing by white dwarfs, red giants, and neutron stars, we do not suffer from a lack of subjects worthy of our interest. But more than that, we also have to focus on the environment in which these objects evolve and from which they come from. This place in which stars are born is called the interstellar medium (**ISM**) – even if an accurate description of the birth of stars requires a more complete separation of the ISM into different regions and components as we will see in the following subsections.

1.1.1 The phases of the ISM

The ISM approximately contains 6.7×10^9 $M_\odot$ of gas (De Becker, M. 2023) essentially composed of hydrogen (∼732% of the mass) and helium (∼27%). Many heavier elements aresuch as C, O, N, and others also represent, but in trace amou $\sim 1\%$ of the total mass and are necessary for the chemical diversity of the interstellar medium (Pinto, C. 2013). (All the molecules studied in this master's thesis require the presence of these heavier elements.) More importantly, this gas component is not randomly distributed in the ISM

but rather forms phases that are described in seven phases following in De Becker, M. 2023. It is important to point out that the phases of the ISM should not be seen as phases in the usual thermodynamical meaning. Indeed, even if this remark is still debated by the scientific community, they do not show any usual phase transitions. In the following text, they are seen as different parts of the ISM even if the term "phase" is kept by simplicity. These phases are written here:

- The HIM - Hot Ionized Medium: Also named "Coronal gas", it is a rarefied (10^{-3} cm^{-3}) gas out of thermodynamical equilibrium with a temperature ranging from 10^5 to 10^6K (Carraro 2021). It fills between 20% and 50% of our galaxy.

- The WIM - Warm Ionized Medium: Or HII region if the density is high enough. They are regions containing ionized hydrogen. Their temperature is typical of the order of 10^4 K, their densities range between 0.2 to 10^4 cm^{-3}, and this phase is known to fill up to 10% of our galaxy (De Becker, M. 2023). The state of the hydrogen is usually due to the presence of an O or B spectral-type star of which the emitted light will ionize the H atoms. Given some physical processes, UV light absorbed by the hydrogen is transferred into visible light leading to shining regions of the ISM (Séguin and Villeneuve 2002).

- The WNM - Warm Neutral Medium: A phase of the ISM characterized by neutral atomic hydrogen heated up to 5000 K with a density of 0.6 cm^{-3}. It fills up to 40% of the galaxy (De Becker, M. 2023).

- The CNM - Cold Neutral Medium: A phase of the ISM characterized by neutral atomic hydrogen cooled down to 100 K. Its density is typically 30 cm^{-3} and it fills up to 1% of the galaxy (De Becker, M. 2023). Due to the lack of a strong thermal emission, this phase of the ISM is hardly detectable. Nevertheless, its presence has been observed using the 21 cm emission line of hydrogen (Séguin and Villeneuve 2002). Nowadays, optical and UV absorption lines are also used (Bruce T. Draine 2011).

- **The Diffuse Molecular Gas:** From the moment when atomic hydrogen (and other elements) can sufficiently bind to form a molecular phase, we talk about molecular clouds – which are the main environment for this master's thesis. Diffuse molecular clouds are characterized by a temperature ranging from 10 to 50K. Their densities are about 100 cm^{-3} and they fill 0.1 % of the galaxy (De Becker, M. 2023).

- **The Dense Molecular Gas:** When the molecular cloud is denser, we are now confronted with dense molecular clouds. With densities ranging from 10^3 to 10^6 cm^{-3}, temperatures ranging from 10 to 20 K, and a filling factor for the galaxy of the order of 0.01% (De Becker, M. 2023), their characteristics enable the presence of more complex molecules. More particularly, the opacity of these clouds will shield and protect molecules enabling a richer chemistry.

- Stellar outflows: Depending on the author, stellar outflows are considered part of

the ISM and not part of a stellar system. They are highly variable depending on the star, which is the stellar wind's base. With a temperature of a few ten degrees for cool stars and several thousand for hot stars, their densities can also range from an order of magnitude of 1 cm^{-3} to 10^6 cm^{-3} for hot and cold stars (De Becker, M. 2023).

As the bold writing emphasizes, two phases are of first interest in my studies – the diffuse and dense molecular clouds. As said earlier – and clearly defined in the following sections – this master's thesis is about astrochemistry and requires molecules by definition. In the seven phases described above, molecular clouds are among the most interesting ones when we study the molecular content of the ISM.

More than the gas, we also have to mention **the presence of dust** in the interstellar medium. With a life cycle covering many astrophysical environments, dust is of first importance due to its different optical, thermal, chemical, and electric properties (Van Grootel, V. 2023) that will directly influence and shape its neighborhood. Taking its origin in AGB stars, Supernovae, Novae, ... and evolving in the numerous phases of the ISM, dust is known to play a key role in various processes such as star and planet formation (David A. Williams and Cecchi 2016). One has to note its limited contribution to the mass percentage of the ISM – of the order of 1% (De Becker, M. 2023). Nevertheless, dust is impacting enough to constrain astrophysicists to take into account its influence on most of the processes in space.

1.1.2 The energy components of the ISM

Now that we have met the gas – or the main material – component of the ISM, it is time to focus on the energetic aspects ruling the evolution of the medium. Different features have been identified in space and their census is necessary if we want to simulate astrophysical phenomena of the ISM without suffering from a lack of completeness. Following Bruce T. Draine 2011, we can quote the following components and their importance in Table 1.1:

As visible in Table 1.1, the main reservoirs of energy in the ISM can be divided into four main categories – radiation energy, kinetic energy, magnetic energy, and cosmic rays – with the same order of energy. This fact is known as equipartition of energy (De Becker, M. 2023).

1.1.3 Supernova remnants

When talking about the interstellar medium, a book or a course on the subject will usually mention the presence and importance of Supernovae. When the radiation energy sources found in Table 1.1 are easily understood by the regular reader, the presence of kinetic energy, magnetic energy, and cosmic rays is harder to understand. Concerning kinetic energy and cosmic rays, a main source can be Supernovae. Indeed, Supernovae approximately release 10^{51} erg of mechanical energy. The material released by the explosion constitutes what is called a Supernovae remnant (De Becker, M. 2023). Nevertheless, when we talk about the energy budget, it is worth mentioning the energy released per

Component	u (eV cm^{-3})
Cosmic microwave background ($T_{CMB} = 2.725K$)	0.265
Far-infrared radiation from dust	0.31
Starlight ($h\nu < 13.6$ eV)	0.54
Thermal kinetic energy ($\frac{3}{2}nkT$)	0.49
Turbulent kinetic energy ($\frac{1}{2}\rho v^2$)	0.22
Magnetic energy ($\frac{B^2}{8\pi}$)	0.89
Cosmic rays	1.39

Table 1.1: Energetic components of the ISM expressed in energy densities - Table 1.5 in Bruce T. Draine 2011.

unit time. With events occurring about 2.5 times per century, we are still dealing with 10^{42} erg s^{-1} (De Becker, M. 2023).

Concerning the influence of the energy released by Supernovae remnants on the ISM, two main contributions have to be quoted:

- Cosmic rays: Through acceleration processes such as the Diffusive Shock Acceleration (Drury 1983), a part of the energy is transferred to charged particles that will be accelerated to high velocities (approaching the speed of light). This is one of the main investigated sources of cosmic rays.

- **Shocks**: The Supernovae remnants are a huge amount of gas and dust grains expelled at possible very high velocities. The collision of this matter with the surrounding interstellar medium can lead to the formation of shocks if the difference in velocities is high enough. As guessed from the title of this master's thesis, shocks are of first interest and will be deeply described in the following sections. Nevertheless, their influence can already be considered as we can expect that it will feed the kinetic energy component of the ISM and enable the supply of many processes such as chemical reactions or grain destruction.

Even if Supernovae remnants are commonly envisaged as the source of shocks, this master's thesis wants to keep the concept of shock physics the most general possible. For this purpose, sources are not discussed in detail and future results can be applied to other

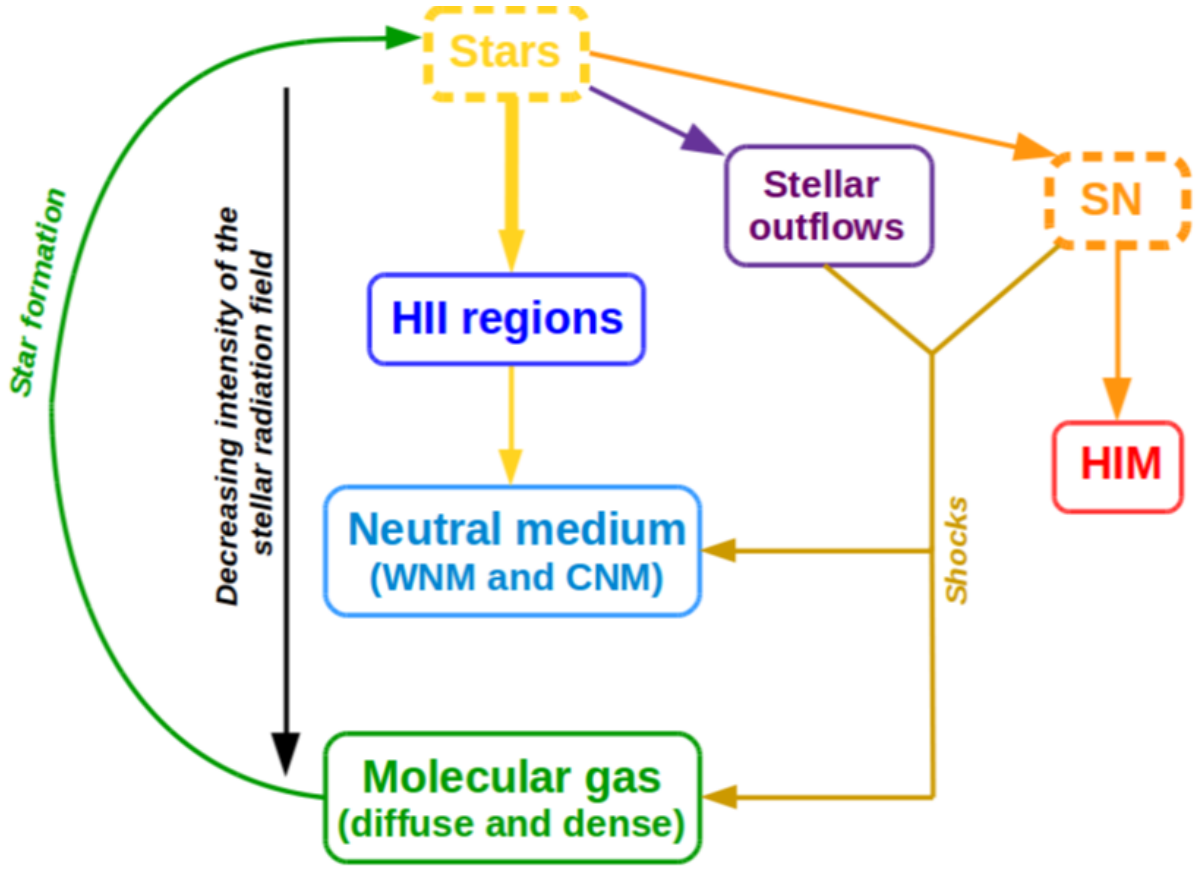

Figure 1.1: Global view of the ISM presenting the interconnections between its different phases, stars and Supernovae.

astrophysical cases such as (Bruce T. Draine 2011):

- The contact of stellar winds with the interstellar medium.
- The case of expanding HII regions.
- The passage of molecular clouds in the arms of spiral galaxies.
- The shock between two molecular clouds.

1.1.4 A global view of the ISM

Now that the main components of – or influencing – the ISM have been analyzed, it is time to emphasize their interconnections. As mentioned earlier, the phases of the ISM are not static and are directly impacted by the inputs and outputs of energy. A first global view of the connections between the different phases, light sources, and Supernovae is visible in Figure 1.1.

This paragraph ends the subsection describing the environment of our research: the interstellar medium. However, due to the diversity of the ISM and the processes taking

place in it, certainly, we cannot study and analyze it entirely during this master's thesis, and we have to decide where we want to pursue our efforts. As we study the impact of shock physics on astrochemistry, we will focus on the molecular content, and thus on molecular clouds. The understanding of these phases is critical to have a global view of many processes such as star formation and their exhibition to Supernovae remnants – or other sources of shocks – has to be considered.

1.2 The scientific field: Astrochemistry

Now that the environment studied in this master's thesis is clearly defined, it is time to focus on the research field giving the point of view of my analyses and the methods available to do them. In my case, this master's thesis is about astrochemistry. Even if the following statement becomes less true over time, astrochemistry is quite a recent discipline and a good description of its basic features is necessary. As said in De Becker, M. 2021, astrochemistry can be defined as follows:

"Astrochemistry is the science devoted to the study of the chemical processes at work in astrophysical environments, including the interstellar medium, comets, circumstellar, and circumplanetary regions."

This means that chemical reactions and molecules exist in space – which is the case. Actually, and this will be emphasized in the following sections, at least 256 different molecules have been identified in astrophysical environments (Guélin and Cernicharo 2022). This diversity of species and the presence of unusual, but important, molecules is proof that a specific chemistry takes place in space. From this fact, and knowing that chemistry is strongly dependent on physical conditions, one can already estimate the importance of studying chemical contents to have indications of the astrophysical environment he/she is studying. This is the approach adopted in this master's thesis to study interstellar shocks.

1.2.1 Methods in astrochemistry

A scientific field is not only described by its subjects but also by its methods. Concerning astrochemistry, my subdivision is based on my experience with the domain and contains three main methods and two approaches. This certainly does not do justice to the diversity of the field, but it already gives a first overview of the context of this master's thesis.

- **Method - Observational astrochemistry:** The first way to apprehend chemistry in space is to observe it. Using techniques such as molecular spectroscopy, it is possible to take advantage of the unique molecular signature of chemical species to identify them. With this powerful tool, the main goal of observational astrochemistry is to make an inventory of the molecular diversity and its dependence on the astrophysical conditions – (ISM, star-forming regions, planetary systems, comets, ...)

  Methods in astrochemistry are correlated. If observations give us matter to study

in the other methods, our current models and experiences also drive observations to detect such specific molecules. The last important point to stress is the fact that observations of molecular signatures require instrumentation in many domains of the electromagnetic spectrum. Good examples are the ground-based "Atacama Large Millimeter / Submillimeter Array (ALMA)" or the space telescope "JWST" able to detect infrared photons corresponding to molecular vibration transitions.

- **Method - Experimental astrochemistry:** With the development of experimental astrophysics, the subdiscipline of experimental astrochemistry has grown up. The goal is to mimic astrophysical conditions – including density, temperature, and abundance values and the presence of cosmic rays, magnetic fields, etc, using experimental setups. This kind of experiment already exists such as in *Setups—Laboratory for Astrophysics—Leiden Observatory* n.d.

  Like other main scientific disciplines, the main purpose of experimental astrochemistry is to enable direct manipulations on the subject of studies – to better apprehend the response of the system to exterior factors. Nevertheless, this method still faces various challenges such as the difficulty of reproducing astrophysical conditions. As we have seen, the ISM can be characterized by very low density and temperature values. Another major problem is linked to the temporality. Chemical processes taking place in space can span millions of years when experiments are limited to very much shorter periods. These problems constitute thus the challenges of current and future scientists.

- **Method - Computational astrochemistry:** The last method included in my vision is the use of computational methods to simulate, as accurately as possible, the chemical evolution in astrophysical environments. As chemists know (and as explained in Sect. 7.1), chemical reactions can be mathematically described by a set of ordinary differential equations dependent on the abundance of species and physical conditions. This set is too big to be evaluated with a pen and a sheet of paper and computational calculations are thus fundamental.

  We can still divide computational astrochemistry into two sub-methods depending on whether the chemical reactions are computed in physical conditions that are **parametrized** previously (and thus fixed) or if the chemical reactions are computed in the same time as the physical conditions – which is mainly referred to as **chemodynamics**. **Chemodynamics** enables us to evaluate the impact of chemistry on physical conditions and vice versa but at the expense of high computational costs – and thus often a reduced chemistry contrarily to **parametrized simulations** which usually contain a bigger set of chemical reactions and components.

Before talking about the approaches scientists can follow to analyze the astrochemistry of an environment, we have to explain the concept of **molecular complexity**. In chemistry, all molecules are not equal in terms of complexity and one can guess that the most abundant molecule H_2, constructed from two atoms of hydrogen, is simpler than $C_6H_{12}O_6$ - the molecule of glucose. The concept of complexity is not clearly defined in

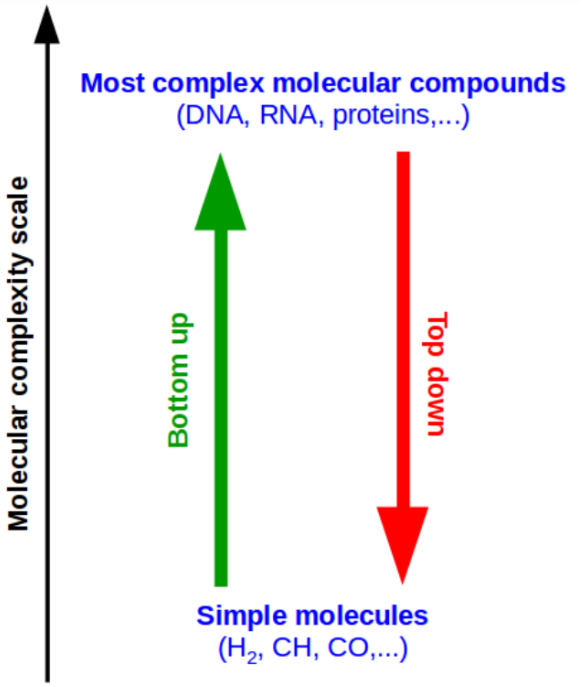

Figure 1.2: Two approaches can be followed in astrochemistry depending on whether we progressively increase or decrease the molecular complexity in our studies. These approaches are respectively called **bottom-up** and **top-down** approaches.

the scientific literature and, this master's thesis is not about this specific aspect, we will not try to give a clear definition. Nevertheless, we can imagine that the complexity of a molecule depends on the number of atoms, the presence of organic functions, and the chemical properties evolved such as chirality.

Knowing this concept and as illustrated in Figure 1.2, it is possible to define two approaches, depending on whether we choose to go down or up on the complexity arrow:

- **The Bottom-up approach:** it starts from the simplest compounds found in space such as the common diatomic molecules (H_2, CO, CH, ...), and tries to develop chemical reactions to reach, reactions after reactions, more complex molecules. This approach is often used when we do not know how far the molecular complexity can go and if this limit of complexity has yet to be assessed.

- **The Top-down approach:** it starts from specific complex macromolecules of interest such as proteins or nucleic acids, and tries to go back on the track of the reactions to find possible molecular precursors – stepping down the scale of molecular complexity. Precursors of the most complex molecular species can be for instance amino acids or sugars.

Having defined the different methods and approaches in astrochemistry, it is useful to put the astrochemical bases of this master's thesis where we study the impacts of interstellar shocks on astrochemistry. Beneficiating from the computational support of Liege

University, we will use computational tools as described in 1. This master's thesis is thus about **computational astrochemistry**. To be more precise and as the dynamical aspect of shocks is very relevant to me, it will be all about **chemodynamics**. Concerning the approaches, as we do not already know that much about the complexity reached in shocks (shocked environments suffer from a lack of investigations in terms of astrochemistry), it will be a **bottom-up approach** where the complexity will be assessed at the end of my analysis.

Differences between astrochemistry and molecular spectroscopy:

Before ending this subsection on the methods and approaches in astrochemistry, we want to make clear the distinction that exists between molecular spectroscopy and observational astrochemistry. Even if the two are deeply connected in the context of space studies, molecular spectroscopy should be seen as the tool that the astrochemists will use to identify molecules in space. Of course, as it is the main tool, astrochemical observations are highly dependent on the progress of techniques of molecular spectroscopy. More than that, astrochemistry would not exist if spectroscopic observations of molecules in astrophysical environments (such as CH, the first molecule identified in space in 1937 (Swings and Rosenfeld 1937)). This proves that this tool is essential. Nevertheless, this distinction has to be made to have a clear view of what astrochemistry is and what astrochemistry is not.

1.2.2 The molecular component

Now that the research field is well-defined, the next step is to perform a small overview the astrochemical situation of the ISM. To do so, we have to clarify the chemical compounds and the chemistry linking them together. This subsection will begin by indicating the envisaged abundance for constituents of main interest in the interstellar medium and the assumptions made to reach our conclusions.

Molecules are made of atoms. As a direct consequence, elemental abundances of atoms in the interstellar medium are critical information to foresee the possible molecules in space. Nevertheless, the ISM is not uniform in space and time. In time, because of the nucleosynthesis of heavy elements in stars, the universe – principally made of hydrogen and helium from the primordial nucleosynthesis – has seen an enrichment of heavy atoms. As an example, the astrochemistry of the early universe was mainly limited to hydrogen, helium, their ions, and electrons (D. A. Williams et al. 2018). We can thus expect that chemistry in space is directly dependent on the redshift of the source we are observing. In space, even in our galaxy, we can detect a gradient of abundances concerning the heavy elements. For the quantitative aspect, we think that the center of the Milky Way is two times richer in heavy elements than the solar neighborhood (Bruce T. Draine 2011). Knowing this is important to know what scientists are generally talking about when they state elemental abundances. Due to the difficulty that we have in measuring these abundances when they are far from us, we measure solar abundance and make the hypothesis that the interstellar neighborhood should have a similar abundance of elements. The solar abundance for the 32 first atoms can be seen in Tables 1.2 and 1.3.

Z	X	$\langle m_X \rangle$ / amu	N_X / N_H	M_X / M_H
1	H	1.0080	1	1
2	He	4.0026	$9.55 \times 10^{-2\pm0.01}$	3.82×10^{-1}
3	Li	6.941	$2.00 \times 10^{-9\pm0.05}$	1.38×10^{-8}
4	Be	9.012	$2.19 \times 10^{-11\pm0.03}$	1.97×10^{-10}
5	B	10.811	$6.76 \times 10^{-10\pm0.04}$	$7.31 \times 10-9$
6	C	12.011	$2.95 \times 10^{-4\pm0.05}$	3.54×10^{-3}
7	N	14.007	$7.41 \times 10^{-5\pm0.05}$	1.04×10^{-3}
8	O	15.999	$5.37 \times 10^{-4\pm0.05}$	8.59×10^{-3}
9	F	18.998	$2.88 \times 10^{-8\pm0.06}$	5.48×10^{-7}
10	Ne	20.180	$9.33 \times 10^{-5\pm0.10}$	1.88×10^{-3}
11	Na	22.990	$2.04 \times 10^{-6\pm0.02}$	4.69×10^{-5}
12	Mg	24.305	$4.37 \times 10^{-5\pm0.04}$	1.06×10^{-3}
13	Al	26.982	$2.95 \times 10^{-6\pm0.01}$	8.85×10^{-5}
14	Si	28.086	$3.55 \times 10^{-5\pm0.04}$	9.07×10^{-4}
15	P	30.974	$2.82 \times 10^{-7\pm0.03}$	8.73×10^{-6}
16	S	32.065	$1.45 \times 10^{-5\pm0.03}$	4.63×10^{-4}

Table 1.2: Protosolar Abundances of the Elements with $Z \leq 16$. Data come from photospheric and meteoritic measurements. From Bruce T. Draine 2011.

Z	X	$\langle m_X \rangle$ / amu	N_X / N_H	M_X / M_H
17	Cl	35.453	$1.86 \times 10^{-7\pm0.06}$	6.60×10^{-6}
18	Ar	39.948	$2.75 \times 10^{-6\pm0.13}$	1.10×10^{-4}
19	K	39.098	$1.32 \times 10^{-7\pm0.02}$	5.15×10^{-6}
20	Ca	40.078	$2.14 \times 10^{-6\pm0.02}$	8.57×10^{-5}
21	Sc	44.956	$1.23 \times 10^{-9\pm0.02}$	5.53×10^{-8}
22	Ti	47.867	$8.91 \times 10^{-8\pm0.03}$	4.27×10^{-6}
23	V	50.942	$1.00 \times 10^{-8\pm0.02}$	5.09×10^{-7}
24	Cr	51.996	$4.79 \times 10^{-7\pm0.01}$	2.49×10^{-5}
25	Mn	54.938	$3.31 \times 10^{-7\pm0.01}$	1.82×10^{-5}
26	Fe	55.845	$3.47 \times 10^{-5\pm0.04}$	1.94×10^{-3}
27	Co	58.933	$8.13 \times 10^{-8\pm0.01}$	4.79×10^{-6}
28	Ni	58.693	$1.74 \times 10^{-6\pm0.01}$	1.02×10^{-4}
29	Cu	63.546	$1.95 \times 10^{-8\pm0.04}$	1.24×10^{-6}
30	Zn	65.38	$4.68 \times 10^{-8\pm0.04}$	3.06×10^{-6}
31	Ga	69.723	$1.32 \times 10^{-9\pm0.02}$	9.19×10^{-8}
32	Ge	72.64	$4.17 \times 10^{-9\pm0.04}$	3.03×10^{-7}

Table 1.3: Protosolar Abundances of the Elements with $17 \leq Z \leq 32$. Data come from photospheric and meteoritic measurements. From Bruce T. Draine 2011.

These atoms are thus necessary to build molecules. Actually, hundreds of these molecules have been identified in space and it is again useful to have an inventory of them to gain an idea of the diversity and molecular complexity reached in astrophysical

Table 1.4

Number of atoms	Chemical species
2 atoms	AlCl, AlF, AlO, C_2, CF^+, CH, CH^+, CN, CN^-, CO, CO^+, CP, CS, FeO, H_2, HCl, HF, NH, KCl, N_2, NO, NO^+, NS, NaCl, O_2, OH, OH^+, PN, SH, SH^+, SO, SO^+, SiC, SiN, SiO, SiS, SiP, TiO, ArH^+, NS^+, VO, HeH^+, PO^+
3 atoms	AlNC, AlOH, C_3, C_2H, C_2O, C_2P, C_2S,CO_2, H_3^+, CH_2, H_2Cl^+ , H_2O, H_2O^+, H_2S, HCN, HCO, HCO^+, HCS^+, HCP, HNC, HN_2^+, HNO, HOC^+, KCN, MgCN, NH_2, N_2H^+, N_2O, NaCN, OCS, SO_2, c-SiC_2, SiCN, SiNC, SiCSi, FeCN, TiO_2, CCN, S_2H, HCS, HSC, NCO, , NCS, CaNC, MgC_2, NCS, HSO
4 atoms	l-C_3H, c-C_3H, C_3N, C_3O, C_3S, C_3H^+, H_3O^+, C_2H_2, H_2CN, H_2CO, H_2CS, HCCN, HCCO, $HCNH^+$, HCNO, HOCN, $HOCO^+$, HNCO, HNCS, HSCN, NH_3, SiC_3, PH_3, H_2O_2, HMgNC, MgCCH, NCCP, CNCN, HONO, HCCS, HNCN, $HCCS^+$, H_2NC
5 atoms	C_5, CH_4, c-C_3H_2, l-C_3H_2, H_2CCN, H_2C_2O, H_2CNH, H_2COH^+, C_4H, C_4H^-, HC_3N, HCCNC, HCOOH, NH_2CN, SiC_4, SiH_4, HCOCN, HNCNH, HC_3N^-, CH_3O, $NCCNH^+$, CH_3Cl, MgC_3N, NH_2OH, HC_3O^+, HC_3S^+, H_2CCS, C_4S, HCCCO, HCOSH, HCSCN, NaCCCN, MgC_3N^+
6 atoms	c-H_2C_3O, C_2H_4, CH_3CN, CH_3NC, CH_3OH, CH_3SH, l-H_2C_4, HC_3NH^+, $HCONH_2$, C_5H, HC_2CHO, HC_4N, CH_2CNH, C_5N^-, C_5S, SiH_3CN, z-HNCHCN, MgC_4H, HC_3CO^+, CH_2CCH, H_2CCCS, HCSCCH, MgC_5N, CH_5^+, $HCCNCH^+$, CH_3CO^+, C_5O, c-C_5H, C_5H^+, HCCCCS, MgC_4H^+

environments. A temporary census of this inventory for the ISM is visible in Tables 1.4 and 1.5. "Temporary" is here very relevant since new molecules are discovered every year.

1.2.3 Chemical reactions

The molecular components of the ISM are not fixed in time but evolve through chemical reactions – linking them together by the creation and destruction of molecular bonds. Nevertheless, these chemical reactions differ greatly from the usual chemistry from which we are used on Earth due to the high differences in the physical conditions of the environment. Indeed, if basic laboratory chemistry is usually performed in aqueous solutions or any other solvents, we do not possess any equivalent in space. To understand chemical processes in the ISM, we must know that the chemistry is mainly achieved in two or three phases depending on the author. These phases are:

- The gas phase
- The grain-surface mantle

Table 1.5

Number of atoms	Chemical species
7 atoms	c-C_2H_4O, CH_3C_2H, H_3CNH_2, CH_2CHCN, H_2CHCOH, C_6H, C_6H^-, HC_4CN, CH_3CHO, CH_3NCO, HC_5N^-, HC_5O, $HOCH_2CN$, HNCHCCH, HC_4NC, CH_2CHCCH, C_3HCCH, H_2C_5, MgC_5N, CH_2CCCN, NC_4NH+, MgC_5N^+
8 atoms	H_3CC_2CN, $H_2COHCOH$, CH_3OOCH, CH_3COOH, C_6H_2, CH_2CHCHO, CH_2CCHCN, C_7H, NH_2CH_2CN, $(NH_2)_2CO$, CH_3SiH_3, $(NH_2)_2CO$, CH_2CHCCH, $HCCCH_2CN$, MgC_6H, HC_5NH^+, $C_2H_3NH_2$, Z-$(CHOH)_2$ HCCCHCCC, C_7N^-, CH_3CHCO, HMgCCCN, MgC_6H^+
9 atoms	CH_3C_4H, CH_3OCH_3, CH_3CH_2CN, CH_3CONH_2, CH_3CH_2OH, C_8H, HC_6CN, C_8H^-, CH_2CHCH_3, CH_3CH_2SH, CH_3NHCHO, HC_7O, H_3C_5CN (2 isomers), HCC-CHCHCN, H_2CCHC_3N, C_5H_4, $H_2CCCHCCH$, OHCHCHCHO, $CH_2CHCHNH$
10 atoms	CH_3COCH_3, CH_3CH_2CHO, CH_3C_5N, CH_3OCH_2OH, C_6H_4, HC_2CCHC_3N, HC_7NH^+, $C_2H_5NH_2$, C_2H_5NCO, t-$CH_3CHCHCN$, c-$CH_3CHCHCN$, $CH_2C(CH_3)CN$
>10 atoms	HC_8CN, CH_3C_6H, $CH_3OC_2H_5$, $HC_{10}CN$, C_6H_6, C_2H_5OCHO, C_3H_7CN, CH_3COOCH_3, $C_2H_5OCH_3$, CH_3CHCH_2O, C_6H_5CN, CH_3COCH_2OH, C_{60}, C_{60}^+, C_{70}, c-C_5H_5CN, $C_{10}H_7CN$ (2 isomers), c-C_5H_6, c C_9H_8, $NH_2CH_2CH_2OH$, CH_3C_7N, i-C_3H_7OH, n-C_3H_7OH, CH_2CCHC_4H, g-CH_2CHCH_2CN, $HC_{11}N$, C_5H_5CCH (2 isomers), C_6H_5CCH, CH_3C_7N, c-CH_2CHCH_2CN, c-$C_5H_4CCH_2$, c-C_9H_7CN, $C_{10}H^-$, $C_{10}H$, E-1-C_4H_5CN, $C_{11}H_{12}N_2O_2$
Deuterated	HD, H_2D^+, HDO, D_2O, DCN, DCO, DNC, N_2D^+, NHD_2, ND_3, HDCO, D_2CO, CH_2DCCH, CH_3CCD, D_2CS, NH_3D^+

- The icy mantles of grains (if they exist)

A good analysis of the chemistry of an astrophysical environment should take care of each of these phases as they have each different properties and effects on the surrounding medium and the evolution of the molecular components. Before attacking the specific chemical aspects of these phases, it is particularly relevant to clarify how we describe chemical reactions in a general way. These parts will take as known some chemical concepts of chemical kinetics such as the concept of elementary reactions, rate constants, or activation barriers. If the reader is unfamiliar with these concepts, he/she can refer to the associated content in Sect. 7.1. When a computer simulates the evolution of species through chemical reactions, a method is to see each chemical reaction (Re. 1.1) as an ordinary differential equation (ODE) (Eq. 1.2):

$$A + B \rightarrow AB \tag{1.1}$$

$$\frac{d[A]}{dt} = -k \cdot [A] \cdot [B] \tag{1.2}$$

Where [A] is the concentration of the species A, and k is the rate constant of the reaction. The minus term comes from the fact that reactants are consumed in the reaction. (It would have been a "+" term if it was a product created during the reaction.) Formally, the ODE describing the evolution of the density of A is only dependent on the densities of the reactants, and on the rate constant k. All dependencies on the specificity of the reactions such as the activation barrier and on the physical conditions such as the temperature, the ionization by cosmic rays, the number of energetic photons, ... are hidden in the rate constant and we will write that as a function:

$$k_i = f_i(T, other\,parameters) \tag{1.3}$$

Where i is the type of elementary reaction considered. (All types will be defined in the following subsection.) Each type of elementary reaction will thus have its reaction rates determined through a specific function f_i. Now, when a code computes the evolution of each component of the system through the computation of a system of reactions, it only has to find the type of each reaction to compute the reaction rates and form a set of ODE – which can be numerically solved.

Gas phase chemistry

Following De Becker, M. 2021, gas phase chemical reactions can be divided into 13 reaction types as shown in Table 1.6. As these reactions depend on different physical conditions, their relevance highly depends on the studied environment. Some considerations have to be made:

Reaction type	k_i (typical value)	General chemical reaction
Photodissociation	$k_{pd} = \int_{\nu_d}^{\nu_H} 4\pi J_{IS}\alpha(\nu)\, d\nu$	$AB + h\nu \rightarrow A + B$
	$k_{pd} = \alpha exp[-\gamma A_\nu]$	
	$(10^{-9} \sim 10^{-11})$	
Photoionization	$(10^{-10} \sim 10^{-12})$	$A + h\nu \rightarrow A^+ + e^-$
Cosmic-ray induced	$(10^{-9} \sim 10^{-17})$	$AB + CR^{(+)} \rightarrow A^+ + B + CR^{(n)}$
	$(10^{-17} \sim 10^{-18})$	$A + CR \rightarrow A^+ + e^-$
	$k_{CR} = \alpha(T/300)^\beta \gamma/(1-\omega)$	$AB + CR \rightarrow A + B$
	(10^{-17})	
Neutral-neutral reactions	$k = \gamma \cdot (T/300)^\alpha \cdot exp[-\beta/T]$	$A + B \rightarrow C + D$
	$(10^{-11} \sim 10^{-14})$	
Ion-molecule reactions	$(10^{-9} \sim 10^{-10})$	$A^+ + B \rightarrow C^+ + D$
D.E.R	$(10^{-7} \sim 10^{-8})$	$A^+ + e^- \rightarrow A^* \rightarrow C + D$
Charge transfer	$(10^{-9} \sim 10^{-10})$	$A^+ + B \rightarrow A + B^+$
Associative detachment		$A^- + B \rightarrow AB + e^-$
Collisional association		$A + B + M \rightarrow AB + M$
Collisional dissociation		$AB + M \rightarrow A + B + M$
Radiative association	$k_{ra} = (\frac{k_a}{k_r + k_d})k_r$	$A + B \underset{k_d}{\overset{k_a}{\rightleftarrows}} AB^* \xrightarrow{k_r} AB + h\nu$

Table 1.6: Reaction types encountered in the gas phase of the ISM from De Becker, M. 2021 with the function f_i describing the rate constant, and the general pattern of the chemical reactions. Not-defined terms and general comments are presented in the main text.

- Photodissociation is the dissociation of molecules through the absorption of energetic photons (typically in the far ultraviolet – FUV) and these radiative processes are thus mainly relevant in environments where the FUV radiation field is not too attenuated (by dust for example). Photodissociation is thus mainly important at the edges of molecular clouds. Another important factor to be taken into account is the presence of H_2. The energy required to dissociate dihydrogen is 13.6 eV. Due to its major contribution, we can consider that all photons with an energy above 13.6 eV are absorbed by H_2 and are not available to dissociate other minor molecules (This explains the integral from ν_d, the dissociation limit of the molecule AB and ν_H, the dissociation limit of H_2.). In the rate constant, J_{IS} is the mean intensity of the interstellar radiation field, and $\alpha(\nu)$ is the photodissociation cross section at a given frequency ν. A more convenient way to write the rate function is to parametrize it with α and γ which are dependent on the reactions. In this case, k depends on visual extinction A_ν.

- Photoionization enables the creation of cations – such as C^+ – and electrons given that energetic photons are available. Nevertheless, the question of H_2 and the limit at 13.6 eV has to be taken into account again. Indeed, elements or molecules with an ionization potential higher than 13.6 eV will never be ionized by photoionization. This is the case of atomic oxygen and nitrogen.

- The other factor that will deeply impact the chemistry of the ISM is the presence of cosmic-ray (charged energetic particles). As visible in Table 1.6, cosmic rays are important in many types of reactions as they can dissociate or ionize molecules. Even if the efficiency of these processes is rather weak, cosmic rays can penetrate the core of molecular clouds and become the only source of ions when the radiation field is too strongly attenuated. More than that, through the excitation of molecules and their relaxation (the third line), cosmic rays are a source of UV photons in the inner parts of the densest regions of the ISM such as the interior of molecular clouds. As seen later, these UV photons are important in the context of dust grains. Concerning the rate constant shown for cosmic-ray-induced photoreactions on the third line, α is the cosmic-ray photoreaction rate, β is a parameter characterizing the dependence of the reaction on the temperature, γ is an efficiency factor, and ω is the average albedo of dust grains.

- For other chemical processes (third part of Table 1.6), a convenient way to express the rate constant is to parameterize it as a function of α, β, and γ - valid in a specific range of temperature. In the parameterization given here, one can recognize that the parameter β exponentially decreases the rate constant and acts as the activation barrier of the reaction (in temperature units).

- Neutral-neutral reactions are only driven by the Van der Waals forces which are not very efficient low-range forces. Due to the weakness of the interaction and the need to break bonds before creating new ones, they are usually characterized by a high activation barrier but if the reaction includes atoms or radicals which are more chemically active. Neutral-neutral reactions particularly concern environments with

great kinetic energy as in **shocks**. Another important point is in the creation of two products C and D. The explanation resides in the fact that the kinetic energy of the reactants before the collision in the rest frame is conserved. If we only had one product with all the remaining energy, it would dissociate too easily into two molecules. Even if this statement tends to be false when the product of the reaction is big enough to stabilize the excess of energy before radiating it – enabling the formation of only one product.

- Polarization-induced interactions between ions and molecules lead to reactions faster than their neutral-neutral homologue. This is true if the reactants present a permanent dipole which makes the interaction easier. Due to these more efficient ion-molecule reactions, the level of ionization of the medium is of great importance in evaluating the efficiency of the chemistry in it.

- D.E.R or Dissociative electron recombination reactions enable the breaking of an ionized molecule (which can be the product of ion-molecule reactions) into smaller neutral molecules which could be hard to form otherwise. As for neutral-neutral reactions, if the excited A^* molecule is large enough to stabilize the excess energy for long enough – until the emission of a photon, D.E.R. may not be necessarily dissociative.

- Even if the photoionization reaches a limit at the level of hydrogen (13.6 eV) resulting in a very efficient creation of cationic hydrogen H^+, charge transfer reactions help in the balance of ionic species in the ISM. Due to these reactions, trace molecules such as O-bearing molecules can be ionized and trigger the beginning of ion-molecule pathways.

- Collisional associations solve the problem of excess energy by enabling its evacuation through a third body M. Nevertheless, with low densities, three-body reactions are unfavorable. This kind of reaction will be particularly relevant in the context of the grain-surface phase.

- Collisional dissociations require the collision between two species. The transferred energy gives rise to an excited molecule that will tend to break. As we can expect, stable molecules able to radiate away the excess of energy will be more resistant to collisional dissociations. We should also expect that the violence of collisions will affect the efficiency of the collisions. Knowing this, we predict that hotter mediums such as **shocks** should enhance collisional dissociations.

- As illustrated by the formula of their rate constants, radiative association reactions are strongly dependent on the efficiency of the radiative relaxation of the newly formed molecule. Indeed, the excited molecule AB^* needs to perform a relaxation before breaking again into two fragments. This thus becomes effective only for large molecules which are more stable than the smaller ones.

From these general considerations, it is already possible to imagine the general form of

gas phase reactions. Two pathways emerge from this picture: a fast ion-driven pathway containing mainly ion-molecule reactions to increase the complexity and a slower one with neutral-neutral reactions. Interconnections between these pathways are assured by charge transfers and terminations of the ion-molecule reactions path can be achieved through some processes such as electron recombination. From this picture, we guess the importance of the creation of ions and thus a strong dependency on photoionization or cosmic-ray-induced ionization according to the environment.

Grain-surface phase chemistry

As we have seen, due to energetic considerations, chemical reactions between relatively small molecules should give at least two products to enable a runaway of the excess energy. This consideration should be compared to the fact that the most abundant molecule in the universe is H_2. The first question that emerges from this is: "How can we efficiently form H_2 without using more complex molecules?". The condition that we imposed to the formation of H_2 takes into account the fact that even if formation reactions such as (Re. 1.4 or Re. 1.5) exist, they raise the question of the formation of their reactants – which would require the existence of H_2. This is thus a "Chicken and egg" problem.

$$H + H_3^+ \rightarrow H_2 + H^+ \tag{1.4}$$

$$CH + H \rightarrow H_2 + C \tag{1.5}$$

Associative detachments (Re. 1.6) and collisional associations (Re. 1.7) could be a good alternative to form H_2 without the call of more complex molecules. Nevertheless, the anion H^- required in associative detachments is formed too slowly to account for the actual abundances of dihydrogen (David A. Williams and Cecchi 2016) and the densities in the ISM are way too low to enable collisional associations to be efficient enough.

$$H + H^- \rightarrow H_2 + e^- \tag{1.6}$$

$$H + H + H \rightarrow H_2 + H \tag{1.7}$$

We thus see that gas-phase reactions are not a good explanation for the formation of all molecules found in the ISM. To be more complete, we can also ask the question of the formation of the most complex molecules (with several atoms) as we know that gas-phase reactions tend to fragment their products – and limit the increase of the molecular complexity. These facts leaded scientists to investigate reactions on grain surfaces. Indeed, the grain can absorb the excess energy as the third body M in associative collisions to enable simple addition reactions. Nowadays, grain surface chemistry is well-confirmed

by observations and laboratory experiments. Here are the basics that the reader should know to plainly understand the importance of grains in our chemical modelling.

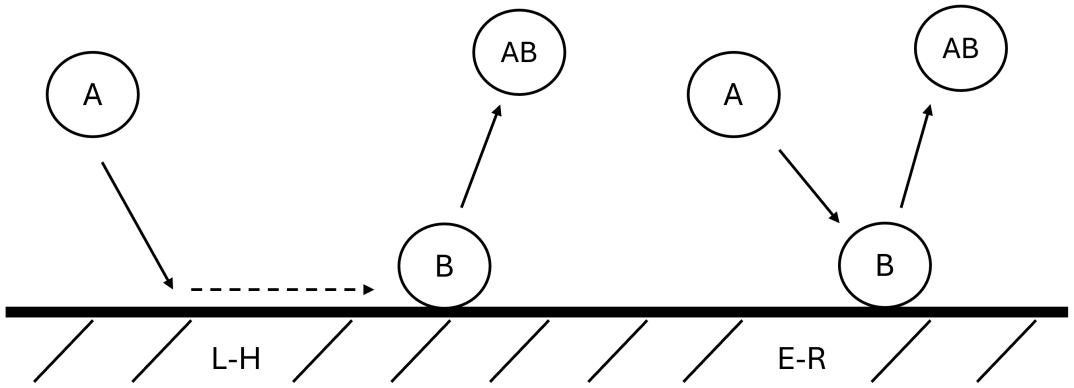

Figure 1.3: Diagram of the Langmuir-Hinshelwood and Eley-Rideal mechanisms in grain surface chemistry. From David A. Williams and Cecchi 2016.

As visible in Figure 1.3, two main mechanisms explain addition reactions on grains. Both depend on the ability of compound B to adsorb – physically or chemically – on the grain surface and to stay sufficiently long on it. In the first mechanism known as the Langmuir-Hinshelwood (L-H) mechanism, a second compound A adsorbs the surface and moves on it using thermal energy and quantum tunneling until it finds the compound B, reacts with it, and desorbs as a product. The second mechanism is the Eley-Rideal (E-R) one. In this second scenario, compound A directly lands on compound B to react and desorbs as a product. When the efficiency of the L-H mechanism is deeply affected by the temperature of the grain and the mobility of species, the E-R mechanism is more dependent on the surface coverage of the grain (David A. Williams and Cecchi 2016). Another point emphasized in Figure 1.3 is the ability of these processes to simply add molecules to others without fragmentation. As already mentioned, this fact ensures the importance of grains to increasing molecular complexity. Another feature of grains can be the presence of an ice layer in some conditions that will modify and impact the chemical reactions. Nevertheless, simulations are limited in terms of physical processes and this will not be strongly covered in this master's thesis. The main point to be drawn from this is that grains can add new atoms and fragments to molecules with basic reactions – adsorptions, reactions on surfaces, and desorptions.

Addition reactions on grains are possible. Now, one has to evaluate the importance of this reactional phase before indicating it as an important feature to incorporate into modelling. To do so, scientists compared abundances in hot star atmospheres (where compounds on grain are completely evaporated) and in the ISM. Results are shown in Table 1.7. We directly evaluate the high impact of grain adsorption on the ISM abundances. Even if this impacts more metals, significant percentages of carbon and oxygen

participate in making grains impacting.

Element	Carbon	Nitrogen	Oxygen	Magnesium	Silicon	Iron
Hot star atmospheres	214	62	575	36.3	31.6	33.1
Abundance in the IS gas	91	62	389	1.5	2.2	0.3
Percentage in the IS gas	43%	100%	68%	4%	7%	0.9%
Abundance in the IS dust	123	0	186	34.8	29.4	32.8
Percentage in IS dust	57%	0%	32%	96%	93%	99.1%

Table 1.7: Comparisons between abundance in dust grains and the gas phase. Grain phase abundances are inferred from the difference between the gas phase and hot star atmospheres. Units are relative to one million H atoms. From Van Grootel, V. 2023.

1.2.4 The chemical network

Before ending this subsection on the wonderful field that is astrochemistry, we have to present an efficient and current tool used to visualize chemical processes – the chemical network. We have discovered the high diversity of chemical reactions occurring in space covering the gas phase and the grain-surface phase. Due to this diversity, current astrochemical models compute several thousands of chemical reactions. The use of computers allows us to transform them into ODEs and easily calculate the evolution of the abundance of the different chemical compounds from a big set of chemical reactions. More suitable to our way of thinking, we can represent our set of reactions as a chemical network where compounds are the nodes and reactions are the lines. An example of a chemical network is shown in Figure 1.4.

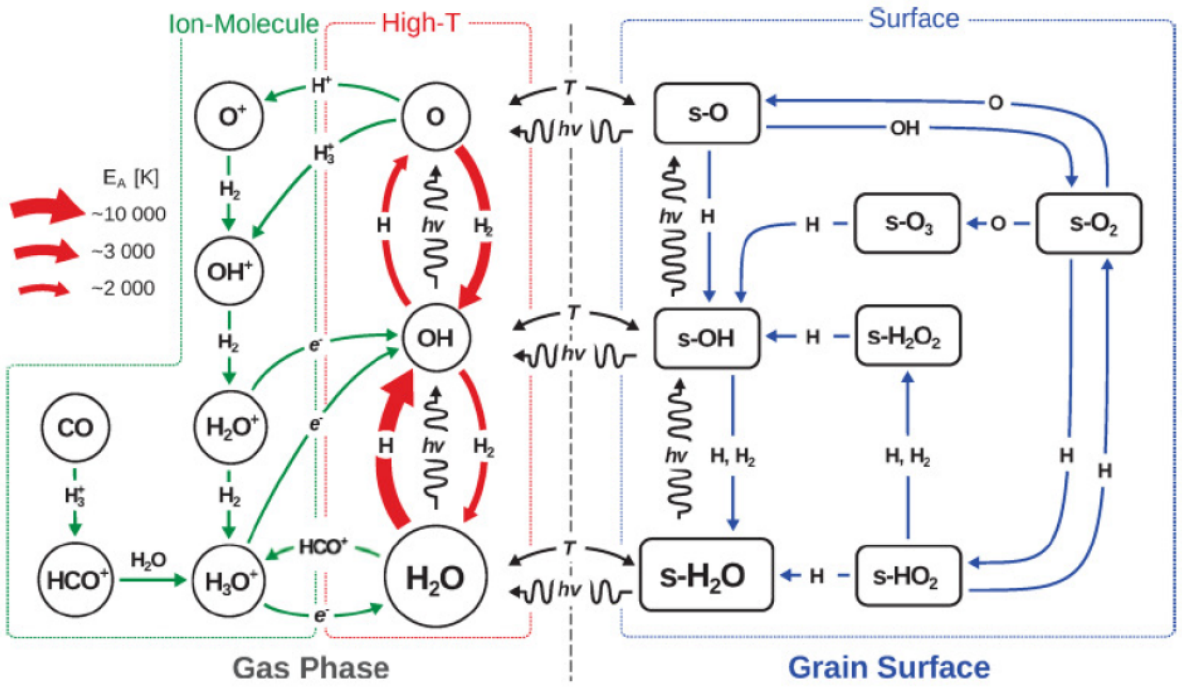

Figure 1.4: Chemical network of the H_2O molecule in the gas phase and on grain surfaces. From van Dishoeck, Herbst, and Neufeld 2013.

As visible in Figure 1.4, the chemical network enables to showing of the main molecules of interest and represents the different pathways linking them together. When both are present, a chemical network should differentiate between the gas phase and the grain surface processes. As discussed in the gas phase discussion, an ion-molecule road and a neutral-neutral one mainly form the gas phase. The neutral-neutral path is mentioned as the High-Temperature path given that neutral-neutral reactions have a greater activation barrier and are thus more likely to occur when enough energy is available.

1.3 Objectives of this master's thesis

Now that we are familiar with the scientific field of astrochemistry, as well as the scientific context, it is time to identify the main objectives of this master's thesis and the main results that it will provide to the scientific community. Given the wealth of the results reached by our methods that will be described in 2, two main research questions are addressed in this work:

- **How can we make use of astrochemistry to characterize interstellar shocks?**
- **How do shocks influence the overall chemistry of the interstellar medium?**

The first question is justified by the huge distance between interstellar shocks – the main subject of this master's thesis – and scientists. As usual in astronomy, this distance prevents any direct experiments on what we observe. It is thus essential to determine observational ways to identify our subject and the physical phenomena happening in it. One of these ways is to identify which molecular tracers – molecules specific to an environment observable with spectroscopy – are abundant enough to fulfill this task of identification. A good prediction of these molecular tracers will enable astrophysicists to more easily identify and characterize interstellar shocks from spectroscopic observations. Also, as will be seen in the next section, shocks are divided into different types. Molecular tracers identified in this master's thesis should be able to characterize the presence of shocks, but also their types.

As it will be described, our methods are computational and make use of simulations. This way of proceeding pushes us to simulate and compute the evolution of a big part of the physical and chemical aspects of the shocked environments including the chemical abundances of chemical components through the shock. Taking advantage of these outputs, it will be possible to deeply analyze how changes in shocks influence the evolution of these chemical abundances, and thus the overall chemistry – in the context of the various assumptions made by our simulations. This will give us first and interesting insights into the chemistry of interstellar shocks – justifying the second question.

To do so, including this introduction giving the scientific context of this master's thesis, my work is divided into eight parts. **The model: The Paris-Durham Shock code** 2 describes in detail the computational methods used in this work. Emphasizing the different aspects of the shocks, the physics, and the chemistry implemented in the code, this step is mandatory to understand the strengths and weaknesses of the results reached at the end of my simulations. **The exploration of the parameter space** 3 details the initial conditions of my simulations and the treatment of the raw data that has been done to perform the exploration. This section also gives the first results obtained during my master's thesis. **Discussion – The molecular tracers** 4 discuss the first results based on previous works and the real case of L1157 – a shocked region described in detail in this chapter. The question of the identification of molecular tracers is highlighted and answered through this discussion. While **Discussion – The astrochemistry of interstellar shocks** 5 focuses on the second question. Relying on computational tools

described in this part, the evolution of the chemical network for our main element CH_3OH will be plotted and analyzed in the first instance. The **conclusion** 6 will end the main part of this work by summarizing the context, the research questions, the methods, the results, the discussions, and the scientific perspectives that can follow what has been done during this work. More details concerning some aspects of the work or some results that did not find their place in the master's thesis can be found in the **Appendix** 7. An overall picture summarizing the organization of the master's thesis is displayed in Figure 1.5.

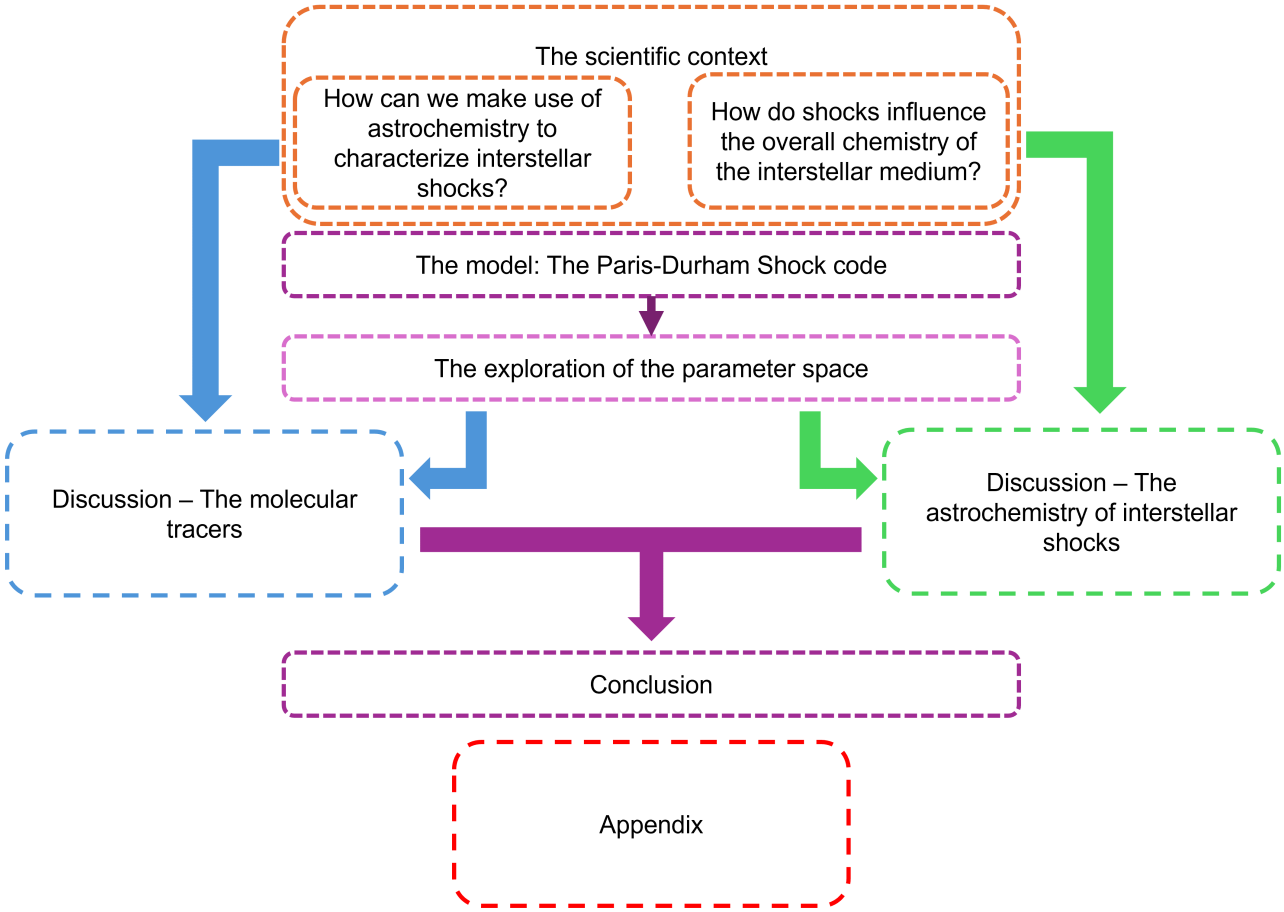

Figure 1.5: Organization of the eight different components as presented in the objectives of this master's thesis.

Chapter 2

The model : The Paris-Durham Shock code

All simulations carried out as part of this Master's thesis are calculated using the Paris-Durham Shock code (Flower and Pineau des Forêts 2003a; Godard et al. 2019). A large proportion of the results are analyzed using the tools available on the ISMServices website (*Interstellar Medium Services Platform* n.d.), which are the ISM Data Analysis Toolbox (2.1.4), and The Chemistry Analyser tool. As numerical methods are always limited by the precision of the calculation tools, this chapter looks in detail at the functioning of the Paris-Durham Shock code. But more than the computational details, looking through the code functioning enables us to discover more about shock physics, which is an primordial step in analyzing the consequences of shocks on astrochemistry.

2.1 What does the Paris-Durham Shock code do ?

The Paris-Durham Shock code simulates shocks in galactic and extragalactic environments. Solving the physics and chemistry of shocks in parallel, the code appropriately calculates the physical evolution of shocks, taking into account the chemical influence of their components. As we will see in this chapter, the ionization fraction of the medium determines the importance of what we call magnetic precursors, which have an impact on the shock structure. Thus, chemical reactions that have been influenced by changes in the physical properties of the medium will lead to significant feedback on the evolution of shocks. Nevertheless, the physics of shocks is complex, and the Shock code is forced to follow certain major assumptions to limit computational cost. These assumptions can be summarized as follows: (The ISM Team of Paris Observatory 2020)

- We calculate only the plane-parallel shock in the reference frame of the shock wave.
- We consider a steady-state shock. Consequently, all time derivatives are set to 0.

- The medium studied is homogeneous and impregnated with a magnetic field transverse to the shock propagation. The magnetic field is frozen into the ionized gas.

As we will see in the next subsection, different types of shocks can occur in space. Concerning the Shock code, five types of shock can be calculated: J-type, C-type, young C-type, steady C*, and C-J shocks. In this master's thesis, all simulations were carried out with J-type and C-type shocks. For all these shock types, the Shock code enables certain observational predictions by calculating the predicted surface brightness for certain atomic lines (O, C, C+, N, N+, Si, Si+, S, S+, Fe+) and optically thin H_2 lines (lines computed in the optically thin regime where the total optical depth is approximated to be very small ¡¡ 1.). These predictions will be used as a first means of validating the results plotted by the Shock code.

Concerning limitations, although the chemical network of the Shock code includes ionization, it can only study singularly ionized species and does not calculate the transfer of Lyman photons in its current version. As a result, overly violent J-type shocks cannot be calculated, and jump speeds are limited to 30 km/s. Similarly, grain-grain collisions are not yet included in the Shock code and must be taken into account when discussing Shock code results. More specifically, the absence of grain-grain collisions will lead to an underestimation of the release of refractory species and ice into the gas phase (The ISM Team of Paris Observatory 2020).

2.2 Properties of shocks and their different types

To clarify the subject of these simulations, it is useful to spend a little more time on shocks. According the description byDe Becker, M. 2023, shocks can be seen as a significant discontinuity in the flow of a fluid. This situation can occur in many contexts such as collisions between two different clouds for example with the condition that the shock velocity $|u_u - u_d|$ is high enough to have more than a simple perturbation. Where u_u and u_d are the velocities of the upstream and downstream regions. To be precise, the shock velocity has to be supersonic for the shock to occur. As visible in Figure 2.1, this discontinuity leads to a separation of shocks into three different components: the upstream (pre-shock) region, the downstream (post-shock) region, and the shock front where occurs the discontinuity. Justifying the discontinuity aspect of the shock, the shock front is known to be very thin compared to the other two components. The upstream and downstream regions of the shock are characterized by different values for their physical parameters which are the densities ρ, the pressure P, and the temperatures T. As it will be described soon, it is possible to be more precise in separating by defining the relaxation layer in the downstream region. The relations between these different parameters are expressed by the magneto-hydrodynamics laws which will be introduced in the next subsection.

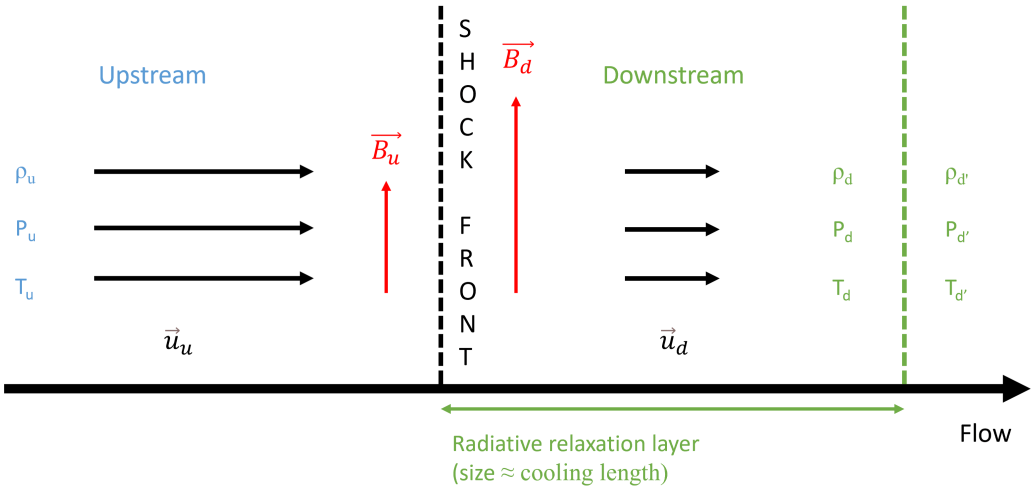

Figure 2.1: Illustration of a magneto-hydrodynamic shock where the magnetic field is perpendicular to the fluid flow. The shock is separated into three major components: the upstream (pre-shock) region, the shock front, and the downstream (post-shock) region. The downstream region contains in itself a radiative relaxation layer. Inspired from De Becker, M. 2023.

In the Paris-Durham Shock code, we also consider a magnetized medium. This is taken into account by introducing a magnetic component perpendicular to the fluid flow. Via the Lorentz force, the magnetic field acts on ions. Thus, the strength of the magnetic field can have a great impact on the shock structure by acting on all charged species as we will see in C-type shocks. The last important feature implemented in the code visible in Figure 2.1 is the presence of the radiative relaxation layer. As well as the code includes heating processes able to significantly increase the temperature of shock components, it also includes mostly radiative cooling processes. These processes will evacuate the energy in the form of photons, bringing the temperature back to the initial pre-shock temperature. As discussed by De Becker, M. 2023, these radiative processes could create a feedback loop having a major impact on the upstream region of the shock. Nevertheless, a necessary condition to warrant enough photons to produce a significant radiative precursor is a pre-shock velocity of the order of $100 km\, s^{-1}$. Knowing that in this master's thesis, we will evaluate shock velocities of the order of $10 km.s^{-1}$, radiative precursors are negligible.

Even if these components are general for almost every shock, it is important to know that **different types of shocks exist**. Figure 2.1 principally describes J-type shocks where the transition of the properties between the upstream and the downstream region is abrupt, in the form of a Jump. Nevertheless, another significant type of shock occurs when the transition is smoother or even Continuous. These are called C-type shocks. C-type shocks are essentially the fruit of the combination of a moderate magnetic field and a high-density medium characterized by a low degree of ionization (De Becker, M. 2023). In these conditions, we are confronted to a case where we can not necessarily assume

that the magnetic field is frozen in the flow due to the fact we do not have a strong coupling between charged and neutral particles. As the magnetic field acts only on ions and electrons, their strong coupling by collisions with the neutral medium is necessary to assume a frozen-in-flow magnetic field as described by B. T. Draine 1980.

The uncoupling of ions and electrons on the one hand, and the neutral medium on the other hand, can lead to magnetic precursors. These magnetic precursors constitute the feedback effect that will shape the structure of the C-type shock. As described by B. T. Draine 1980, the structure of magneto-hydrodynamic (MHD) shocks with magnetic precursors is strongly different from MHD shocks showing a J-type behavior. A part of the dissipation of the energy in C-type shocks is done in the magnetic precursor. For this reason, we do not encounter a sudden increase in the temperature. Thus, good radiative cooling should prevent a temperature as great as in J-type shocks. The general aspect of the effects of magnetic precursors in interstellar shocks is depicted in Figure 2.2. This will also be visible in the simulations presented later in this work. Another strong difference between these two main types of shocks is the necessity to describe C-type shocks using multi-fluid models since the coupling between charged and neutral particles cannot be assumed. As a consequence of this uncoupling, C-type shocks possess a region where ions can stream into the neutral medium, driven by the magnetic field. These two major components (i.e. the temperature profile and the ion stream) should lead to interesting differences in the astrochemistry of shocks. Indeed, chemical reactions are strongly dependent on the temperature via the energy barrier they have to pass through. A huge increase in the temperature could enable endothermic reactions, almost impossible at low temperature, or leads to destructive chemistry if the medium becomes too hot. The stream of ions and electrons in the neutral medium, also called ion-neutral drift (The ISM Team of Paris Observatory 2020), should have a great impact on ion-neutral reactions. Nevertheless, it exists also specific conditions for C-type shocks to appear. To have magnetic precursors, information about changes in physical conditions must reach the upstream region. This can be done only if the magnetosonic velocity (at which perturbation in the plasma is conveyed upstream) becomes greater than the shock velocity. We should emphasize that the magnetosonic velocity grows with the magnetic field, and decreases with the charged particles density according to (Eq. 2.1):

$$v_{Magnetosonic} = \sqrt{v_{sound}^2 + \frac{B^2}{4\pi\rho_i}} \tag{2.1}$$

As previously mentioned, other types of shocks exist such as C*-type shocks and CJ-type shocks, in which the shock can be temporarily subsonic as analyzed by Godard et al. 2019. But their existence being very specific for a special set of physical conditions in irradiated shocks, they are not covered by our simulations or by this master's thesis in general.

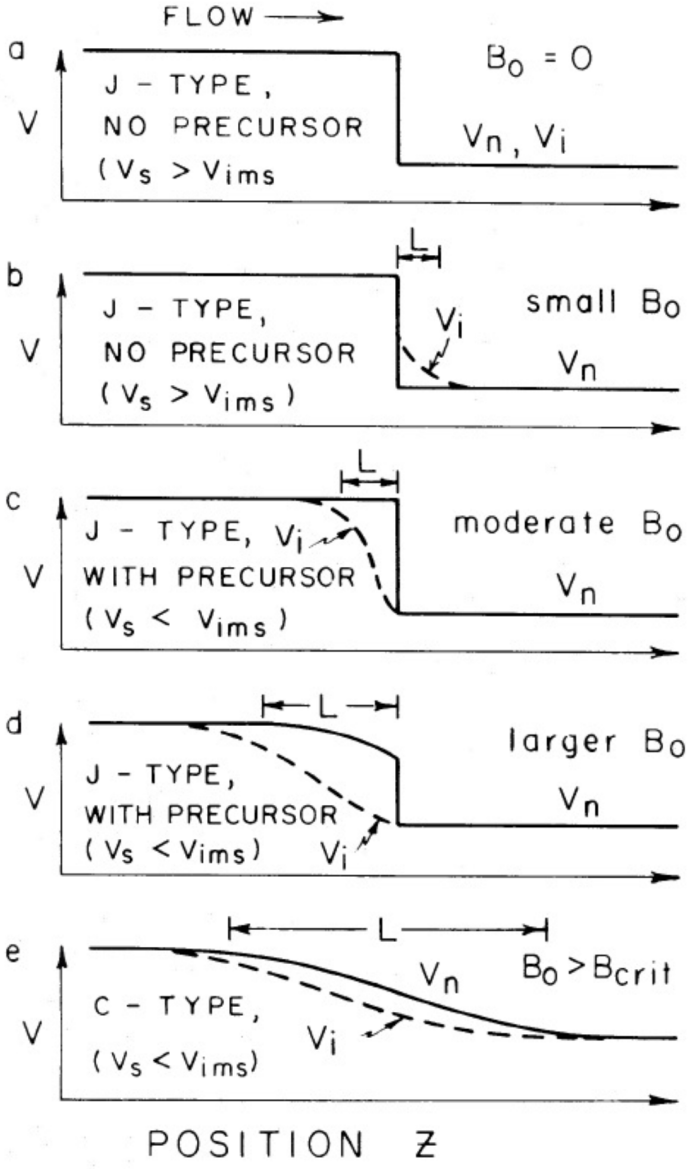

Figure 2.2: Illustrations of the effects of magnetic precursors on the behavior of interstellar shocks. As mentioned in the main text, C-type shocks appear only if the magnetosonic speed of ions – v_{ims} on the schema – is greater than the shock velocity. Magnetic precursor effects thus directly depend on the strength of the magnetic field. From De Becker, M. 2023.

2.3 Physical basis of the Shock Code model

2.3.1 The conservation equations

The first step toward modelling of shock physics is to describe the underlying physics laws. In our case, as we want to discuss MHD shocks, we can use the fundamental equations of magneto-hydrodynamics. It is also important to note that differences between C-type shocks and J-type shocks will bring some differences in how we have to mathematically

treat them. This is the result, as we just saw, of C-type shocks occurring when the medium is characterized by a low ionization fraction. In this case, the entrainment of neutral species by ionic species cannot be assumed to be sufficiently strong. They are decoupled. We therefore need to model a multi-component fluid when describing C-type shocks. To this end, the Shock code models one global fluid when calculating J-type shocks and three fluids - neutral species, positive ionized species and negative ionized species (mainly electrons) - when calculating C-type shocks.

Shock modelling and, more specifically, the modelling of its fluid components requires the solution of conservation equations. According to the first paper about the Shock code (Flower, Pineau des Forets, and Hartquist 1985), the conservation equations concern the conservation of particle number density (Eq. 2.2 and 2.3), the conservation of mass (Eq. 2.4 and 2.5), the conservation of momentum (Eq. 2.6 and 2.9), and the energy conservation (Eq. 2.10 and 2.11).

Particle number density conservation is divided into neutral species, positive ionized species and negative ionized species:

$$\frac{d}{dz}(\frac{\rho_n \cdot V_n}{\mu_n}) = N_n \tag{2.2}$$

where ρ_n is the mass density, V_n is the velocity of particles, μ_n is the mean molecular weight, and N_n is the number of neutral particles created/consumed per unit volume and time. A very similar equation can be written for positive ionized species,

$$\frac{d}{dz}(\frac{\rho_i \cdot V_i}{\mu_i}) = N_i \tag{2.3}$$

Since the Shock code model is electrically neutral, the conservation equation for negative ions is identical to that for positive ions.

The conservation of mass for neutral species is written as follows:

$$\frac{d}{dz}(\rho_n \cdot V_n) = L_n \tag{2.4}$$

where L_n is the source term of the neutral species. In the same way, we can consider positive ionized species using:

$$\frac{d}{dz}(\rho_i \cdot V_i) = L_i = -L_n \tag{2.5}$$

The last equality comes from the fact that ionized species originate from neutral

species (we only consider the first ionizations). In the first paper, Flower, Pineau des Forets, and Hartquist 1985 considered electron mass to be negligible, since electrons were the only component of negative ions. Today, the chemical network of the Shock code includes some negative ions, and a corresponding mass conservation equation must be written for negative ionized species.

It is now time to write down the third conservation equation which concerns **momentum conservation**. This is shown in the following equation concerning neutral species:

$$\frac{d}{dz}(\rho_n \cdot V_n^2 + \frac{\rho_n \cdot k_B \cdot T_n}{\mu_n}) = A_n \tag{2.6}$$

with k_B, the Boltzmann constant, T_n, the temperature of the neutral medium, and A_n stands for the momentum changes per unit volume and time for the neutral medium. When we have to consider charged species, we know that the magnetic field will lead to a compression term which as to be added as in the following equation:

$$\frac{d}{dz}(\rho_i \cdot V_i^2 + \frac{\rho_i \cdot k_B \cdot T_i}{\mu_i} + \frac{B^2}{8\pi}) = -A_n \tag{2.7}$$

As described in the assumptions made by the Paris-Durham Shock Code, we consider a magnetic field frozen into the ionized gas. This is useful to simplify the last equation given that this assumption leads to a relation between the perturbed magnetic field and the unperturbed one (Eq. 2.8). In the following equation, V_s stands for the shock velocity,

$$B_i \cdot V_i = B_0 \cdot V_s \tag{2.8}$$

This enables us to rewrite Eq. 2.7 as Eq. 2.9). This second equation makes it easier to computationally describe the momentum conservation.

$$\frac{d}{dz}(\rho_n \cdot V_n^2 + \frac{\rho_n \cdot k_B \cdot T_n}{\mu_n} + \frac{B_0^2}{8\pi} \cdot (\frac{V_s}{V_i})^2) = -A_n \tag{2.9}$$

The last equation concerns energy conservation. Here, the main difference between the neutral and the ion-electron fluids resides in the fact that we consider the mean internal energy per neutral particle in the neutral medium (Eq. 2.10). As an approximation, this term is neglected in the case of the ions-electrons fluid (Eq. 2.11). In its place, a contribution from the magnetic field is written (where the frozen field assumption is already taken into account.). These equations are the following:

$$\frac{d}{dz}\left(\frac{1}{2}\cdot\rho_n\cdot V_n^3+\frac{5}{2}\cdot\frac{\rho_n\cdot V_n\cdot k_B\cdot T_n}{\mu_n}+\frac{\rho_n\cdot V_n\cdot U_n}{\mu_n}\right)=B_n \tag{2.10}$$

This equation is for the neutral medium. U_n describes the mean internal energy per neutral particle and B_n is the adequate source term. For the ion-electron fluid, we have:

$$\frac{d}{dz}\left(\frac{1}{2}\cdot\rho_i\cdot V_i^3+\frac{5}{2}\cdot\frac{\rho_i\cdot V_i\cdot k_B\cdot(T_i+T_e)}{\mu_i}+\frac{V_s^2}{V_i}\cdot\frac{B_0^2}{4\pi}\right)=B_i+B_e \tag{2.11}$$

More than these usual MHD equations, it is computationally important to follow changes in the abundances of our chemical species. When the MHD equations follow the behavior of our fluids (one for J-type shocks and three for C-type shocks), the following equation (Eq. 2.12) individually follows each atomic or molecular species:

$$\frac{d}{dz}(n_\alpha\cdot V_\alpha)=C_\alpha \tag{2.12}$$

where C_α is the rate at which the species α are being formed (or consumed) by chemical reactions per unit of volume and time, and n_α is the density. These rates can be directly related to the number of neutral (or ionized) particles created per unit of volume and time with N_n (or N_i) by the equations:

$$N_n=\sum_{\alpha,neutralspecies}C_\alpha \tag{2.13}$$

$$N_i=\sum_{\alpha,ionizedspecies}C_\alpha \tag{2.14}$$

Another relation can be made between the global mean energy per neutral particle per unit of volume and the individual ro-vibrational levels of energy of the specific species:

$$\frac{\rho_n}{\mu_n}\cdot U_n=\sum_{\nu J}n_\alpha(\nu,J)\cdot E_\alpha(\nu,J) \tag{2.15}$$

where $n_\alpha(\nu, J)$ describes the density of species α at the ro-vibrational level (ν, J) and $E_\alpha(\nu, J)$ is the energy of ro-vibrational level (ν, J) concerning the specie α.

2.3.2 The source terms

Continuing to follow the article of Flower, Pineau des Forets, and Hartquist 1985 and the dedicated part of the Shock Code documentation (The ISM Team of Paris Observatory 2020), we now have to describe the source terms implemented in the MHD equations. These were L_n, A_n, and B_n. The first one, L_n, appears in (Eq. 2.4) and describes the rate at which mass is transferred from the ionized fluid to the neutral one per unit of volume and time. This can be related to the rate of formation/destruction C_α by writing:

$$L_n = \sum_{\alpha, neutral\, species} C_\alpha \cdot m_\alpha \tag{2.16}$$

Similarly, the mass transfer from the neutral fluid to the ionized one is simply written:

$$L_i = \sum_{\alpha, ionized\, species} C_\alpha \cdot m_\alpha \tag{2.17}$$

As specified by Flower, Pineau des Forets, and Hartquist 1985, the requirement $L_n = -L_i$ can serve as a required check in the code. The next source term is A_n which describes momentum transfers between the ionized and the neutral medium. There exist different ways to transfer momentum, and the code takes into account three of them which are:

- (i) Reactive inelastic collisions between ionized and neutral species
- (ii) Elastic ion-neutral scattering. (Ambipolar diffusion)
- (iii) Elastic collisions between grains and neutral species (Ambipolar diffusion)

The first momentum transfer between ionized and neutral species is accurate when reactive ion-neutral collisions occur. To mathematically describe them, we introduce a similar factor to C_α, but that will take into account the specific reaction β in which the species α is involved. This new factor is denoted $C_{\alpha\beta}$ and should be related to C_α with:

$$C_\alpha = \sum_\beta C_{\alpha\beta} \tag{2.18}$$

It is now possible to mathematically write the source term A_n describing the momentum transfer from the ionized medium to the neutral one (Eq. 2.19) (or from the neutral medium to the ionized one, EQ. 2.20) per unit of volume and time. In the frame of the center of mass of the reaction, we can use V_β and write:

$$A_n^{(i)} = \sum_{\alpha, neutral species} \sum_{\beta} C_{\alpha\beta} \cdot m_\alpha \cdot V_\beta(CM) \tag{2.19}$$

$$A_i^{(i)} = \sum_{\alpha, ionized species} \sum_{\beta} C_{\alpha\beta} \cdot m_\alpha \cdot V_\beta(CM) = -A_n^{(i)} \tag{2.20}$$

It is useful to describe more the value of the velocity V_β as described in the documentation of the code. In neutral-neutral reactions (or ion-ion reactions), we can directly expect V_β to be V_n (or V_i). But in the context of a momentum transfer, we consider neutral-ion reactions where we can write:

$$V_\beta = \frac{(m_i \cdot V_i + m_n \cdot V_n)}{(m_n + m_i)} \tag{2.21}$$

Again, we can describe the relation $A_n^{(i)} = -A_i^{(i)}$ as a check-up to perform during the run of the code. The next process we take into account is the scattering between ionized and neutral species. The rate coefficient of these processes can be written and implemented in the second part of the source term $A_n^{(ii)}$ through the following equations:

$$< \sigma v >_{in} = 2.41\pi \cdot (\frac{e^2 \cdot \alpha_n}{\mu_{in}})^{1/2} \tag{2.22}$$

$$A_n^{(ii)} = \frac{\rho_n \cdot \rho_i}{\mu_n + \mu_i} \cdot < \sigma v >_{in} \cdot (V_i - V_n) \tag{2.23}$$

Where $< \sigma v >_{in}$ is the rate coefficient, e is the charge of the electron, α_n is the polarizability of the neutral species, and μ_{in} is the reduced mass. As indicated B. T. Draine 1980 and emphasized by Flower, Pineau des Forets, and Hartquist 1985, Eq. 2.23 is more precise when the shock velocity does not exceed $24 km \cdot s^{-1}$. This is respected in our simulations. The third way to transfer momentum concerns elastic collisions between charged grains and neutrals. This is also a kind of ambipolar diffusion. The formula used in the code is the following:

$$A_n^{(iii)} = n_g \pi a^2 \cdot |V_i - V_n|(V_i - V_n) \cdot \rho_n \tag{2.24}$$

Where n_g is the charged grain density, and a is the rms radius of the grain size distribution at a certain point as described in The ISM Team of Paris Observatory 2020. The final momentum transfer source term can be written as a sum of its three components:

$$A_n = A_n^{(i)} + A_n^{(ii)} + A_n^{(iii)} \tag{2.25}$$

The last source term we have to explain is B_n. It represents the transfer of energy between the ionized and neutral medium per unit volume and time. It is a little bit harder to describe mathematically these transfers. For the sake of simplicity, we do not think that it is an absolute necessity to get into the details since the equations are not as expressive as their predecessors. Nevertheless, it is important to note that these transfers can also be separated into different processes which are summarized as the following:

- **Ions-ions, neutrals-ions, and neutrals-neutrals reactive collisions** describe the transfer of kinetic energy between the products of the reaction.
- **Transfer of energy between reactants**
- **Endothermicity and exothermicity** of reactions
- **Elastic scattering between ionized and neutral species**
- **Elastic scattering between electrons and neutral species**
- **Elastic scattering between electrons and ionized species** which is also named the "Joule Heating".
- **Photoionization and photodissociation**
- **Photoelectric effects on grains and PAHs**
- **Cosmic rays ionization**

A detailed treatment of these energy transfers including the corresponding equations can be found in Appendix 7. As a first view, it is only important to note that these transfers of energy can lead to a heating or a cooling of the medium.

2.3.3 The molecular cooling

Even if we do not focus on energetic source terms, it is relevant to explain at least one given that it is at the base of the radiative relaxation layer described earlier. Initially implemented in the Paris Durham Shock Code, it is the radiative cooling by molecules (Flower, Pineau-Des-Forets, and Hartquist 1986). The radiative cooling enables the medium to lose energy through ro-vibrational transitions. Here, even if the Shock Code considers radiative cooling from several molecules of interest: H_2, CO, and H_2O, we will mainly focus on molecular dihydrogen H_2.

Following the documentation of the Shock Code, our goal is to define the source term corresponding to this radiative cooling "B_n". The first step is to denote the population

density of the rotational level of H_2 as in the next equation (we call these levels "J".):

$$n(H_2) = \sum_j n_J \tag{2.26}$$

where the total density of hydrogen is (considering the most important hydrogen-bearing compounds):

$$n(\mathbf{H}) = n(H) + 2n(H_2) \tag{2.27}$$

Knowing that possible de-excitations require a jump from J to $J-2$, the next step requires comparing spontaneous radiative decay rates $A(J \rightarrow J\text{–}2)$ in s^{-1} and collisional de-excitations where rates $C(J \rightarrow J\text{–}2)$ are written:

$$C(J \rightarrow J-2) = n_j \cdot (n(H) + n(H_2)) \cdot < \sigma v >_{J \rightarrow J-2} \tag{2.28}$$

where $< \sigma v >_{J \rightarrow J-2}$ denotes the rate coefficient of collisional de-excitation. As an assumption made and discussed by the code, this rate coefficient does not change if we consider atomic or molecular collisions. A detailed balance where we consider the relations between collisional excitations and de-excitations is written:

$$(2J-3) \cdot C(J-2 \rightarrow J) = (2J+1) \cdot C(J \rightarrow J-2) \cdot exp\left(\frac{2(2J-1) \cdot B}{k_B \cdot T_n}\right) \tag{2.29}$$

In Eq. 2.29, $(2J+1)$ is the degeneracy of the rotational level J, and B is the rotational constant of the ground state of H_2. Now that these terms have been defined, we can also describe more precisely the rate coefficient of collisional de-excitations used in the code:

$$< \sigma v >_{J \rightarrow J-2} (cm^3 s^{-1}) = 4.6 \cdot 10^{-12} \cdot (2J-3) \cdot T_n^{\frac{1}{2}} \cdot \left(1 + \frac{2 \cdot (2J-1) \cdot B}{k_B T_n}\right)^{\frac{1}{2}} \times exp\left[-5.01 \cdot \frac{\frac{2 \cdot (2J-1) \cdot B}{k_B T_n}}{1 + \frac{BJ(J+1)}{k_B T_n}} - 0.1187 \cdot (4J-2) \right] \tag{2.30}$$

It is of course not mandatory to retain all the mathematical details of this rate coefficient. Nevertheless, its writing remains useful in determining what are its dependencies on physical conditions. Now that we possess the expressions of the spontaneous radiative

decay and the collisional excitations/de-excitations, we can write the equation denoting the gradient of the flux of the level J population as a stationary state:

$$\begin{aligned}\frac{d}{dz}(V_n n_J) = &[C(J+2 \to J) + A(J+2 \to J)] \cdot n_{J+2} + C(J-2 \to J) \cdot n_{J-2} \\ &- [C(J \to J+2) + C(J \to J-2) + A(J \to J-2)] \cdot n_J \\ &+ \frac{n_J}{n(H_2)} \frac{d}{dz}[V_n n(H_2)] \end{aligned} \quad (2.31)$$

Equation 2.31 denotes a stationary state - not time dependant - of level J where creation and destruction terms of molecular hydrogen in level J are dispatched in three lines. The first line describes radiative and collisional transitions from other rotational states to the J state. The second line (be aware of the $-$ sign) describes the decrease of the J state population due to transitions. Concerning the third line, it describes chemical reactions populating (or depopulating) rotational states. We now have to recall what we are describing in this subsection: molecular cooling. The final important step is thus to mathematically write the rate of radiative cooling and implement this in our previous equations. Knowing A, the spontaneous radiative cooling, we can describe the source term:

$$B_n(H_2)_{radiative} = -\sum_{J \geq 2} n_J \cdot A(J \to J-2) \cdot 2(2J-1)B \quad (2.32)$$

This source term is important in the equations of energy conservation (Eq. 2.10). Also, a good knowledge of the ro-vibrational level densities enables us to know the value of (Eq. 2.15) and is required for its implementation in Eq. 2.10. This was the first description of molecular cooling (by H_2 even if other molecules participate in this process.). As already mentioned, the other source terms concerning the energy conservation equations do not require a detailed mathematical treatment at our level. Nevertheless, we still encourage curious readers to see the developments in the documentation of the Paris-Durham Shock code (The ISM Team of Paris Observatory 2020).

2.4 Chemical basis of the Shock Code model

After describing the physical evolution of the shock (the temperatures, the densities, the velocities, ...), we now focus on the chemical content of the system. As specified in the scientific context, the Paris-Durham Shock code can be assimilated into chemodynamics simulations. This means that the physical evolution is computed parallel to the chemical reactions. The main point of chemodynamics is that it enables to study of the interconnections between the physical and the chemical laws.

As already mentioned, the code reads a chemical network and transforms it into a set of ODEs which is solvable by the computer. In the actual version (1.1 – rev 122) of the

Paris Durham Shock code, the chemical network is constituted of 141 chemical species, and 5 artificial species (which are not direct chemical species but are present in specific chemical reactions). These 141 chemical species are divided into 51 neutrals, 16 species in grain icy mantles, 5 species inside grain refractory cores, 66 cations, and 3 anions as shown in Table 2.2. All these species are coming from more fundamental elements (H, D, He, C, N, O, Na, Mg, Si, S, Fe, and G). G is a representative grain species necessary to track the grain charge during the simulation. The elemental abundances of these elements are based on solar abundances and can be found in Table 2.1.

H :	1.00E+00	D :	0.00E+00
He :	1.00E-01	C :	3.01E-04
N :	7.94E-05	O :	4.41E-04
Na :	0.00E+00	Mg :	3.70E-05
Si :	3.40E-05	S :	1.88E-05
Fe :	3.23E-05	G :	6.94E-11

Table 2.1: Elemental abundances as initially used in the Paris-Durham Shock code. (Gas + Mantles + PAH)

All these species are linked together by 3270 chemical reactions of several types as covered in the astrochemical part of the scientific context. It contains 20 types of reactions which are standard chemical reactions, H_2 and HD formations, collisional dissociations of H_2, reactions with excited H_2, radiative recombinations, gaseous 3-body reactions, photo-reactions, self-shielded photoreactions, cross section photoreactions, CR ionizations or dissociations, photoelectric effects, recombinations on grains, adsorptions on grain surfaces, photodesorptions from grain surfaces, CR induced grain desorptions, secondary photon induced desorptions, thermal desorptions from surfaces, erosions of grain cores, sputtering of grain mantles, and three body reactions on surfaces. The specific reactions that we have seen during the description of what astrochemistry is dispatched into these new categories. It is not useful to fully describe the meaning of these new categories given that the usual names are taken back in the chemical network of the Paris-Durham Shock code.

The main chemical aspects described earlier governing the gas phase and the grain-surface phase are thus found in the code. Nevertheless, some points should be emphasized (The ISM Team of Paris Observatory 2020):

- The grain phase is divided into the core bulk and the ice mantle with different sets

of chemical equations. Different parameters such as the size, the power-law grain size distribution, the thickness of the ice layer, etc., will influence the cross-section involved in the chemical reactions. (Nevertheless, these parameters are too specific in the context of this master's thesis and their influence is not deeply investigated.)

- The grain-surface phase – even if it is divided into grain cores and icy mantles – stays very general and, certainly due to computational costs, is only described by basic chemical reactions (more advanced techniques exist nowadays such as branching ratios) and some assumptions. The major assumption that is made concerning the adsorption of species onto grain mantles is the direct and fast saturation of these species (additions of hydrogen atoms until the molecule is saturated). This is typically written:

$$C + GRAIN \rightarrow CH_4^* \tag{2.33}$$

- The chemical network also contains artificial species as listed in Table 2.2 which do not correspond to real chemical species. GRAIN describes adsorption when it is a reactant and is used as a product in case of sputtering, erosion, and photodesorption. PHOTON as a reactant is used in dissociation and ionization processes. CRP denotes the ionization or dissociation by impact of secondary electrons which result from the interaction with cosmic rays. SECPHO is used in the same processes but with secondary photons coming from H_2 UV fluorescence. The last one – VOISIN – is a necessary computational artifact for thermal evaporation reactions on grains. As reactions are written under the form A + B → C + D – thus, with two reactants – thermal evaporation reactions are written A* + VOISIN → A + GRAIN.

- The code considers the enthalpy formation of each chemical species and is thus able to compute the endo/exothermicity of each reaction. More than that, the code takes into account the reverse reaction of each chemical reaction if the endothermicity is less than 2 eV (23200 K). To do so, it multiplies the rate constant k with an exponential term containing the activation barrier: $exp^{-\Delta E/kT}$.

These scientific considerations concerning the physical and chemical evolution as computed in the Paris-Durham Shock code are now done. It is now time to focus on the input files the user has to provide and the output files with the data he/she will receive.

2.5 The input files

Concerning the initial setup of the Paris-Durham Shock code we have to clarify before any simulations, three main files need to be called by the code. The "species.in" file provides the species list and the initial abundances. The "chemistry.in" file contains the chemical network as the one described earlier. The input file we have to adapt before each simulation is "input_mhd.in". It is a file containing a list of parameters that we can change to specify the specific features of the simulation. The important parameters in our

Neutrals	H, H_2, He, C, CH, CH_2, CH_3, CH_4, C_2, C_2H, C_2H_2, C_3 C_3H, C_3H_2, O, OH, H_2O, O_2, CO, HCO, H_2CO, CH_3OH, CO_2, HCO_2H N, NH, NH_2, NH_3, N_2, CN, HCN, HNC, NO, S, SH, H_2S, CS SO, SO_2, OCS, Si, SiH, SiH_2, SiH_3, SiH_4, SiO, SiO_2, Mg, Fe, $C_{54}H_{18}$, G
Grain icy mantles	CH_4^*, H_2O^*, O_2^*, CO^*, H_2CO^*, CH_3OH^*, CO_2^*, HCO_2H^* NH_3^*, H_2S^*, OCS^*, SiH_4^*, SiO^*, SiO_2^*, Mg^*, Fe^*
Grain refractory cores	C^{**}, O^{**}, Si^{**}, Mg^{**}, Fe^{**}
Cations	H^+, H_2^+, H_3^+, He^+, C^+, CH^+, CH_2^+, CH_3^+, CH_4^+, CH_5^+ C_2^+, C_2H^+, $C_2H_2^+$, $C_2H_3^+$, C_3^+, C_3H^+, $C_3H_2^+$, $C_3H_3^+$, O^+, OH^+ H_2O^+, H_3O^+, O_2^+, CO^+, HCO^+, H_2CO^+, H_3CO^+, CH_3OH^+ CH_5O^+, HCO_2^+, N^+, NH^+, NH_2^+, NH_3^+, NH_4^+, N_2^+, N_2H^+ CN^+, HCN^+, H_2CN^+, H_2NC^+, C_2N^+, NO^+, HNO^+, S^+, SH^+ H_2S^+, H_3S^+, CS^+, HCS^+, SO^+, HSO^+, HSO_2^+, $HOCS^+$, Si^+, SiH^+ SiH_2^+, SiH_3^+, SiH_4^+, SiH_5^+, SiO^+, $SiOH^+$, Mg^+, Fe^+, $C_{54}H_{18}^+$, G^+
Anions	$C_{54}H_{18}^-$, G^-, ELECTR
Artificial	GRAIN, PHOTON, CRP, SECPHO, VOISIN

Table 2.2: List of the 146 chemical species included in the chemical network of the Paris-Durham Shock code.

	File parameters
modele	**Model name**. subdirectory output/modele will be created containing all output files; also added as prefix to the .hdf5 binary output files.
specfile	**Path of file with species list and their initial abundances.** Can be the output file species.out created by a previous "initialization" run (types S1, S2, P1 or P2, see below).
chemfile	**Path of file with chemical reactions list.**
h2exfile	**File with initial H_2 level populations.** Standard value "none" initializes H_2 levels at LTE at temperature = Tn with an ortho to para ratio = op_H2_in. Can be the file H2_lev.out from preshock run.
	Environment parameters
Zeta	**Cosmic ray ionization rate per H_2 molecules** (s^{-1}). For a gas with 10% of Helium, it is related to the usual cosmic ray ionisation rate per H nucleus, ζ_{CR}, through $Zeta = \zeta_{CR}/0.54$.
RAD	**Mean intensity** G_0 of the FUV field over the interval 910-2066 $\dot{A}$, in Habing units.
Av0	**Visual extinction at** z = 0 (in magnitudes); Typical value is 1.00E-01.

Table 2.3: File and Environment parameters in the input_mhd.in file of interest as described in The ISM Team of Paris Observatory 2020.

simulations are found in Tables 2.3, 2.4 and 2.5. Other parameters exist to make the code more general. An exhaustive list can be found in The ISM Team of Paris Observatory 2020.

2.6 The output files

Again, it is not possible and useful in our context to detail all the outputs obtainable with the Paris-Durham Shock code. For the development of this master's thesis, four main outputs should be emphasized:

- **info_mhd.out:** contains a complete resume of the simulation including the parameters as written in mhd_input.in, the date and time of the simulation, the lists of the chemical elements and reactions used, the final shock properties (required to

	Grain properties
F_TGR	**Grain temperature flag.** 0 = constant (Standard), 1 = computed at each position.
Tgrains	**Initial grain temperature** (in K).
rho_grc	**grain core bulk density** (in g cm^{-3}). The number of grains per unit volume of gas is inversely proportional to *rho_grc*. Standard value = 2 g cm^{-3}.
rho_grm	**ice mantle bulk density** (in g cm^{-3}). Determines the thickness of the ice layer, hence the total grain cross-section for collisions with gas. Standard value = 1 g cm^{-3}.

Table 2.4: Grain parameters in the input_mhd.in file of interest as described in The ISM Team of Paris Observatory 2020.

evaluate the smooth running of the simulation), and the run duration. This output file is of all importance to analyze and characterize shock simulations in the Python code developed for the data treatment (see Sect. 3).

- **mhd_phys.out:** contains all the produced data concerning the evolution (at each distance z in the shock) of the different physical properties. The densities, the temperature of each fluid, the velocity of each fluid, and other properties are read from this file to perform the data treatment.

- **mhd_speci.out:** contains all the fractional abundances (as a function of the distance z in the shock) of the different chemical elements that are present in the chemical network. Another more specific file is "species.out" and contains all these abundances at the last computed point. It can be specified to be the file "species.in" at the beginning of a new simulation.

- The code also computes some emission lines for the following compounds. (H_2, Fe, C^+, C, Si^+, Si, H, O, S^+, S, N^+, and N.) These lines are necessary to evaluate the importance of species in terms of emissions and thus their possibilities to be a molecular tracer.

This subsection concludes this first description of the Paris-Durham Shock code. Of course, the code has existed for more than thirty years with continuous development and cannot be explained with all its details (the bibliography of the main code contains more than 37 articles.) More specific aspects will thus appear in due course during the next sections depending on the requirements of the discussion.

	Shock parameters
shock_type	Type of model can take the following values
	C = Continuous C-type shock (with ion-neutral decoupling)
	J = Jump J-type shock (neutral viscosity term added to dynamical equations)
	preshock with Sideways irradiation:
	S1 = isodensity advection at Vs with constant FUV flux
	S2 = isobaric advection at Vs with constant FUV flux
	Preshock buffer with upstream irradiation:
	P1 = isodensity advection at Vs with FUV attenuation along z
	P2 = isobaric advection at Vs with FUV attenuation along z
Nfluids	**Number of fluids** can take the following values
	1 (standard for J-shocks), 2 (neutrals and ions decoupled, but $T_e = T_i$), 3 (standard for C-shocks - neutrals and ions decoupled, and $T_e \neq T_i$)
Bbeta	**Magnetic field parameter** $b = B(\mu G)/\sqrt{n_H(cm^{-3}}$
Vs_km	**Shock entrance speed** (types C, J) or advection speed (types S1, S2, P1, P2) (km/s).
nH_init	**Initial proton density** (cm^{-3}) related to gas volumic density through $\rho = 1.4 \times m_H n_H$ (for 10% of Helium by number). V1.1 is only validated up to $n_H \leq 10^8 cm^{-3}$.
Tn	**Initial temperature of neutrals** (in K).

Table 2.5: Shock parameters in the input_mhd.in file of interest as described in The ISM Team of Paris Observatory 2020.

Chapter 3

The exploration of the parameter space

The first work done in this master's thesis is an exploration of the parameter space considered in our simulations. Using the different features introduced in (Sect. 2), we performed 48 simulations at different shock velocities (from 5 km s^{-1} to 19 km s^{-1} with a footstep of 2 km s^{-1}), and at different hydrogen densities (100 cm^{-3}, 1000 cm^{-3}, and 10 000 cm^{-3}). In this section, we will deeply discuss the initial conditions of these simulations. We will also see what the Python code used to treat the resulting data did, and we will expose the different results we obtained.

3.1 The initial conditions

As indicated in the tutorial furnished with the Shock code (The ISM Team of Paris Observatory 2022), running a shock code model requires simulations of the pre-shock region. To do so, we performed at each density a simulation without any shock (what is called an S1 shock type by the code). Doing this, we calculated a molecular equilibrium state coming from solar abundances. The idea that the ambient medium was at equilibrium before the shock is an abrupt assumption. But this assumption should be put into perspective. Even if this will be discussed, we already foreshadow that small chemical differences in the abundances due to the equilibrium state assumption will be negligible compared to changes brought by the huge variations in the shocks. Except for the initial density, each pre-shock simulation was done using the same parameters to enable valid discussions on the results. As shown in Figure (3.1), we took standard parameters : a cosmic ray ionization rate of 5×10^{-17} s^{-1}, a temperature of 10 K, and no external irradiation. The molecular content of the pre-shock region found as an output (The species.out file) of these simulations served as an input of the shock simulations.

```
date :  6/11/2023     time : 13 H  7 min

input files
          modele           :example_preshock
          specfile         :species_2022_05.in_depl
          chemfile         :chemistry_2022_05_all.in_noadso
          h2exfile         :none
          gridfile         :none

shock parameters
          shock type       :S1
          Nfluids          :        1
          Bbeta            : 1.00E+00
          B (micro Gauss)  : 1.00E+01
          Vs (km.s-1)      :     10.0
          Dv (cm.s-1)      :   1000.0
          nH_init (cm-3)   : 1.00E+02
          Tn (K)           :     10.0
          o/p H2 init      : 3.00E+00

environmental parameters
          Zeta H2 (s-1)    : 5.00E-17
          F_ISRF           :        1
          RAD              :     0.00
          Av0 (mag)        :     0.10
          F_COUP_RAD       :        0
          F_AV             :        0
          F_invAv          :        0
          Av conv factor   :     0.00
          N_H2_0 (cm-2)    :1.000E+06
          N_CO_0 (cm-2)    :1.000E+06
          vturb (cm s-1)   :3.500E+05

grains parameters
          F_TGR            :        0
          Tgrains (K)      : 1.50E+01
          amin_mrn (cm)    : 1.00E-06
          amax_mrn (cm)    : 3.00E-05
          alph_mrn         : 3.50E+00
          rho_grc (g cm-3) : 2.00E+00
          rho_grm (g cm-3) : 1.00E+00

excitation & cooling
          ieqth            :        1
          Cool_KN          :        0
          NH2_lev          :      150
          NH2_lines_out    :      200
          H_H2_flag        :BOTH
          iforH2           :        1
          ikinH2           :        2
          pumpH2           :        0
          NCO_lev          :       50

integration parameters
          integ_type       :        0
          Nstep_max        :    30000
          timeJ (yr)       : 1.00E+09
          duration_max (yr): 1.00E+09
          XLL/nH (cm)      : 1.00E+12

DVODE parameters
          Eps_V            : 1.00E-07
          T0_V             : 0.00E+00
          H0_V             : 1.00E+05
          Tout_V           : 1.00E+05
          MF_V             :       22
          Itask_V          :        1
          Istate_V         :        1
          Hdone            : 0.00E+00
          Hnext            : 0.00E+00

outputs parameters
          F_W_HDF5_STD     :        1
          F_W_HDF5_CHE     :        1
          F_W_ASCII        :        1
          Npthdf5          :    10000
          Nstep_w          :        5
          speci_out        :FD
          H2_out           :AD
          line_out         :local
```

Figure 3.1: A summary of the input conditions indicated to perform the simulations of the pre-shock region. We did three pre-shock simulations at different densities (100 cm^{-1}, 1000 cm^{-1}, and 10 000 cm^{-1}). The physical conditions included a temperature of 10 K, a cosmic ray ionization rate of 5 $\times$ 10^{-17} s^{-1}, and no external radiation.

3.2 Simulations of shocks

Since we possess all the required inputs, we could perform our 48 shock simulations with different shock velocities, and densities. 24 simulations were about J-type shocks and the other 24 concerned C-type shocks. Two major differences had to be taken into account between J-type shocks and C-type shocks.

- **The number of fluids:** We counted one fluid for J-type shocks and three fluids (The neutral medium, the ionized medium, and electrons) for C-type shocks.

- **The strength of the magnetic field:** C-type shocks are characterized by a strong magnetic field than J-type shocks. Following the parametrization of B. T. Draine, Roberge, and Dalgarno 1983, the magnetic field is described by the equation $B_0 = b_0 \cdot \sqrt{n_H}$ where b_0 is a free parameter fixed at 0.1 for J-type shocks, and at 1.0 for C-type shocks.

3.3 The enhancement factor $f_{enhance}$ and the comparison factor $f_{comparison}$

When we explore the parameter space, we have to choose what we want to analyze. It will be a function of our parameters. In our case, as we want to analyze the impact of shock types on astrochemistry, we followed the idea of James et al. 2020 and defined the enhancement $f_{enhance}[A]$, the factor describing how much a specific species A is magnified in the post-shock region, as follows:

$$f_{enhance}[A] = \frac{\chi_A(R)}{\chi_A(0)} \tag{3.1}$$

Where $\chi_A(R)$ is the fractional abundance of molecule A in the post-shock region. Note that the fractional abundance is simply $n(A)/n_H$, and $\chi_A(0)$ is the fractional abundance of molecule A in the pre-shock region. We can also define a comparison factor to directly compare J-type shocks and C-type shocks with the following equation:

$$f_{comparison}[A] = \frac{\chi_A(J)}{\chi_A(C)} \tag{3.2}$$

Where the label "J" or "C" describes a fractional abundance of the molecule A in the post-shock region of a J-type or a C-type shock. As we deal with abundances computed at many points in the post-shock region, it is relevant to indicate that we talk about the average value. We decided to compare fractional abundances in the post-shock regions for two main reasons. Firstly, the post-shock region has a bigger size (several orders of magnitudes) than the shock front, it contains shock-impacted molecules, and it can be measured by astronomical observations. Secondly, since the work of James et al. 2020 is

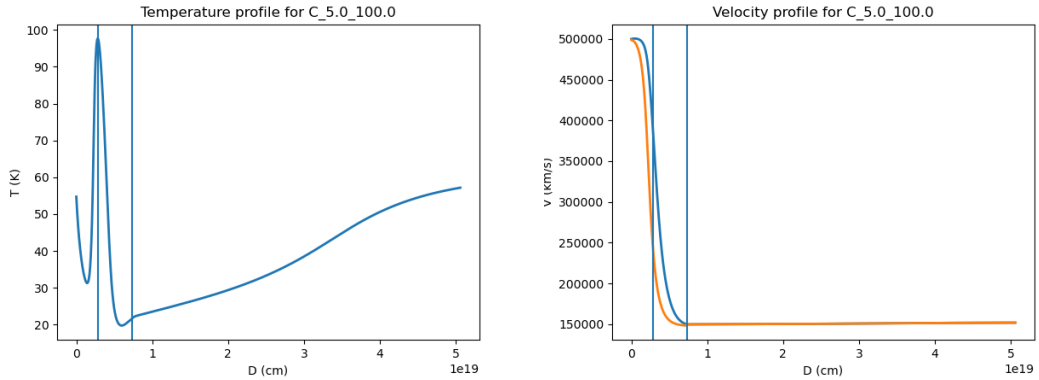

Figure 3.2: Temperature and velocity profiles for the simulation of a C-type shock with a shock velocity of 5 km s^{-1} and a density of 100 cm^{-3}. On the temperature profile, the maximum of temperature marks the beginning of the post-shock region. On the velocity profile, the convergence of the ionized and neutral velocities indicates the end of the post-shock region.

taken as a reference for this work, it is useful for the discussions to compare the same quantities. We will still follow their methods to decide the limits of the post-shock region in the next subsection.

3.3.1 Dissipation length of C-type shocks

Originally described by B. T. Draine 1980, the dissipation length marks the end of the post-shock region. As mentioned earlier, the ionized medium in C-type shocks can stream into the neutral medium. This means that the velocity for ionized species and the velocity for neutral species will differ throughout the shock. The dissipation length is characterized by the length at which the two velocities have equalized again. If this is the end of the post-shock region, we also have to mark its beginning. To do that, we choose the distance at which the neutral temperature reaches its maximum. This should mark the end of the shock front. A visual representation of this zone has been plotted by our data treatment code in Figure [3.2].

3.3.2 Dissipation length of J-type shocks

Even if we can still consider the maximum temperature as the beginning of the post-shock region, it is impossible to evaluate the convergence site of the two medium velocities as the end of the region. In J-type shocks, we consider a strong coupling between ions and neutral species, and we thus only have one fluid, and one velocity to simulate. At this place, we consider that we have reached the end of the post-shock region when the temperature reaches its equilibrium. In our data treatment code, we consider a temperature equilibrium when we do not have variations more than 50K. The post-shock region can be visualized on the temperature profile of J-type shocks in Figure [3.3].

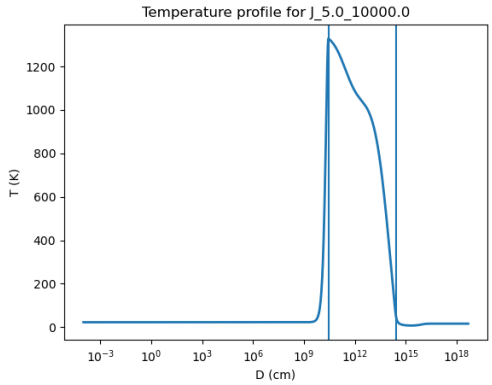

Figure 3.3: Temperature profile for the simulation of a J-type shock with a shock velocity of 5km/s and a density of 10 000/cm^3. The maximum temperature marks the beginning of the post-shock region. For its end, we consider the distance at which we do not have variations more than 50K.

3.4 The results

We thus designed graphics representing the enhancement factor in J-type shocks and in C-type shocks, and the comparison factor. We did it for each species in our chemical network to discover which molecules could be interesting. As an example, the three graphs concerning the ion SiH_4^+ are shown in Figure [3.4]. All the important plots for each species can be found in Appendix 7. In terms of pertinence, the knowledge of the enhancement factor is what can be the most useful to compare our shock models with observational data. Our grid of shock models and their enhancement factors covering an ensemble of potential shocked systems will thus be essential to link raw results coming from the Paris-Durham Shock code and real shocked astrophysical environments (as will be the case for L1157 B2 in the next chapter). As a starting point for future discussions, the coverage of the parameters space in the annexes already shows that we should expect some dependencies on the shock type and the parameters of the shock such as the velocity. This can be seen from the fact that the enhancement and comparison factors are not only a series of 1.0 proving that some differences occurred. More than that and as it will used in the following sections, it is possible to imagine and define new functions that are directly related to these enhancement factors and that will be useful to feed the discussion (such as the geometric standard deviation discussed later in the text).

We should emphasize that our results are not limited to these graphics and some other information coming from the simulations will be shown in due time. Indeed, and it will be the subject of Chapter 5, a good understanding of the different pathways followed by the chemical species can be extracted from our raw resources using the tools available with the Paris-Durham Shock code. This will be of first use to analyze the impact that shocks can have on the chemistry of the perturbed environment.

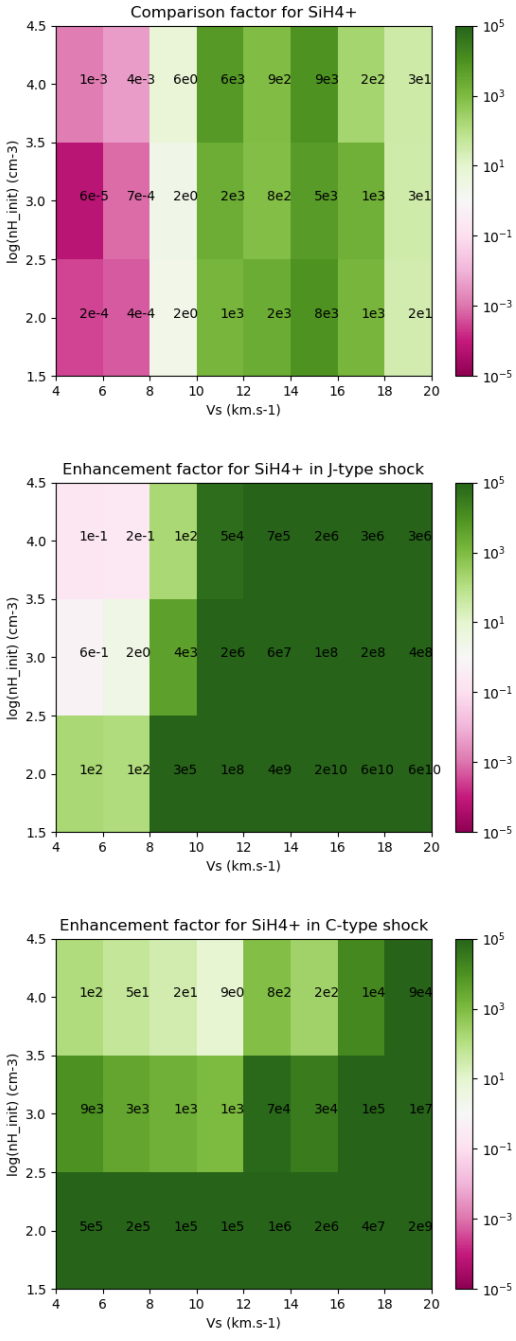

Figure 3.4: Exploration of the parameter space concerning the comparison factor, the enhancement factor in J-type shocks, and the enhancement factor in C-type shocks of SiH_4^+ as a function of the velocity shock and the density.

Chapter 4

Discussion - The molecular tracers

The first question we will address is that of the identification of molecular tracers of interstellar shocks. More than just making a list of all the molecules created with a fractional abundance above an arbitrary threshold, we will also separate molecules depending on their ability to characterize the type of shock (more specifically, we want to differentiate tracers of J-type and C-type shocks using their chemical signatures). Nevertheless, basing all our discussions on our results alone is not enough. Indeed, our results come from computational methods – shock models with personal inputs – and their validity is not proven. Knowing these considerations, this discussion begins with a comparison of our results and previous research. The identification of molecular tracers of interstellar shock types seems to be a young (but interesting) question and papers studying this subject (with a focus on the chemical diagnostic) are relatively rare. Due to that, our method is mainly based on the work of James et al. 2020. The first part of this discussion will thus be a comparison between what they get, the similarities, and the differences with our results – using the main molecules that were already identified as tracers. We will take advantage of this comparison to describe recent papers in the domain. Once this stage has been completed, we will use our simulations to characterize shocks in real cases such as L1157 B2 (the environment already studied in James et al. 2020). This first application will enable us to define our methods of characterization and to identify our first molecular tracers and their specificities.

What is the objective? The comparison with other studies and the application of a real case "L1157 B2" to seek after molecular tracers is here to answer our first question **"How can we make use of astrochemistry to characterize interstellar shocks?"**. This is why we will define and summarize during this discussion a complete method we made to analyze and characterize shocks with our astrochemical simulations.

4.1 The comparison with previous results

In 2020, James et al. 2020 performed a similar work by using the code UCLCHEM, a time-dependent chemical code with astrophysical applications to identify molecular tracers of

shock types. With the help of this code, they performed an exploration of the parameter space. For the shock velocities, they considered values from 5 km/s to 15 km/s with a step foot of 1 km/s. For the densities, they selected a range from 10^3 cm^{-3} to 10^6 cm^{-3}. With their results, they deeply discussed the physico-chemical differences between J-type shocks and C-type shocks by an analysis of important molecules that are CH_3OH, H_2O, SO, SO_2, and HCN. Armed with these discussions, they could compare their work with the observations done on the system L1157 B2. Three main conclusions were brought by their work and will serve as comparison points for this master's thesis:

- The main differences between J-type shocks and C-type shocks occur at low shock velocities and low densities in molecules such as HCN and H_2O. These differences come from the dependence of sputtering and evaporation on the physical conditions.

- CH_3OH enables us to determine the pre-shock density. Nevertheless, no major differences have been found between C-type shocks and J-type shocks. With an assumption of low temperature, they found that their chemical network suffers from a lack of destructive reactions for this molecule.

- L1157-B2 region presents both behavior from C-type shocks and J-type shocks. This could be explained by a multi-component shock. The authors also emphasize the fact that the astrochemistry of shocks is more dependent on the initial conditions than on the shock type.

In this part of the discussion, we will describe their code as it is necessary to discuss our differences. We will also make the same analysis of their important molecules. Since these molecules have been intensively discussed by the authors, this will enable us to understand the variations seen in our two models.

4.1.1 The differences between UCLCHEM and the Paris-Durham Shock code

As we have seen, the first part of this master's thesis is based on the paper of James et al. 2020 as it makes easier the comparisons. Nevertheless, the two codes are not the same and present several major differences. These have to be identified as they influence the results we obtain. The first main difference we can emphasize is that UCLCHEM (Holdship et al. 2017) parameterizes shocks contrary to the Paris-Durham Shock code. Their parameterized model is partially based on an older version of our code "mhd_vode" as described in Flower and Pineau des Forêts 2015 and on analytical results. The parameterization means that the physical conditions have been induced as space-dependent initial conditions that will not change in time. The direct remark is that the feedback of the chemical composition is neglected. With this parameterization, the UCLCHEM code works in two phases. The first phase consists of an isothermal collapse from a user-supplied temperature, density, and chemical composition to a final density (also supplied by the user). During this collapse, the code computes the chemical composition through the density changes. The second phase follows the chemical evolution through physical conditions indicated by the user - The physical conditions modify the values of the chemical reaction rates.

The second main difference stands in the chemical network. The chemical network furnished with the Paris-Durham Shock code only contains 141 different species while the UCLCHEM code has 215 molecules. We can already suppose that the chemical diversity will be greater in their code – or said otherwise – the chemical complexity will be more limited in our code. Indeed, all compounds that are not present in the Paris-Durham chemical network just do not exist and can not enrich the molecular diversity of my simulations. Nevertheless, this fact did not affect our choice concerning which code we wanted to use in this master's thesis. Indeed, complex molecules are rarer and will thus have a significantly reduced impact on the shock physics. More than that, molecular tracers of shock types should be produced in a sufficiently significant way to be easily observed. More than the species included, we also have to take into account the number of reactions connecting our molecules. In the UCLCHEM code, they possess 2456 reactions while our code works with 3270 different reactions as described in (Sect. 2). This has to be emphasized. When we increase the number of species, we should increase the number of reactions at the same time. Even if our code possesses fewer different species, we have a significantly more complete chemical network.

The third difference is in the initial conditions we used in our simulations. Some observations of L1157-B2 were already done and the observed chemical composition was used as an initial input in the UCLCHEM model of James et al. 2020. In our case, we took solar abundances. Knowing that L1157 is estimated to be at only 250 parsecs from us (Looney, Tobin, and Kwon 2007a), this assumption should be tolerable. Thus, we do not expect strong impacts due to these differences.

The last main difference between our two codes is the physical conditions. Small changes in temperature and density can be seen between our results and their parametrizations, even if they are not greater than a factor 2. Nevertheless, the Paris Durham Shock code possesses a too-strong cooling. Due to that, the temperature in our results decreases to $10K$ before coming back to an initial temperature of $50K$ which is physically unrealistic. Benefitting from a parametrization, they do not encounter this problem. An attentive reader could have noticed that our initial temperature is $50K$ and not $10K$. This is due to an increase in the temperature during the pre-shock simulation. Nevertheless, $50K$ is still acceptable (particularly for not-too-dense clouds) and the variation from $10K$ to $50K$ is insignificant compared to the shock conditions. In the physical conditions, they took interstellar values for the radiation field (without defining it) while it was not taken into account in our simulations. This will be discussed.

We take advantage of this section to indicate that these major differences were the main reasons for us to choose the Paris-Durham Shock code instead of the UCLCHEM code. Even if this has to be discussed, our first physical insight motivates us to focus more precisely on the physical and chemical processes and their interconnections. From the beginning of this master's thesis, we have been deeply convinced that these interconnections could lead to major impacts on global astrochemistry in shocks. It is also sure that these main differences are not the only ones. Nevertheless, it would be too long to cite them all (and not very relevant to do it now). Other changes between the two codes will be presented and discussed during the discussion when we will judge it necessary.

4.1.2 Differences in the comparison factors

Now that differences between the two codes have been clarified, we can compare their results as displayed in Figures 4.1, 4.2, 4.3, 4.4, and 4.5 and our results obtained in the context of this master's thesis shown in Figures 7.3, 7.4, 7.5, 7.6, and 7.7. The main point where we have to be careful is in the different ranges we took for the densities and the shock velocities. Also, color markers are not the same and could induce misunderstandings for those who would not be attentive. That being said, we can begin the direct comparisons between previous results and ours. In the following description, we only take care of the values taken by the comparison factor and not the underlying chemistry able to explain it. This will be the subject of the next section (S5).

- **For the H_2O molecule (Figures 7.3 and 4.1),** James et al. 2020 did not find any differences between fractional abundance in J-type shocks and C-type shocks except for low-density shocks (10^3 and 10^4 cm^{-3}) with a small shock velocity of 5 km s^{-1} where the comparison factor is about 10^3. The transition between these low-velocity shocks and other shocks is found to be very abrupt, showing a clear discontinuity explained in their paper by the fact that, if evaporation of species from grains occurs in all J-type shocks due to the high temperature, the release of adsorbed molecules in C-type shocks can happen only if sputtering is active. This is the case only for a specific set of physical conditions – typically the one where the comparison factor tends to be 1. In their paper, post-evaporation processes leading to the formation of H_2O molecules are also identified but also the destruction of these molecules is favored by the high temperature reached in J-type shocks. Nevertheless, the specific reactions leading to these results are not deeply described in the paper. In our results, the comparison factor tends to favor J-type shocks for low-velocity shocks with a factor of 10, and C-type shocks with a factor of 3×10^{-1} when we gradually increase the shock velocity. The dependence of the system to changes in the initial conditions is much more continuous and less easily predictable. For example, an increase in the density of the medium leads to an increase in the comparison factor for a shock with a shock velocity of 5 km s^{-1} while it is the opposite for greater shock velocities as visible for a shock velocity of 19 km s^{-1}. Our results are thus quite different from previous ones as seen in the literature. Nevertheless, if we do not take into account the discontinuity for low-velocity shocks, the maximum difference is of the order of a factor of 10.

- **For the SO molecule (Figures 7.4 and 4.2)**, results are more diversified than for the water molecule. Following James et al. 2020, differences in the abundance of the SO molecule are visible only if the density of the medium is below 10^4. In this regime, low-velocity shocks are in favor of J-type shocks for the same reasons that for H_2O: evaporation from the grain phase tends to enrich the gas phase while sputtering in C-type shocks is not effective for these conditions. When we increase the shock velocity, the high temperature reached in J-type shocks enables destructive pathways to occur and SO is destructed. These high temperatures are never reached in C-type shocks, but sputtering becomes more efficient, releasing adsorbed species into the gas phase. The two reasons put together, it is clear that, at higher shock velocities, C-type shocks will have a greater enhancement factor concerning the SO

molecule. If we only increase the density of the medium, they estimate that the destruction mechanisms are density-limited – only controlled by the chemistry on dust grains – and thus differences between J-type shocks and C-type shocks tend to vanish. In our results, we do not observe the peak for simulations with a low shock velocity and a small density. (This is obvious given that SO and SO_2 cannot adsorb on grains in the Paris-Durham Shock code.) Nevertheless, values for greater shock velocities are quite similar to the ones coming from the paper (about 10^{-2} and 10^{-1}). This proves that a similar gas-phase chemistry should take place in the two sets of simulations. We can thus already expect some mechanisms to be incorporated into the two codes and that they are not completely opposite.

- **For the SO_2 molecule (Figures 7.5 and 4.3)**, the results coming from the paper are very similar to the results concerning the SO molecule, and this is the case for the same reasons as before. This was expected due to the high proximity between the SO and the SO_2 molecules. However, a curiosity is pointed out. While the comparison factor is limited to ~ 10 for shocks with a velocity of 5 km s^{-1} for the SO molecule, it reaches ~ 100 for the SO_2 molecule. In the paper, this curiosity does not find any explanations while the similarities in the behavior are justified by the creation of SO_2 through SO-dependent reactions such as SO + O $\rightarrow$ SO_2. Nevertheless, this fact will be discussed in Sect. 5, knowing that direct additions without fragmentation are prohibited in the gas phase. Perhaps the production of SO_2 in their simulations was performed on grains before evaporating, but perhaps other processes are activated in the gas phase. This will be discussed. Concerning our data, our results are again quite similar if we do not take into account the discontinuity for low-density shocks with a low shock velocity. The general trend is a decrease in the comparison factor (in favor of C-type shocks) when we increase the shock velocity – the comparison factor being able to reach 8×10^{-4} for the highest velocities in our simulations.

- **For the HCN molecule (Figures 7.6 and 4.4)**, the results coming from the paper are still highly dependent on the evaporation and sputtering. With the instantaneous evaporation of all species in J-type shocks and the lack of sputtering at low shock velocities, (We have to note that the behavior is here extended to 9 km s^{-1}.) the peaks of the comparison factors are again at low shock velocities and low densities (~ 50). The slow tendency to favor C-type shocks when we increase the shock velocity is again related to the high increase in the temperature that we find in J-type shocks, but not in C-type shocks. This high temperature would be responsible for the activation of destructive pathways that will decrease the fractional abundance of HCN. Nevertheless, without considering the processes of evaporation and sputtering, HCN behaves quite similarly in J-type shocks and C-type shocks, and the comparison factor is never far from ~ 1. In our results, peaks are not identified – let's remark again that it is connected to the treatment of grains – and HCN has a similar behavior in J-type shocks and C-type shocks.

- **For the CH_3OH molecule (Figures 7.7 and 4.5)**, high differences in the two codes appear. With UCLCHEM, the fractional abundance in J-type shocks and C-

type shocks is the same given that the instantaneous evaporation from dust grains in J-type shocks acts in a very similar way to sputtering in C-type shocks when this sputtering is possible. With this in mind, we only have changes for low-velocity shocks with peaks above 10^3 that will favor J-type shocks. Nevertheless, they did not detect any other changes while the behavior of CH_3OH is much more complicated in our simulations. Our results show a continuous variation of the comparison factor that will quickly vary with the shock velocity (and not with density). This will almost always be in favor of C-type shocks with some exceptions at 11 km s^{-1} where the comparison factor is contained between 1 and 10. Otherwise, it decreases when the shock velocity increases – going from 5×10^{-2} to 3×10^{-5} in our set of simulations. This result emphasizes the presence of complex chemistry occurring in shocks that will have to be established in Sect. 5. In every case, the results in our simulations and the simulations of James et al. 2020 are completely uncorrelated for CH_3OH.

Well, the purpose of this subsection was to compare our results and previous results as described in James et al. 2020. The conclusion is that our results are completely different. Nevertheless, the main paper that serves as a basis for this master's thesis can also be questioned as it was not able to characterize the type of the L1157 B2 shocked system. This can be due to a multi-component shocked region, but it can also be due to errors or not appropriate hypotheses in their work. We thus now have to discuss the two sets of simulations to evaluate if one of them is closer to the truth, and – if yes – which one? From our previous considerations, two main differences have to be emphasized. Firstly, CH_3OH does not act in the same way in our simulations and their simulations. Nevertheless, the chemistry occurring in their computations is not deeply described and it is thus impossible to well describe the reasons behind our differences. The second point is the importance of evaporation and sputtering in their shocks which is at the basis of the different peaks in favor of J-type shocks they obtained. Even if it is still possible to have differences coming from different aspects of our simulations (in the chemical networks for example), it is obvious that we have to discuss the treatment of grains in the two codes to decide which work describes the most accurately the reality. The Paris-Durham Shock code already takes well grain sputtering into account in its simulations (The ISM Team of Paris Observatory 2020), we will thus study the other process – evaporation – which is related to the grain temperature.

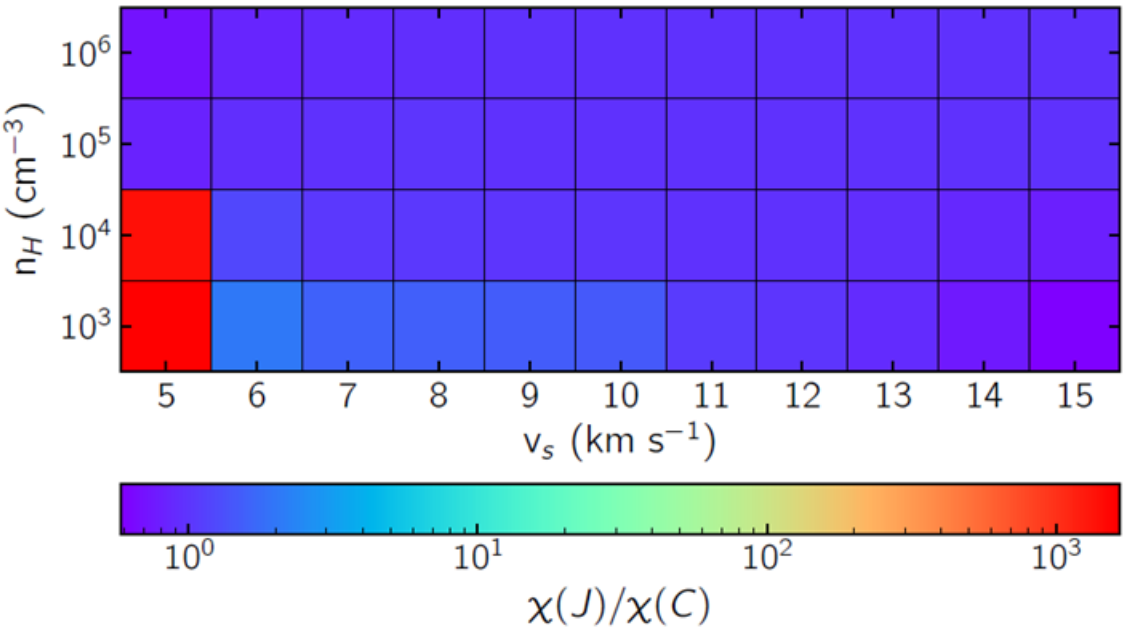

Figure 4.1: Comparison factors in James et al. 2020 for the H_2O molecule. Be careful to note the difference in the colors used and in the range of densities and velocities we studied.

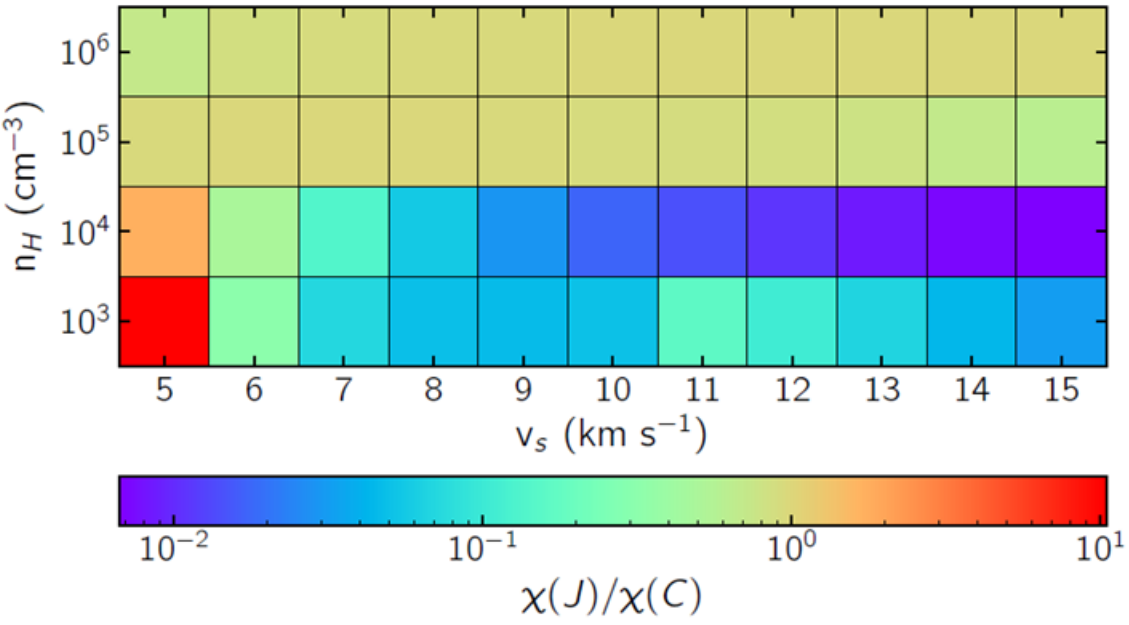

Figure 4.2: Comparison factors in James et al. 2020 for the SO molecule. Be careful to note the difference in the colors used and in the range of densities and velocities we studied.

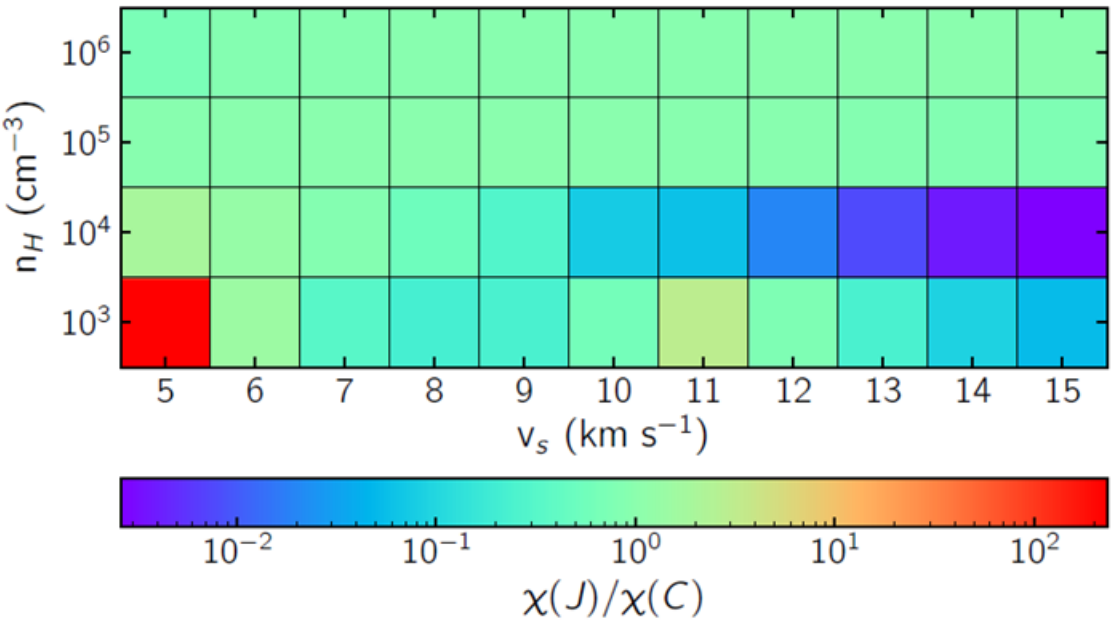

Figure 4.3: Comparison factors in James et al. 2020 for the SO_2 molecule. Be careful to note the difference in the colors used and in the range of densities and velocities we studied.

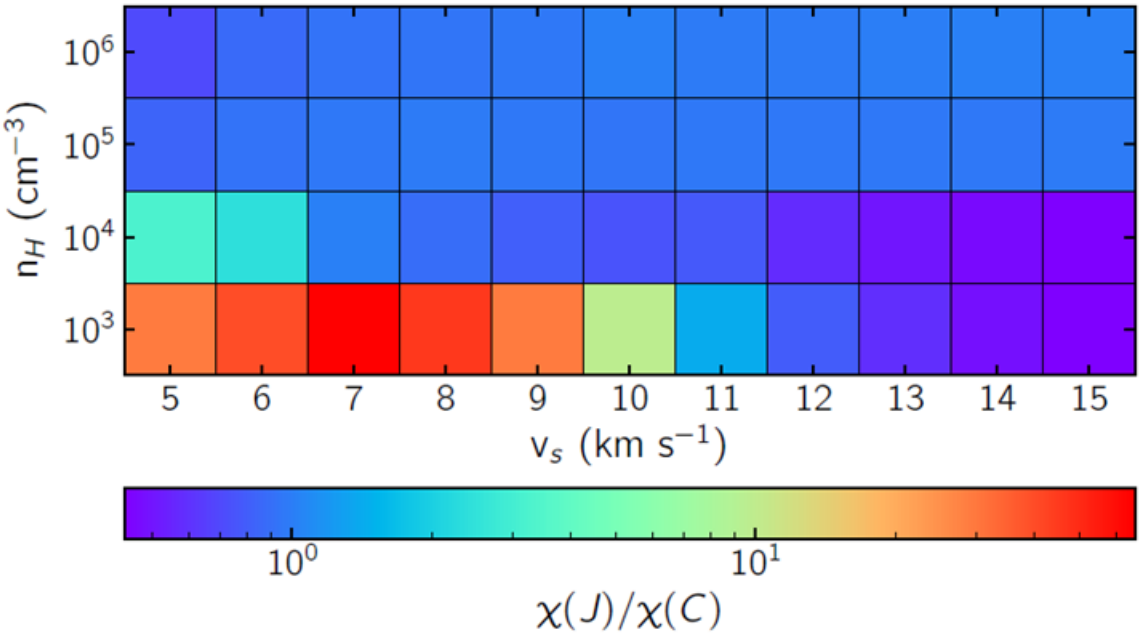

Figure 4.4: Comparison factors in James et al. 2020 for the HCN molecule. Be careful to note the difference in the colors used and in the range of densities and velocities we studied.

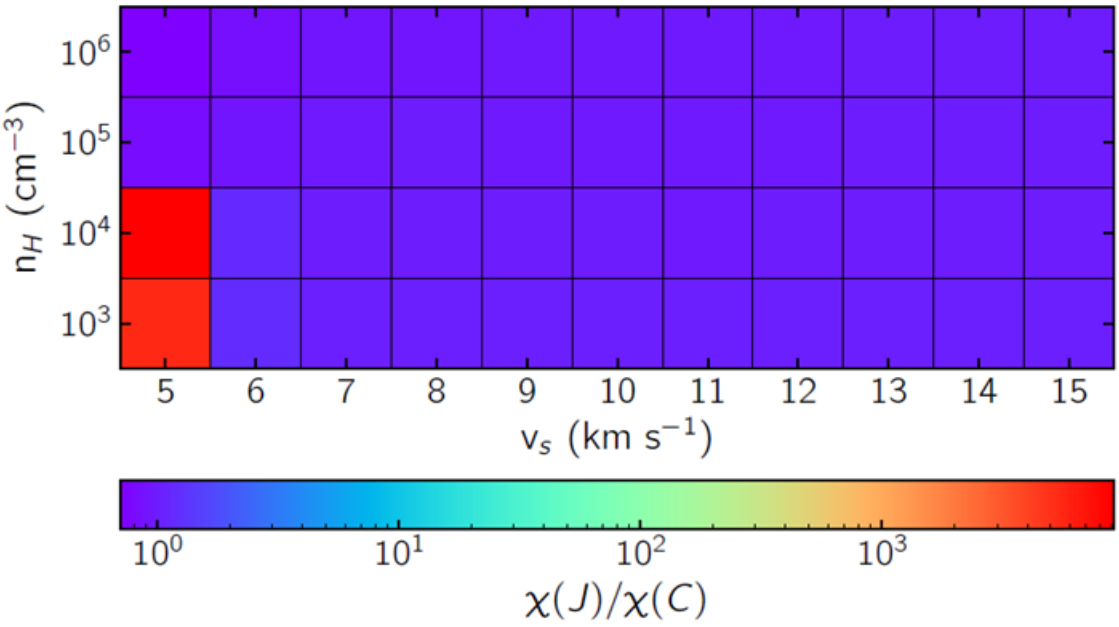

Figure 4.5: Comparison factors in James et al. 2020 for the CH_3OH molecule. Be careful to note the difference in the colors used and in the range of densities and velocities we studied.

4.1.3 Dust grains in the Paris-Durham Shock code

The version of the UCLCHEM code used in James et al. 2020 computes the sputtering of grains that will release adsorbed chemical species into the gas phase (which has been seen to be of major importance in C-type shocks in their simulations), and the evaporation (thermal or not) of these species (important in J-type shocks). As it was explained to be the main reason for the desorption of molecules from the grain phase to the gas phase in J-type shocks, we will focus on the thermal evaporation that happens when the temperature of the grain is high enough to break down the bonds between it and the molecule, leading to evaporation. We do not exactly know the binding energies that were used to link grains and molecules in their simulations but we do not expect them to significantly change from the binding energies used in the Paris-Durham Shock code. The main difference that we find is that they never talk about the specific temperature of grains even though they computed the temperature of the gas phase. We thus think that they took the same temperature along their simulations – considering that the grains are heated at the same time as the gas during the shock. This is a point of view that we were sharing concerning the behavior of grains in interstellar shocks, but this is still only a hypothesis. Is it justified?

To answer this question, we have created a small Python code to display the evolution through the shock of the temperature of the grains. This evolution can be seen in Figure 4.6. We chose our simulations of J-type shocks with the highest density and the high shock velocity as this kind of shock is known to reach the highest temperatures (otherwise, results were sometimes not even visible!). In our simulations, we activated

the parameter F-TGR (Sect. 2) that asks to the code to compute the temperature of the grains at each point in the shock. As you can see, a huge increase in the temperature of the surrounding gas does not lead to a comparable increase in the temperature of the grains. They stay relatively cold during all the shock. We have to recall that one of the assumptions of the Paris-Durham Shock code was the steady state approximation (Sect. 2), and all the time derivatives are thus zero. Said more comprehensively, even if we wait for a long time (assuming that the shock still exists after that), the grains will stay decoupled from the gas in terms of temperature. This result is quite impressive but should not be accepted so easily. After some emails with the ISM Team of Paris Observatory, we learned that the grain temperature is computed as the equilibrium between heating by the external UV field and secondary photons, cooling by dust emission, and heating or cooling through gas-grain interaction. This can be put in parallel with a first model of grains cooling/heating coming from Van Grootel, V. 2023. In this first model, the grain temperature is also led by heating by photons (Eq. 4.1), cooling by radiations (or emissions) (Eq. 4.2), and changes by gas-grain interactions (Eq. 4.3) as you can see in the following equations:

$$\left(\frac{dE}{dt}\right)_{abs} = \langle Q_{abs}\rangle \pi a^2 uc \tag{4.1}$$

were $\langle Q_{abs}\rangle$ is the spectrum-averaged absorption cross section (on all frequencies), a is the radius of the grain (assumed here to be spherical), u is the energy density of the incident photons, and c is the speed of light.

$$\left(\frac{dE}{dt}\right)_{emiss} = 4\pi a^2 \langle Q_{abs}\rangle \sigma T_d^4 \tag{4.2}$$

where $\langle Q_{abs}\rangle$ is the Planck-averaged emission efficiency, σ is the Stefan-Boltzmann constant, and T_d is the temperature of the grain.

$$\left(\frac{dE}{dt}\right)_{gas} = \sum_i n_i \left(\frac{8kT_{gas}}{\pi m_i}\right)^{\frac{1}{2}} \pi a^2 \times \alpha_i \times 2k(T_{gas} - T_{dust}) \tag{4.3}$$

where n_i is the density in species i, T_{gas} is the temperature of the gas phase, m_i is the mass of species i, $(\frac{8kT_{gas}}{\pi m_i})^{\frac{1}{2}}$ is the mean speed of species i, and α_i is the accommodation coefficient ranging from 0 to 1 that will evaluate the inelasticity of the collision (with 0 for purely elastic collisions).

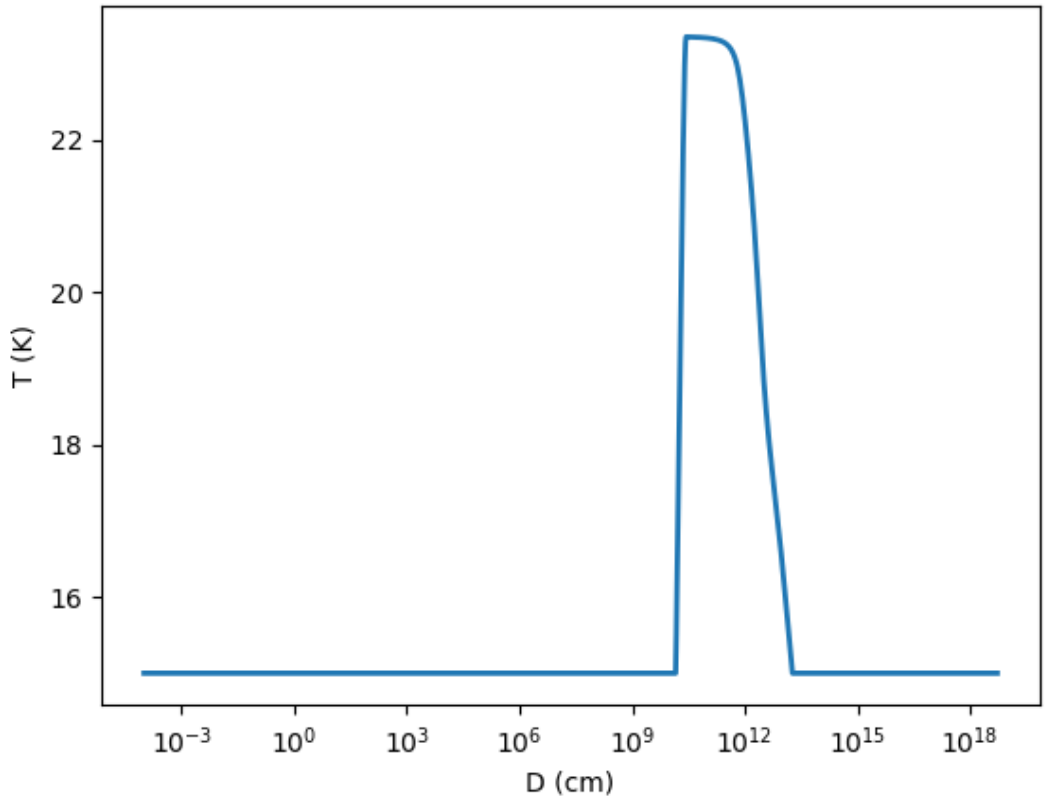

Figure 4.6: Evolution of the temperature of grains through a J-type shock with a density of 10^4 H cm^{-3}, a shock velocity of 19 km s^{-1}, and no external radiation. As specified, the shock is at its steady state.

An equilibrium for the temperature is reached when the sum of all the cooling rates is equal to the sum of all the heating rates. Nevertheless, we can already point out that one of the main heating processes of interstellar gas was made by the external radiation field which is not taken into account in our simulations. To evaluate the impact of this assumption, we performed a longer simulation taking a basic radiation field of 1.7 Habing units as indicated in Parravano, Hollenbach, and McKee 2000 to be the median value, and where we still computed the temperature of grains at each position in the shocks. These simulations are more costly than the previous ones, and this was the main reason behind the lack of an external radiation field in our computations. The evolution of the grain temperature through the shock can be seen in Figure 4.7. Small differences (that are nevertheless the proof that changes occur in the code) are visible, but only unsightly impact the grain temperature in the upstream region and just after the shock front. But the variation is of the order of 5K. That is not enough to deeply impact the whole chemical system.

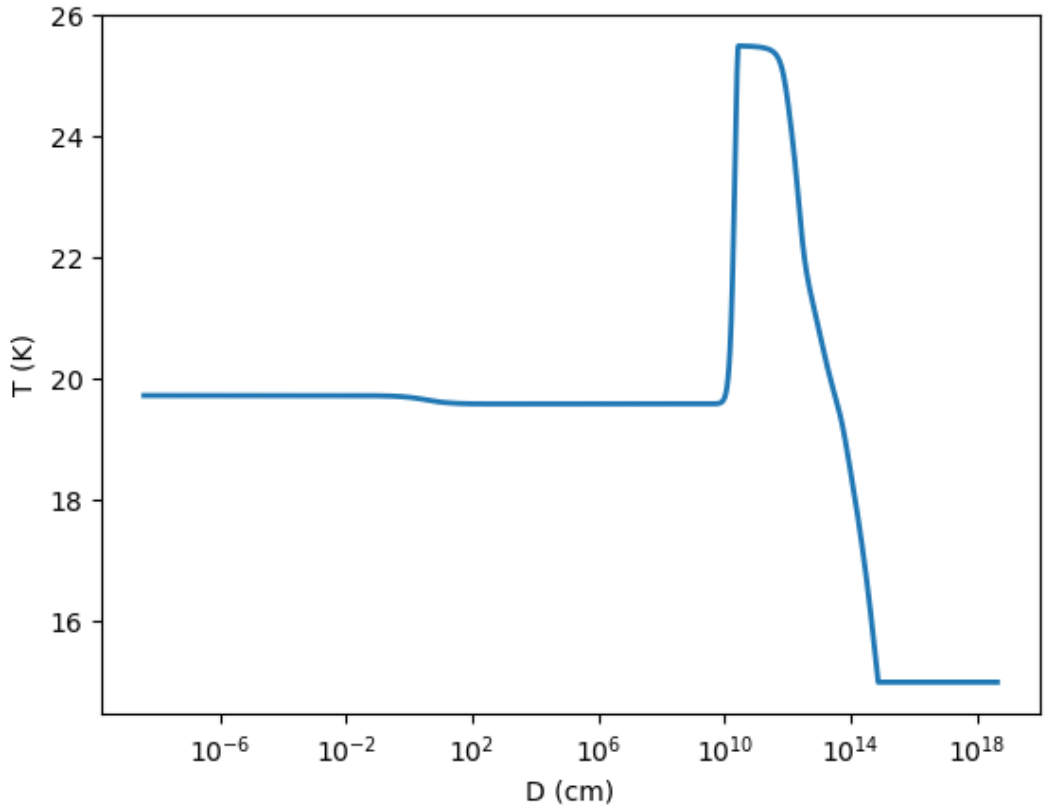

Figure 4.7: Evolution of the temperature of grains through a J-type shock with a density of 10^4 H cm^{-3}, a shock velocity of 19 km s^{-1}, an external radiation of 1.7 Habing Units, and a visual extinction A_0 of 0.1. As specified, the shock is at its steady state.

One more time, it can be highly relevant to find another argument in favor of the decoupling between the gas and the grain phases in terms of temperature. This detail is the one that defines all the results achieved by James et al. 2020 and should not be taken too lightly. To do so, we can use equations (Eq. 4.3 and Eq. 4.2) and evaluate the variation of the collisional heating term (which is the only one that should significantly change through the shock) compared to the radiative cooling term. If the variation is negligible compared to the cooling term, then we can easily assume that the grain temperature variations are negligible in the shocks from our range of initial conditions.

Concerning the collisional heating described in Eq. 4.3, we will consider a pure gas made of atomic hydrogen with a density of 10^4 particles per cm^3. Following the parametrization for the maximum temperature in J-type shocks from David A. Williams and Serena Viti 2014 for a shock velocity of 19 km s^{-1}, we take a temperature of 18050K for the gas phase. The temperature of the grain phase will be taken at 50 K. The mass of a hydrogen atom is 1.67×10^{-27} kg. For the grain radius a, we choose the maximum value that is 0.3 μm in our simulations and we take an accommodation coefficient α_i of 1 to describe a purely inelastic collision. These values have been chosen to give the maximum value of

the heating rate by collisions with the surrounding gas. From this, we find that:

$$\left(\frac{dE}{dt}\right)_{gas} = 3.228 \times 10^{-17} J/s \tag{4.4}$$

It is now time to evaluate the radiative cooling (Eq. 4.2) of the grain. We continue with a radius of 3 μm for the grain. We take a temperature of 50K for the grains, and we choose the Planck-average emission efficiency to be at the smallest value given in Van Grootel, V. 2023 which is the one for the graphite: $8 \times 10^{-7}(\frac{a}{0.1\mu m})(T/K)^2 = 0.006$. With these values, we find that:

$$\left(\frac{dE}{dt}\right)_{emiss} = 2.405 \times 10^{-15} J/s \tag{4.5}$$

It is thus clear that in our conditions the cooling processes are much more efficient than collisional heating. Due to that, grains stay at relatively low temperatures even inside our hot J-type shock and evaporation will not be that impacting. Bounding energies are typically of the order of one thousand degrees in our chemical network. Some papers already analyzed the evolution of the grain temperature for astrophysical environments with a greater density (of the order of 10^8 cm^{-3} for Miura et al. 2017). In that case, and knowing that collisional heating (Eq. 4.3) is directly proportional to the density, the coupling between grains and gas molecules is much more efficient. The collisional heating, results of this coupling, will enable thermal processes on grains in denser environments. Nevertheless, this does not seem to be the case in our studies – due to the low density of diffuse and not dense molecular clouds (Let's remember that our range of densities is typically made to describe these regions). We are not sure that the thermal coupling between gas and grains is sufficiently taken into account in astrochemical models. We thus emphasize its impact in this master's thesis.

We thus know that grains do not heat significantly in low-velocity shocks when the density is not high enough. Consequently, grains do not reach temperatures comparable to the binding energies of the molecules we study. Nevertheless, it does not necessarily mean that evaporation processes should be left behind in simulations of molecular clouds. In fact, Miura et al. 2017 have studied the evaporation of species depending on the strength of the binding energy (from 1000K to 5000K). But, contrary to the Paris-Durham Shock code, they do not describe the binding energy with a single mean value E_{d0}, but as a Gaussian which is also characterized by standard deviation ΔE_d. They found that the ratio $\frac{\Delta E_d}{E_{d0}}$ will deeply impact the fraction of atoms or molecules that will desorb from the grain surface. An increase in this ratio leads to an increase of several orders of magnitude in the desorption fraction. Concerning our reactions with a size of grains that is of the order of 0.1 μm, they indicate that nearly all the molecules have been desorbed if their binding energies are between 1000K and 2000K (with a desorption fraction which is about 0.5 to 0.99999). This will be the case in our simulations for CH_4, O_2, and CO. However, molecules with greater binding energies will keep a relatively low desorption

fraction. For example, the desorption fraction of a molecule with a binding energy of 5000K will be limited to 2.57×10^{-3} in their studies with this size of grains. This is typically the expected behavior of water which has a binding energy of 4800K. From these more advanced studies on the behavior of grains, we deduce that the reality is not in a simulation with zero evaporation due to the limited grain temperature, nor a simulation with complete evaporation due to a perfect coupling between grains and gas, but is between these two extrema.

Unfortunately, the main paper that served as a basis for this master's thesis (James et al. 2020) was mainly impacted by a too-high temperature of grains. Due to that, thermal desorption took the lead in their chemical network, changing all the fractional abundances and giving unrealistic results for molecules with high binding energies. On the opposite, simulations in the Paris-Durham Shock code drastically underestimated evaporation processes. (All the kinetic constants for these reactions contained a negative exponential with the binding energy that will strongly attenuate the desorption.) With the Paris-Durham Shock code, it is currently too difficult to take good grain processes into account. (Branching ratio techniques exist in other methods and will be briefly discussed in the conclusion (Chap. 6)). The main consequence is that we will underestimate the number of molecules that will be released in the gas phase and thus impact the chemical network – this is more true for molecules with a small binding energy. Knowing these differences, we do not have any reasons anymore to limit ourselves to the molecular tracers quoted in James et al. 2020 and will try to identify which one we can use from our simulations. Nevertheless, we have to be aware that all our enhancement (and thus comparison) factors have potentially been deeply impacted. The importance of evaporation processes will be evaluated in the next discussion (Chap. 5). This will be particularly relevant for high-binding-energies species from which the results can eventually be more trusted.

4.2 L1157-B2

The shocked region that will serve as a basis to evaluate the possibilities given by astrochemistry to identify and characterize shocks is L1157 B2. L1157 is a well-known astrophysical environment containing a class-0 protostar with two main outflows B and R as visible in Figure 4.8. These outflows have led to shocked regions known as clumps which are mainly referred to as B1 and B2. B1 and B2 are shocked regions characterized by different temperatures (80-100K (Tafalla and Bachiller 1995) and 20-60K) and different ages (1000 years and 4000 years) (James et al. 2020). That is coherent with the relative position of these clumps compared to the protostar. If both have been studied through the past few years, the B2 clump was less investigated. We already know from previous studies that B1 should be a C-type shock, with a density of 10^4 cm^{-3}, and a shock velocity of 40 km s^{-1} (S. Viti et al. 2011). More than that, L1157 is recognized as one of the best astrochemical laboratories in space given the high diversity of molecules found in its clumps. More particularly, important complex molecules have been identified in L1157 B1 during the observations such as $HCOOCH_3$, CH_3CN, HCOOH, C_2H_5OH (Arce et al. 2008). Fewer molecules have been identified in L1157 B2, but the different physical properties of the shock may have impacted the chemical composition of the medium. From comparisons between astrochemical models of which one detailing NH_3 and H_2O profiles

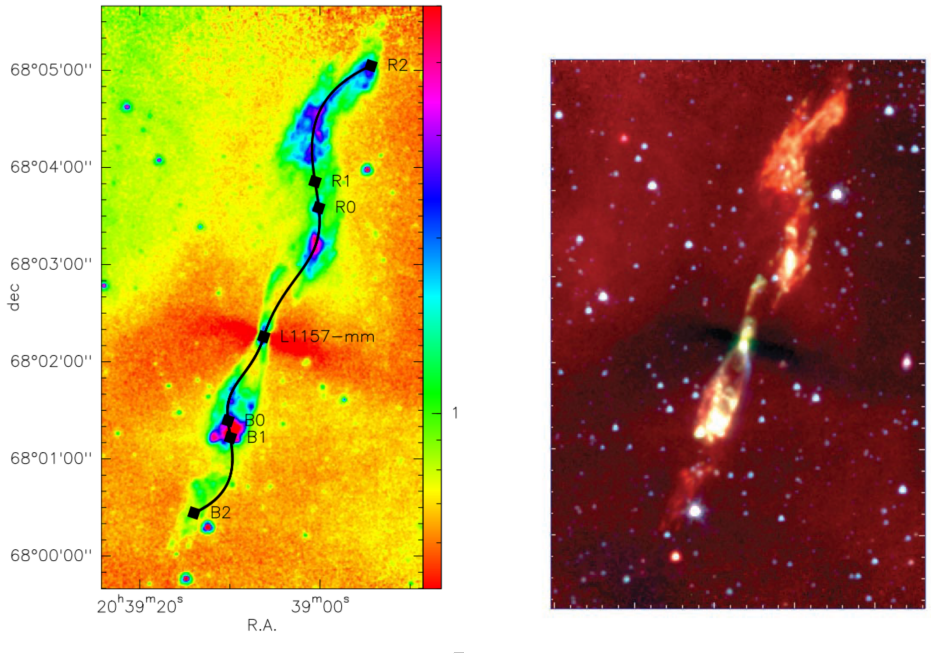

Figure 4.8: On the left panel, color IRAC image in blue, green, and red of L1157 from Looney, Tobin, and Kwon 2007b. On the right panel, 8 μm observations of L1157 from Podio et al. 2016.

and observed lines (Gómez-Ruiz et al. 2016), we mainly think that L1157 B2 may be a shocked region with a smaller density (of the order of 10^3 cm^{-3}) and a shock velocity of 10 km s^{-1}. Nevertheless, these previous studies do not show a satisfactory concordance between predictions and observations, and a great uncertainty remains in the B2 region (Vasta et al. 2012). The type of shock is not already determined and C-type behavior as well as J-type behavior can potentially be extracted from comparisons with our new simulations. A new characterization of L1157 B2 will be the purpose of the following section.

4.2.1 A first attempt to identify the best model

As previously mentioned, the lack of evaporation from dust grains has impacted our reactions at different levels. And some molecules are more affected than others. In this context, it is impossible to base our argumentation on only one or two molecular tracers as their computed abundance can be completely unrealistic. As a first try and to avoid our discussion being compromised by a potentially bad molecule, we firstly decided to compare observations from L1157 B2 and our results for a maximum of chemical species. A comparison between observational and computational data with a maximum of molecular tracers should be more reliable as we decrease the potential impact of molecules that would have been badly simulated. Nevertheless, suppose we incorporate a high number of molecules that do not vary with the shock properties. In that case, we would reduce the contrast between the results obtained for various shock models. It will be more difficult to choose one of them as being the best one to describe reality. This has to be kept in mind, but let's begin with a maximum of molecular tracers. Firstly, we need to list the

enhancement factors that were observed for a maximum of species. These data can be found in Table 4.1.

Molecule	$\chi(X)_{unshocked}$	$\chi(X)_{B2}$	$f(X)_{B2}$
CH_3OH	4.5×10^{-8}	2.2×10^{-5}	500
CN	4.8×10^{-9}	$\sim 5 \times 10^{-8}$	~ 10
CS	2.8×10^{-9}	1.9×10^{-7}	66
H_2CO	$4 - 6 \times 10^{-9}$	$2 - 5 \times 10^{-7}$	$60 - 80$
H_2S	1.1×10^{-8}	4.2×10^{-7}	40
HCN	3.6×10^{-9}	5.5×10^{-7}	150
HCO^+	1.5×10^{-9}	3.0×10^{-8}	20
HNC	1.6×10^{-9}	4.8×10^{-8}	30
SO	$\sim 5 \times 10^{-9}$	$2 - 5 \times 10^{-7}$	$60 - 100$
SO_2	$\sim 3 \times 10^{-8}$	5.7×10^{-7}	~ 20

Table 4.1: Abundances of chemical species as measured in L1157, in the shocked and the quiescent regions. All data come from Bachiller and Pérez Gutiérrez 1997. Only the molecules present in the chemical network are shown.

As we need to compare our shock models with measured values, it is necessary to define a function to minimize. In our case, we have chosen (Eq. 4.6) which is a modified version of the geometric standard deviation where we do not compare a set of values with a fixed geometric mean, but where, for each value of our set, we have an measured value. The choice of a "Geometric" standard deviation stands in the fact that we work with fractions $f(X) = \frac{\chi(X)_{B2}}{\chi(X)_0}$ with orders of magnitude that strongly vary from one molecule to another. An arithmetic deviation would be completely dominated by the molecule with the highest abundance, and we would thus fall back in the issue we wanted to avoid by using multiple molecular tracers.

$$\sigma_g = exp\left(\sqrt{\frac{\sum_X (ln\frac{f(X)_{B2}^{computed}}{f(X)_{B2}^{Obs}})^2}{n(X)}}\right) \tag{4.6}$$

where $n(X)$ is the number of species X included in the geometric standard deviation. From this formula, we obtained the geometric standard deviation for all shock models we made, and thus as a function of the density, the shock velocity, and the type of the shock. The global result is shown in Figures 4.9, and 4.10 while all geometric standard deviations specific for each of our molecules can be found in the Appendix 7.

The first measurement we can extract from these figures is the minimum of our geometric standard deviation which is at ~ 20 for the simulation of a C-type shock with n_H = 100 cm^{-3} and Vs = 9 km s^{-1}. This set of values is in good accordance with previous results seen in the literature. Nevertheless, as previously mentioned, we smoothed the differences in our standard deviation and many models are sufficiently close ($\sigma \leq 3 \times \sigma_{min}$) to our best model to be considered. Due to that, we cannot limit ourselves to the best model and we have to go deeper in the discussion. Firstly:

- If the shock is a C-type shock, our models predict an abrupt separation (of factor 4-5 for the geometric standard deviation) when the shock velocity passes through the barrier of 12 km s^{-1}. We can thus deduce that if other studies prove that L1157 B2 is a C-type shock, we should have a low-velocity shock with a maximum value of 12 km s^{-1}. Concerning the other parameter, we do not have strong variations due to the density of the medium and we can not deduce it from our simulations.

- If the shock is a J-type shock, we do not predict any strong variations in the average enhancement factor due to the physical conditions of the shock. For this reason, we can't determine the parameters of the shock in L1157 B2 as we can not suppress the possibility of a J-type shock at this point of the discussion.

4.2.2 A second attempt to identify the best model

As we have seen, this first try is thus characterized by a minimum in agreement with previous studies. Nevertheless, the large amount of molecules chosen (the maximum enabled by observational data) has too highly broadened the set of possible shock models. For J-type shocks, all shock models are below the limit of 3 σ and no information can be extracted from our method. A second attempt was made with a more specific sorting of the molecules used as molecular tracers. This sorting can be summarized by the following points:

- We have removed the SO and SO_2 molecules as potential molecular tracers. Curiously, the adsorbed on dust grains versions of these molecules are not available in the Paris-Durham Shock code. Nevertheless, there is no reason that these two molecules do not adsorb. Their binding energies are even computationally evalu-

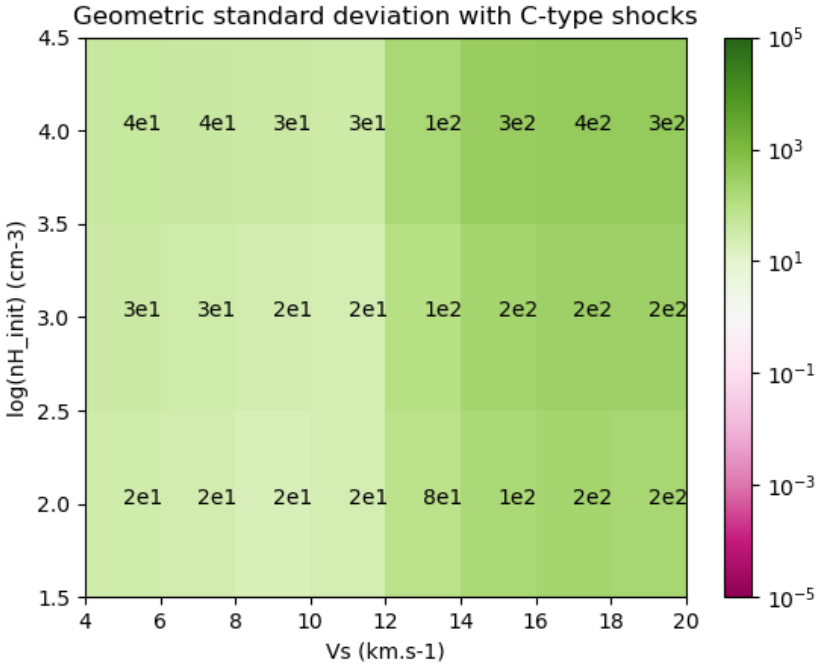

Figure 4.9: Global gometric standard deviations (Eq. 4.6) with all species listed in Table 4.1 for C-type shocks.

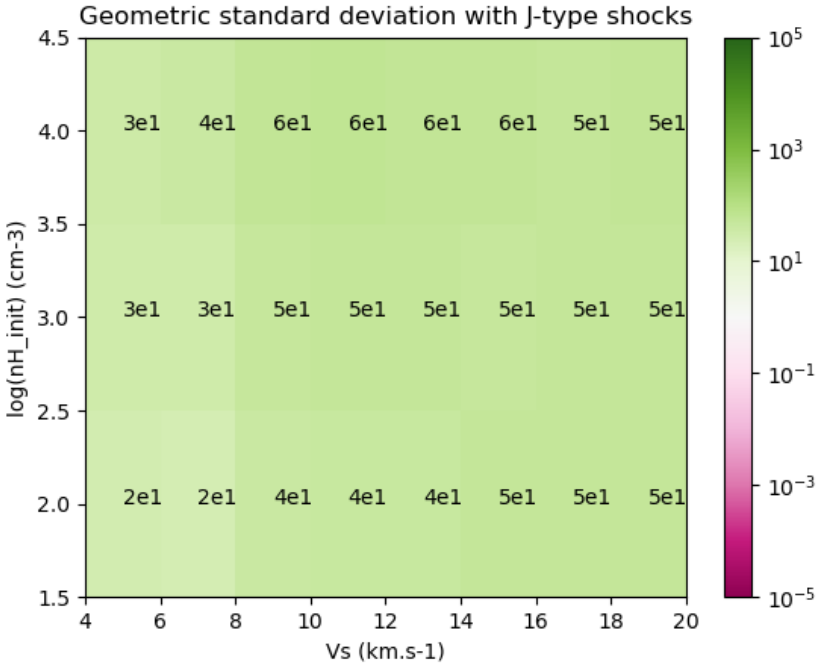

Figure 4.10: Global geometric standard deviations (Eq. 4.6) with all species listed in Table 4.1 for J-type shocks.

n	name	arithmetic standard deviation	n	name	arithmetic standard deviation
1	CH_3OH	65610	5	HCO^+	37,0
2	H_2S	1449,8	6	CS	30,2
3	CN	130,4	7	H_2CO	22,5
4	HCN	42,9	8	HNC	9,9

Table 4.2: List of all the molecular tracers (without SO and SO_2 molecules) with their arithmetic standard deviation in our shock models.

ated. (From DFT methods on crystalline water ice: 3861K and 6880K (Perrero et al. 2022)). From Miura et al. 2017, we should expect a desorption fraction of the order of 0.5 and thus a high impact coming from dust grains. More than that, the chemistry of sulfur is known to be complicated and misunderstood. They have thus been removed from the global geometric standard deviation for these reasons.

- We have sorted all the molecular tracers depending on the arithmetic standard deviation of the geometric standard deviations of all shock models for each species. We thus computed the mean value of the geometric standard deviation for each species and used it to compute a new standard deviation. We sorted the tracers in descending order and decided to keep the first three. The purpose of this step is to remove all molecular tracers that are not very effective in distinguishing between the best models and that will only broaden the results. The list of molecular tracers in descending order is given in Table 4.2. We have to note that the number "3" of kept molecular tracers has been chosen as a good equilibrium between a high number of molecular tracers (to avoid being based on one potentially unrealistic molecule) and a good distinction between shock models in terms of geometric standard deviation. To decide its value, we removed all tracers with an arithmetic standard deviation below the limit of 3 σ_{min} where σ_{min} is the minimum global geometric standard deviation obtained with all molecular tracers.

Our geometric standard deviation is thus now based only on the molecular tracers that are the best to diagnose the shock parameters. These molecules are CH_3OH, H_2S, and CN. The new figures plotting the reduced global geometric standard deviations are Fig 4.11 and 4.12. Compared to our first attempt, the differences between the value of the global geometric deviation of each shock model are more accentuated. It is now easier to differentiate them in the following discussion.

The reduced results are more separated even if we are now confronted with two global minima with a geometric standard deviation at ~ 8 for the C-type shocks with a density of 100 cm^{-3} and shock velocities of 5 and 7 km s^{-1}. Nevertheless, many shock models are

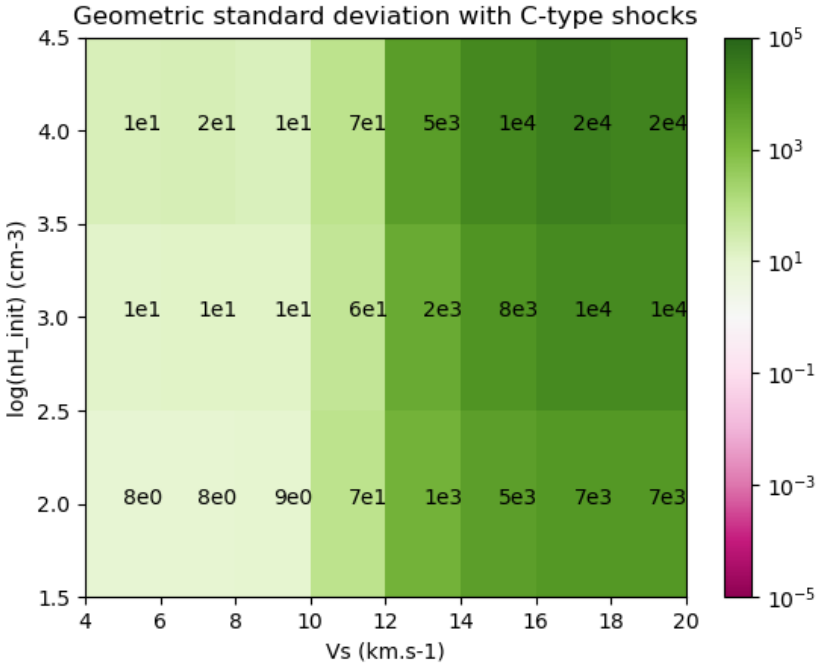

Figure 4.11: Reduced geometric standard deviations (Eq. 4.6) with CH_3OH, H_2S, and CN for C-type shocks.

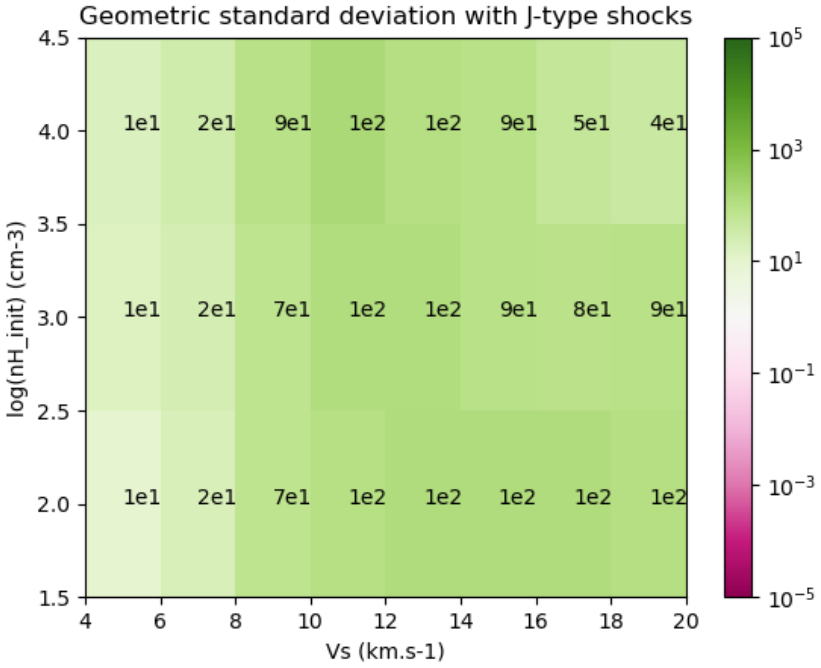

Figure 4.12: Reduced geometric standard deviations (Eq. 4.6) with CH_3OH, H_2S, and CN for J-type shocks.

now above the limit of 3 σ. It is more obvious that whatever the shock type, the velocity of the shock is constrained to be below the limit of 10 km s^{-1} for C-type shocks, and below the limit of 8 km s^{-1} for J-type shocks. Unfortunately, the reduced set of molecular tracers has not deeply impacted the variations along the axis of density. It thus seems that the fractional abundances and thus the relative chemistry is not highly dependent on the density of the medium. Even if we do not exclude that future studies that could be more realistic in terms of physical processes find peculiar molecular tracers that vary with the preshock density, it seems that the density is not very impacting the chemistry. This could be explained by the fact that an increase in the density should enhance almost all the reactions equivalently. Thus, the equilibrium solutions stay the same in terms of relative abundance given that the number of molecules for each species has been multiplied by the same factor. This simplistic assumption should still be evaluated in the case of very high densities where grain-grain processes can bring new behaviors.

Our new results only conclude that the shock velocity of L1157 B2 is below the limit of 10 km s^{-1}, but do not give any clues concerning the preshock density or even the type of the shock. But it is still possible to compare what we have done with previous studies that stipulated that L1157 could be a shock with a shock velocity of 10 km s^{-1}. Doing so could be a source of new insights concerning this shocked region. Indeed, with the Paris-Durham shock code, our shock models with a shock velocity of 10 km s^{-1} are below the limit of 3 σ only for C-type shocks. Even if more studies should be required in the future to clearly diagnose L1157, the pooling information of what has already been done suggests a C-type behavior. Let's recall that the presence of C-type shock behavior does not exclude the possibility of a multi-type shock for the system L1157 B2. However, the methods illustrated here do not enable us to establish the unicity or not of the type of shock.

4.3 A summary of the method

We found that astrochemistry can be used to characterize the shock velocity and potentially, embedded with other studies, the shock type. In the context of this master's thesis, this was done after two major attempts that were explained previously. For the sake of simplicity, it is now useful to briefly remind and synthesize the general method that emerges from our work:

1. We created a grid of parameters characterizing the shocked system we studied. To avoid a too high computational time, the domain for the parameters should be chosen depending on previous studies or the values that could be expected for the shock. (Do we have an old shock and thus a low-velocity shock? Do we have an idea of the density of the medium? Are we in a dense cloud, in a protostellar environment?)

2. Benefitting from the best chemical network available with the Paris-Durham Shock code, we simulated shocks all along the parameters grid and obtained as an output the fractional abundance of all chemical species as a function of the distance in the shock.

3. Through observations (or in our case, through the literature), we obtained fractional abundance for a set of molecular tracers in the shocked region. From the fractional abundance in the shocked region and neighboring quiescent region, we can define and calculate the enhancement factor as in (Eq. 3.1).

4. From the results of our shock models, we computed the enhancement factor for each species in each shock model. By doing so, it was possible to compute for each simulation the geometric standard deviation (Eq. 4.6). The geometric standard deviation is used instead of the arithmetic standard deviation to avoid the ability of only one molecule to take the lead of the global geometric standard deviation. (Knowing that astrochemical simulations currently make strong simplistic hypotheses, this seems to be a critical point.)

5. By taking the geometric standard deviation for all chemical species for each shock model, we obtained the global geometric standard deviation. This gave us a first minimum for the standard deviation which is noted: σ_{min}.

6. We computed for each species the arithmetic standard deviation of their geometric standard deviation and we removed all species with a deviation below the limit of 3 σ_{min}. These molecular tracers do not significantly affect the form of the global geometric standard deviation, but only flatten the results. We also removed all species we thought to be poorly treated by the astrochemical code.

7. Using the new molecular tracers, we obtained the reduced geometric standard deviation that can be used to characterize the shocked region.

L1157 B2 has thus been characterized using the following method. Nevertheless, even if we treated the results of the Paris-Durham Shock code, we did not discuss the reasons behind the astrochemical differences between C-type and J-type shocks. In brief, we know we should expect differences between the both, but we do not know why. This will be discussed in the next chapter, trying to answer our second research question. At the same time, we will focus on the molecular tracers that were useful in the case of L1157 B2 which were: CH_3OH, H_2S, and CN. This step is also a good way to validate or reject the relevance of our results.

Chapter 5

Discussion - The astrochemistry of interstellar shocks

In the first part of the discussion, we used astrochemistry to identify which molecules were significantly impacted by the shock parameters such as their type, density, and velocity. By doing so, we identified three useful molecular tracers to characterize the system L1157 B2 – CH_3OH, H_2S, and CN. However, we extracted these tracers from our results without any analysis of what is physically occurring in interstellar shocks. Said otherwise, we know "What?" but we do not know "Why?". This last part of the discussion will use the remaining data from our simulations and previous work to understand how chemical differentiation emerges from physical differences in the studied shocks. Firstly, taking help from the literature, we will discuss the physical features of shocks able to affect the chemistry. This enumeration will be of first help to apprehend and understand the next part. In this next part, we will recreate the chemical network for some of our molecules of interest at some distances in the shocks. This chemical network will enable us to identify the reactions that will deeply change the chemical composition of our system.

> What is the objective? Understanding the behavior of our molecular tracers in our shock models is necessary to conclude if "Yes or No" we can believe that our astrochemical simulations are suitable to describe interstellar shocks. More than that, we will get a deeper understanding of what is happening in shocks and thus answer the second question **"How do shocks influence the overall chemistry of the interstellar medium?"**.

5.1 The physical behavior of interstellar shocks

Interstellar shocks are a subject that is well documented and a high number of references talk about the physics of shocks. Fortunately, some astrochemists already analyse the main features able to change the chemistry of shocks. It is thus particularly relevant to summarize the main points raised by the community. The following synthesis is mainly based on the textbook "Dynamical Astrochemistry" (D. A. Williams et al. 2018) and on the work of Lesaffre et al. 2013 who already analyzed some signatures of shocks (as a

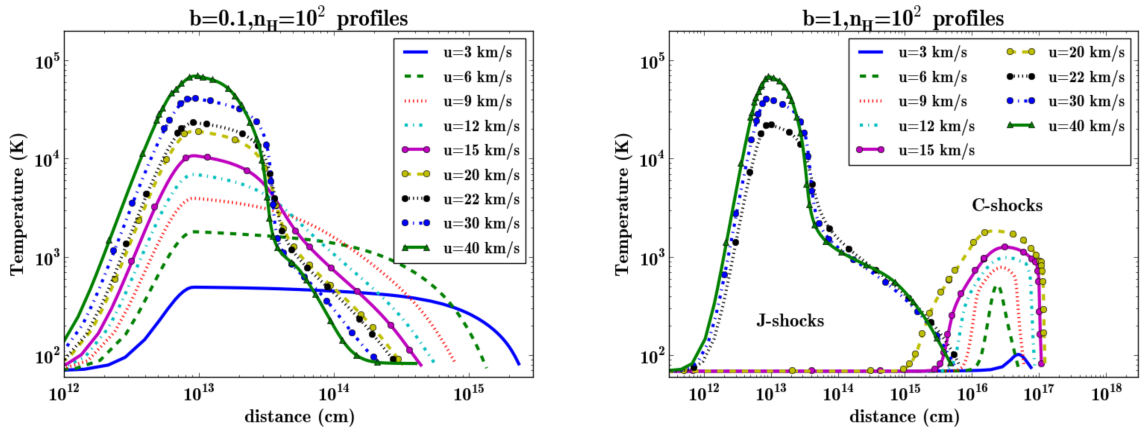

Figure 5.1: Temperature profiles as a function of the shock velocity for shocks with a weak magnetic field on the left side (b = 0.1), and with a strong magnetic field on the right (b = 1). As discussed in the text, the presence of a strong magnetic field enables the presence of C-type shocks. Figures come from Lesaffre et al. 2013.

function of the type and the velocity) with an older version of the Paris-Durham Shock code. As the principal base of the code remained the same between their work and this master's thesis, we could expect to have in first approximation the same physics in their and our simulations (for example, the same temperature and velocity profiles). This was verified by us and confirms the relevance of the following discussion.

5.1.1 The temperature and its impacts

The first physical behavior to study concerns the temperature. As the temperature determines the energetic budget of atoms and molecules, it will deeply impact their abilities to perform chemical reactions. As recalled in Sect. 7.1, energy (and thus temperature) is necessary to pass out the activation barrier that will regulate the reaction rate through an exponential. A sufficient temperature is thus necessary to sufficiently feed pathways with high activation barriers such as the neutral-neutral ones seen in (Sect. 1) or even to enhance the overall chemistry in general. On the other hand, a too-strong increase in the temperature could lead to the dissociation or the destruction of the molecular content. However, such an increase only happens in sufficiently high-velocity shocks with a minimum shock velocity of 50 km s^{-1} (De Becker, M. 2023). In the old version of the Paris-Durham Shock code, a velocity of 35 km s^{-1} is necessary to dissociate H_2 (Lesaffre et al. 2013) which as a dissociation energy of 52000K (D. A. Williams et al. 2018). As these shock velocities are completely out of our range of simulations, we should expect the temperature to enhance the chemistry without being destructive.

As can be seen in Figure 5.1, the temperature profile is highly dependent on the type of shock and varies with the shock velocity. We have to remark that simulations of C-type shocks only happen with a strong magnetic field (b=1) with a not-too-high velocity to ensure that the magnetosonic velocity (Eq. 2.1) is greater than the shock velocity. Let's begin with J-type shocks:

As identified in Figure 5.1, J-type shocks are characterized by a huge increase in the temperature – a jump – that will be more violent than C-type shocks. This jump is sharp in the sense that the temperature is directly followed by a viscous dissipation of the kinetic energy in the so-called "relaxation layer". Two main points have been emphasized in the temperature profile of these J-type shocks. Firstly, the increase in temperature in J-type shocks is particularly strong and leads to significantly higher temperatures than in C-type shocks. It can typically reach several thousands of degrees. This maximum of temperature is proportional to the square of the shock velocity and can be expressed as follows (Lesaffre et al. 2013):

$$T^J_{Max} = 53K \cdot V_s^2 \tag{5.1}$$

where the shock velocity is in km s^{-1}.

Secondly, the viscous dissipation of energy is very efficient, and the temperature quickly comes back to the preshock temperature. Thus, J-type shocks spread out on very small distances compared to C-type shocks. As visible in Figure 5.1, J-type shocks are already suppressed after $10^{14\sim15}$ cm while C-type shocks can easily spread out on $10^{16\sim17}$ cm. It is also interesting to remark that J-type and C-type shocks have opposite tendencies concerning the impact of the shock velocity. In J-type shocks, the higher the shock velocity, the faster the dissipation as the efficiency of the viscous dissipation increases with the shock velocity. Unlike type C shocks, where a higher shock speed means a wider shock. This will be explained when we will discuss temperature profiles in C-type shocks. The huge increase in the temperature will have a huge impact on the chemistry as it will enable endothermic reactions possessing a high activation barrier. This is particularly relevant for the neutral-neutral pathways that will be strongly activated during the jump. Indeed, the simple addition of hydrogen on an atom, a molecule, or even an ion by collision with H_2 typically requires between 3000 and $\sim$ 15000 K that can be reached in J-type shocks with a velocity shock higher than 7.5 and 16.5 km s^{-1} (Lesaffre et al. 2013). We can thus expect an enhancement of hydrogenated species. Nevertheless, the domain of high temperature is quite small in J-type shocks and the enhancement is quickly attenuated by the dissipation of kinetic energy. The effect on the chemistry in J-type shocks can easily be identified in Figure 5.2. Neutrals and ions are enhanced by one to two orders of magnitude (more for H_3^+) while the shock velocity is high enough to reach the temperatures required to activate the endothermic reaction as the basis of their formation, but the density directly tends to a plateau for most molecules as the increase in temperature is counterbalanced by the sharpness of the range in terms of distance. For shocks with a velocity higher than 35 km s^{-1}, we can observe a decrease in the column density. This is related to the dissociation of H_2 (which is enabled at these velocities) which will thus reduce the possibility of the addition of hydrogen. Nevertheless, it only happens for velocities that are out of our range of parameters and it does not have to be taken into account in our future discussions.

Coming back to Figure 5.1, we can observe the temperature profile for C-type shocks.

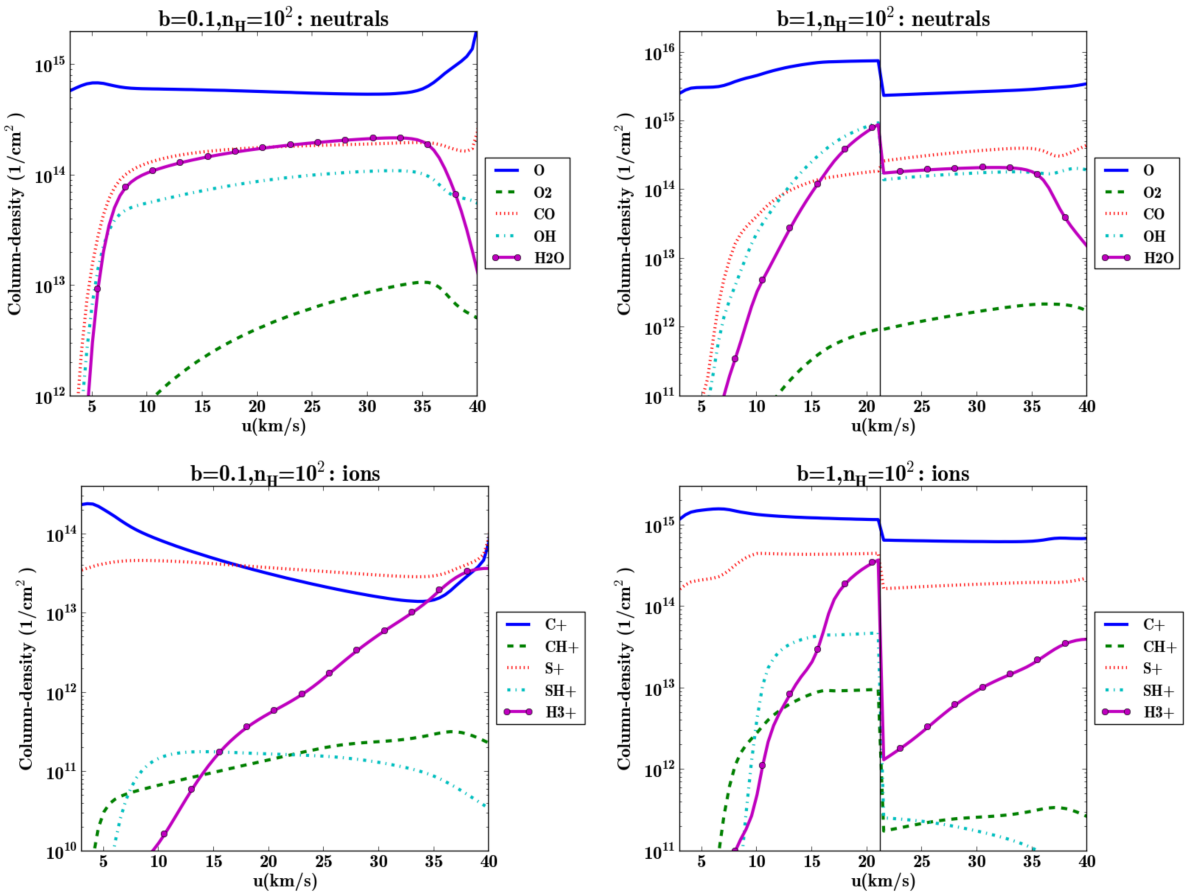

Figure 5.2: Column density profiles for neutrals and ions as a function of the shock velocity for shocks with a weak magnetic field on the left side (b = 0.1), and with a strong magnetic field on the right (b = 1). The line for shocks with a strong magnetic field signals the transition between C-type shocks on the left and J-type shocks on the right. Figures come from Lesaffre et al. 2013.

C-type shocks are characterized by a differentiation in the velocities describing the ionized and neutral content of the medium. The resulting friction between neutrals and ions leads to a transformation of the kinetic energy into thermal energy. For these reasons, the increase in temperature is more continuous and never reaches the high temperature occurring in J-type shocks. We are here limited to some hundreds to one thousand degrees depending on the shock velocity. However, the continuous heating by friction of the material enables C-type shocks to spread out over very large distances and this distance increases with the shock velocity. Even if the gas does not reach the same temperature as in J-type shocks, it stays warm for a greater amount of time. Chemically, we should not expect the temperature to be high enough for high-activation barrier reactions. However, Type C shocks propagate over a greater distance than type J shocks; thus, the molecular content is warm for longer. It gradually enhances the chemistry and the column densities as the maximum temperature increases with the shock velocity. This is observable in Figure 5.2.

5.1.2 The Ion-Neutral drift

The ion-neutral friction occurring in C-type shocks described in the last subsection can do more than warm up the gas along the shock. Its other effect is what we call the ion-neutral drift. Ion-neutral drift is the increase in energetic collisions between ionic and neutral species due to their relative speed. Indeed, the difference in velocities between the ionic and neutral mediums enhances the mean speed at which neutrals collide with ions (as a flux passing through another one). As this relative velocity increases the strength of collisions between ions and neutrals already present due to the thermal agitation, we will describe the effect of the ion-neutral drift by writing an effective temperature that will sum the thermal agitation and the impact of the relative velocity and will use it each time we compute ion-neutral reactions. This effective temperature is written (Pineau des Forets, Flower, et al. 1986):

$$T_{eff} = \frac{m_i T_n + m_n T_i}{m_i + m_n} + \frac{\mu}{3k_b} \cdot (u_i - u_n)^2 \tag{5.2}$$

where m_i and m_n are the masses of the ion and the neutral, T_i and T_n are the temperatures of the ion and the neutral, μ is the reduced mass of the system, and u_i and u_n are the velocities of the ion and the neutral.

The evolution of this effective temperature compared to the maximum temperature in C-type shocks is directly observable in Figure 5.3. From this observation, it is clear that ion-neutral reactions benefit from an effective temperature of the same order of magnitude as the maximum temperature in J-type shocks. This ion-neutral drift only concerns ion-neutral reactions and will thus enhance the corresponding pathway. It explains the greater difference between column densities for neutrals and ions in Figure 5.2 when we pass the line corresponding to the transition of C-type shocks to J-type shocks as ions strongly benefit from collisions with H_2 resulting in an addition of hydrogen.

5.1.3 The sputtering of grains

The drift between the ionized and the neutral content does not only affect ion-neutral reactions. The difference in velocities between neutrals and charged grains can also profoundly affect the chemistry. Collisions between grains and heavy neutrals can provoke the sputtering of the mantle of the grains (Flower and Pineau des Forets 1994) or even an erosion of the grain cores (Field et al. 1997). This sputtering will help the exchanges between the gas and solid phases and will thus participate in the release of freshly saturated species (all double or triple bonds have been replaced by bonds with hydrogen atoms.) into the gas phase. These saturated species can then be partners of other reactions in the gas phase (typically, we can imagine that additions with saturated species are likely to occur as the energetic problem can be more easily overcome by the loss of a fragment of the saturated reactant). As it is a consequence of the drift between ions and neutrals, we already know that it will be very efficient in C-type shocks. It is already interesting to note that it has the same effect as the thermal desorption that was critically discussed in the last chapter. We can thus also expect that the sputtering will lower the issues

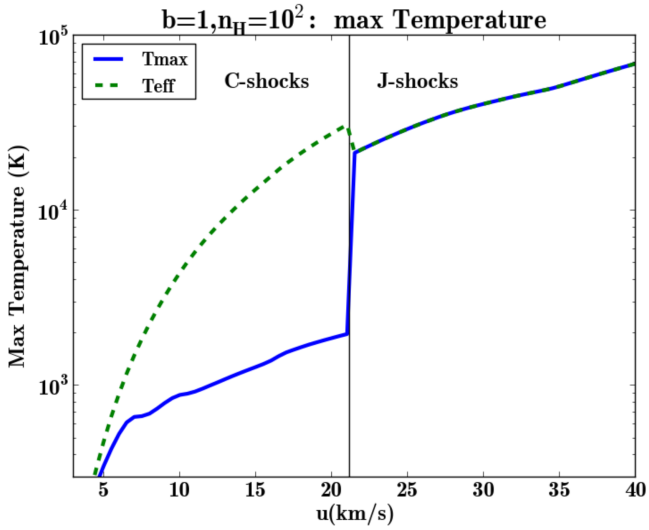

Figure 5.3: Evolution of the effective temperature of ion-neutral reactions compared to the maximum temperature of the gas for shocks with a strong magnetic field (b = 1). The vertical line signals the transition between C-type shocks on the left and J-type shocks on the right. The figure comes from Lesaffre et al. 2013.

associated with the simple treatment of thermal desorption.

In terms of efficiency, the sputtering of the mantle of the grains was already well studied using older versions of the Paris-Durham Shock code (Flower and Pineau des Forets 1994). They found that the mantle could be completely removed in C-type shocks with shock velocities as low as 10 km s^{-1} (with a magnetic field of 30 μG and a preshock density of 10^4 cm^{-3}). This sputtering increases with the densities of grains and gas, with the shock velocity, and with the strength of the magnetic field. It will thus be lower in most of our simulations. Nevertheless, we should still expect sputtering to be efficient enough to remove a significant part of the grain icy mantle species. In these previous studies, they found that the sputtering and thus the release of these mantle species was followed by a phase of readsorption. Knowing that grain reactions lead to the hydrogenation of adsorbed species, we also discovered that the sputtering enables pathways where some molecules such as H_2O or NH_3 are formed and then released in the gas phase, unlocking a more complex chemistry.

Grain refractory core species can also be released into the gas phase through sputtering. Again, this sputtering is particularly efficient when the density is high for high-velocity shocks with strong magnetic fields. Nevertheless, it is still possible for it to be significant in our simulations and can lead to an increase in the gas phase of C, O, Si, Mg, and Fe atoms.

Now that the three major differences between the C-type and the J-type shocks have been pointed out, we can keep them in mind to analyze the chemical network of molecules of interest.

5.2 The case of CH_3OH

The dominant molecular tracer identified in the last chapter was CH_3OH. It has shown a great differentiation due to the velocity of the shock as can be easily seen in Fig 7.10 and it possesses great variations depending on the type of the shock as can be read from the comparison factor in Fig 7.7. Armed with the aspects discussed above, we will analyze in detail the chemistry behind the behavior of this molecule and understand why the Paris-Durham Shock code leads to these differences. Nevertheless, even if the Paris-Durham Shock code mimics at its best the reality of interstellar shocks and their chemistry, we should keep in mind that all the following is the fruit of computational methods and should not be taken as facts without discussion. We also take advantage of this paragraph to emphasize that even if the behavior of CH_3OH can be analyzed (and we are lucky as it is our main molecular tracer), it is not that easy for all the other molecules. Indeed, CH_3OH participates in 53 reactions which can already be a lot for a human brain. However, this number is small and is due to the chemical complexity of the molecule. If we want to analyze smaller and thus more common molecules, we have to investigate several hundreds of reactions. Knowing that we can consider CH_3OH as a good training for more complex chemical networks. Firstly, we sorted all reactions from the overall chemical network to draw a smaller one containing the main reactions impacting our molecular tracer. This chemical network can be seen in Fig. 5.4.

As previously mentioned in the introduction, a chemical network contains a grain phase and a gas phase divided into neutrals and ions. Even if the reactions are not clearly specified in the Figure 5.4 for the sake of clarity, the most important ones will be looked into with more details during the following discussion. This chemical network will be useful to spot the differences between the three astrophysical environments we want to investigate. Namely: the preshock region, the postshock region of C-type shocks, and the postshock region of J-type shocks where the postshock regions were defined in the third chapter. To increase the impact of the shock on the chemistry, we have chosen to analyze shocks at $nH = 10^3$ cm^{-3} and with a shock velocity of 19 km s^{-1}. Even if the numerical values will not correspond to the minima found earlier, this approach allows to better understand the speciation happening in the shock. We already thank the tools available with the Paris-Durham Shock code which help us to easily investigate the evolution of reactions and physical quantities during the shock. From the chemical network, we can already identify the most important molecules that will impact the overall behavior. These molecules are CH_3OH, CH_3OH*, CH_3OH^+, H_3CO^+, and CH_5O^+. The two last ones are important in the sense that the formation of H_3CO^+ seems to express the destruction of our main molecule CH_3OH while CH_5O^+ displays an important interplay with CH_3OH. We will not deeply discuss the other molecules of the network. The reason for this is that they are small enough to be involved in too many reactions, making it unnecessarily difficult to examine them in their entirety. Now that we know where to focus our efforts, we can start the analysis.

Figure 5.4: This chemical network of the CH_3OH molecule is made from the reactions found in the global chemical network of the Paris-Durham Shock code. The black arrows indicate reactions between molecules – Ions or neutrals. A black arrow split in two means a dissociation process. The yellow arrows indicate photo-induced reactions such as photodissociation, photoionization, or photodesorption. Finally, the hollow arrow indicates sputtering processes releasing adsorbed molecules into the gas phase.

5.2.1 The preshock region

As previously mentioned, the preshock region is computed as being at chemical equilibrium assuming solar abundance. Even if the preshock region is considered to be stationary as it does not change with time, it is highly relevant to study it as we will focus later on the differences compared to the initial situation – the preshock region. As visible when we compare data from Table 5.1, CH_3OH is mainly adsorbed on dust grains at the chemical equilibrium. From our shock models, only 1×10^{-8} of CH_3OH molecules are in the gas phase during the preshock phase. We thus expect to have a reservoir of the molecules trapped in dust grains. We can also see that CH_3OH is mainly in its neutral form. (Only 0.04% is in the ionic form.)

As the molecule is mainly trapped in dust grains, it is also relevant to give a special interest to the form of these dust grains. In the preshock region, we computed that the fractional abundance of G, G^-, and G^+ are respectively 2.55×10^{-11}, 4.34×10^{-11}, and 5.85×10^{-13}. The grain is thus mainly negatively charged at equilibrium according to the Paris-Durham Shock code. This point should be discussed. From Van Grootel, V. 2023, we know that interstellar grains are more commonly positively charged in the diffuse interstellar medium due to the photoelectric emission assured by external UV photons. However, these extern photons have been neglected in our shock models, and the negative charge at the preshock phase only stands for densities down to 10^3 cm^{-3} where photons do not pass. We do not expect the assumption of a not-irradiated shock to be highly problematic for lower densities as – as we will see later – it is mainly the fact that the grain is charged that will impact the chemistry. From our dense medium, the charging by external UV photons is negligible compared to other mechanisms taken into account by the code (Flower and Pineau des Forêts 2003b) such as the electron attachment, the electron detachment by the radiation field (primary and secondary photons, and cosmic-rays), the attachment of positive ions, and the neutralization of negatively charged grains by positive ions. Given that, we can believe in the fractional abundance given by the Paris-Durham Shock code for these densities.

Molecule	Preshock abundance	Molecule	Preshock abundance
CH_3OH	7.24×10^{-14}	CH_5O^+	8.45×10^{-15}
CH_3OH*	1.86×10^{-5}	H_3CO^+	1.15×10^{-11}
CH_3OH^+	2.95×10^{-17}		

Table 5.1: Preshock fractional abundance for our molecules of interest.

Knowing the abundance of our elements, it is important to understand the reactions connecting them. Let's start with CH_3OH visible in Figure 5.5. These figures are made using the Chemistry Analyzer Tool furnished with the Paris-Durham Shock code. In the

figure's left part, we plotted the main formation reactions of CH_3OH (at the left) and the main destructive reactions (at the right). Each reaction (or each arrow) can be viewed as "The molecule (at the left) reacts with the reactant (at the middle) to give the product (at the right)". We have to note that the reactant is not necessarily another molecule, but can be some of our artificial species (Sect. 2) such as "secpho" which expresses the interaction with a secondary photon (emitted by excited species). In the figure's right part, all selected reactions are provided with some details allowing us to analyse their evolution through the densities of the reactants, the value of the rate constant, and the global formation rate. At this first step of the shock, the chemistry is not well activated and, due to the low temperature, there are almost only neutral-ion reactions (characterized by a low activation barrier) that will destroy the CH_3OH molecules. However, these destructive reactions are limited by the very low density of CH_3OH and counterbalanced by formation processes (without counting the photodesorption from the grain phase which does not create new molecules – It is just a phase transfer). In the preshock region, CH_3OH* can only be formed from adsorption on grains and destroyed by interactions with secondary photons. But interestingly, adsorption rates are of the order of $\sim 9\times10^{-25}$ cm^{-3} s^{-1} while desorption rates are of the order of $\sim 7 \times 10^{-19}$ cm^{-3} s^{-1}. Even if the difference between these two rates is not enough to drastically change the composition of the medium, we have to note that the code considers that desorption processes begin as soon as the simulation starts. In every case, we can already think that the interplay between the gas and the grain phases is the most impacting aspect of the chemistry of CH_3OH as their reaction rates are greater than destruction processes by 4 orders of magnitude. The chemistry of all the ions is characterized by a total formation rate that is equal to the total destruction rate. This could be assumed knowing that the preshock region is at the equilibrium, and that ions can not directly enter the grain phase and are thus consequently not already affected by desorption processes. As readable from the chemical network of CH_3OH, its ion CH_3OH^+ is only produced from its neutral equivalent (see Figure 5.6). More interesting is the fact that CH_5O^+ is not already well linked with CH_3OH (see Figure 5.7). It is mainly made from the addition of H_2O with CH_3^+ while the products coming from its dissociative electron recombination almost do not contain CH_3OH, but are essentially made of CH_3 and OH molecules. At this step, H_3CO^+ is also not well linked to CH_3OH.

In conclusion, we can stipulate that the preshock region is mainly made of neutral-ion reactions with low activation barriers, and dissociative electron recombination with ions (enhanced by electrostatic forces). The chemical network of CH_3OH is not well activated and molecules are mainly linked to smaller molecules. Also, the main reservoir of CH_3OH is in the grain icy mantles. This information will be important for the comparison with more evolved phases of the shock. Before continuing throughout the shocks, it is also a good idea to see with the enhancement factors (See Figures 7.8 and 7.9) the behavior that we should expect. We should identify mechanisms able to increase the fractional abundance of CH_3OH in C-type and J-type shocks with better efficiency in C-type shocks. Even if we do not try to quantify the enhancements brought by these mechanisms due to the size limitations of this master's thesis, it is important to discuss how C-type shocks can be 10^4 times better than J-type shocks to increase the density of gas phase CH_3OH.

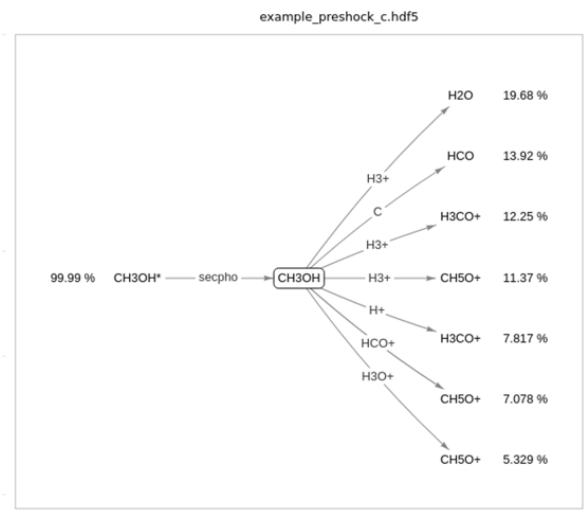

Formation of CH3OH — Total formation rate 7.22e-19 cm-3 s-1

A + B → C + D	n(A) (cm-3)	n(B) (cm-3)	k	rate (cm-3 s-1)	proportion
CH_3OH^* + secpho → CH_3OH + grain	1.86e-2		3.88e-17	7.22e-19	99.99 %

Destruction of CH3OH — Total destruction rate 7.90e-23 cm-3 s-1

A + B → C + D	n(A) (cm-3)	n(B) (cm-3)	k	rate (cm-3 s-1)	proportion
$H_3^+ + CH_3OH \rightarrow CH_3^+ + H_2O + H_2$	9.64e-5	3.43e-11	4.70e-9	1.55e-23	19.68 %
$CH_3OH + C \rightarrow HCO + CH_3$	3.43e-11	1.07e-3	3.00e-10	1.10e-23	13.92 %
$H_3^+ + CH_3OH \rightarrow H_3CO^+ + H_2 + H_2$	9.64e-5	3.43e-11	2.92e-9	9.67e-24	12.25 %
$H_3^+ + CH_3OH \rightarrow CH_5O^+ + H_2$	9.64e-5	3.43e-11	2.71e-9	8.98e-24	11.37 %
$H^+ + CH_3OH \rightarrow H_3CO^+ + H_2$	1.79e-5	3.43e-11	1.00e-8	6.17e-24	7.817 %
$HCO^+ + CH_3OH \rightarrow CH_5O^+ + CO$	3.72e-5	3.43e-11	4.38e-9	5.59e-24	7.078 %
$H_3O^+ + CH_3OH \rightarrow CH_5O^+ + H_2O$	2.47e-5	3.43e-11	4.96e-9	4.21e-24	5.329 %

Figure 5.5: Chemistry of CH_3OH during the preshock phase.

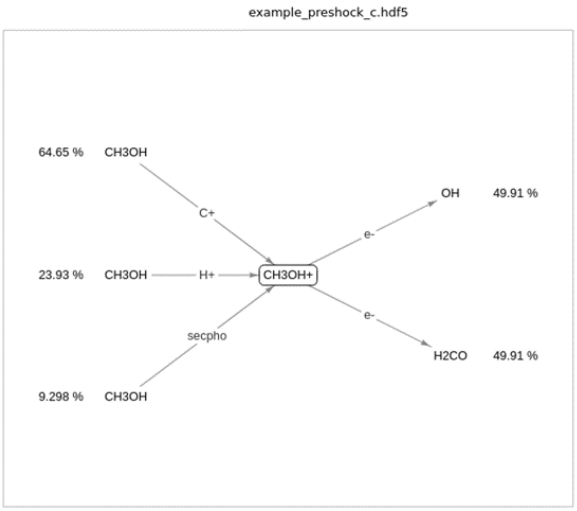

Formation of CH3OH+ — Total formation rate 3.96e-24 cm-3 s-1

A + B → C + D	n(A) (cm-3)	n(B) (cm-3)	k	rate (cm-3 s-1)	proportion
$C^+ + CH_3OH \rightarrow CH_3OH^+ + C$	3.49e-5	3.43e-11	2.14e-9	2.56e-24	64.65 %
$H^+ + CH_3OH \rightarrow CH_3OH^+ + H$	1.79e-5	3.43e-11	1.54e-9	9.48e-25	23.93 %
CH_3OH + secpho → $CH_3OH^+ + e^-$	3.43e-11		1.07e-14	3.68e-25	9.298 %

Destruction of CH3OH+ — Total destruction rate 3.96e-24 cm-3 s-1

A + B → C + D	n(A) (cm-3)	n(B) (cm-3)	k	rate (cm-3 s-1)	proportion
$CH_3OH^+ + e^- \rightarrow CH_3 + OH$	1.00e-14	2.52e-4	7.83e-7	1.98e-24	49.91 %
$CH_3OH^+ + e^- \rightarrow H_2CO + H_2$	1.00e-14	2.52e-4	7.83e-7	1.98e-24	49.91 %

Figure 5.6: Chemistry of CH_3OH^+ during the preshock phase.

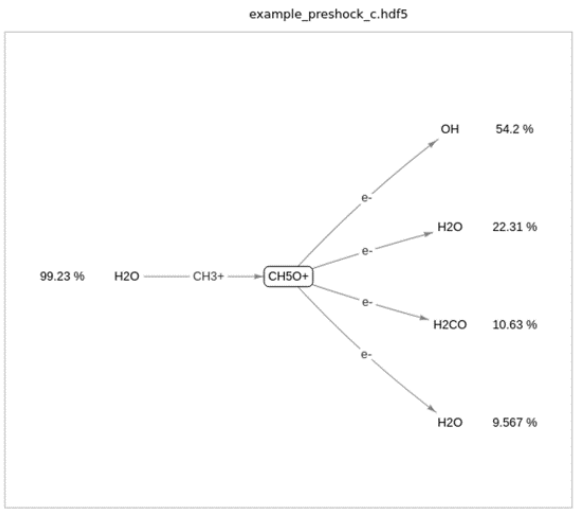

Formation of CH5O+ — Total formation rate 2.43e-21 cm-3 s-1

A + B → C + D	n(A) (cm-3)	n(B) (cm-3)	k	rate (cm-3 s-1)	proportion
$CH_3^+ + H_2O \rightarrow CH_5O^+ +$ photon	1.30e-6	9.26e-4	2.00e-12	2.41e-21	99.23 %

Destruction of CH5O+ — Total destruction rate 2.43e-21 cm-3 s-1

A + B → C + D	n(A) (cm-3)	n(B) (cm-3)	k	rate (cm-3 s-1)	proportion
$CH_5O^+ + e^- \rightarrow CH_3 + OH + H$	3.12e-12	2.52e-4	1.68e-6	1.32e-21	54.2 %
$CH_5O^+ + e^- \rightarrow CH_2 + H_2O + H$	3.12e-12	2.52e-4	6.90e-7	5.42e-22	22.31 %
$CH_5O^+ + e^- \rightarrow H_2CO + H_2 + H$	3.12e-12	2.52e-4	3.29e-7	2.58e-22	10.63 %
$CH_5O^+ + e^- \rightarrow CH_3 + H_2O$	3.12e-12	2.52e-4	2.96e-7	2.33e-22	9.567 %

Figure 5.7: Chemistry of CH_5O^+ during the preshock phase.

5.2.2 The postshock region in C-type shocks

The first type of shock we want to understand chemically is the C-type. To do so, we again analyzed the chemical reactions involved for each chemical species of interest. Nevertheless, we cannot continue to analyze them without simultaneously comparing them with the shock's physical evolution. The main physical parameters able to influence the chemistry were identified to be the temperature and the velocities of the ionic and neutral medium. More specifically, it is the difference between these two velocities that will dictate the strength of the Ion-Neutral drift. The physics of a C-type shock at 10^3 cm^{-3} and 19 km s^{-1} is shown in Figure 5.8. As expected, the physical influence of the C-type shock spans a long distance compared to what we will have with J-type shocks. In future graphics, we should expect to identify the effects of the Ion-Neutral drift from $\sim 2 \times 10^{16}$ cm and the effects of the increase in the temperature from $\sim 3 \times 10^{16}$ cm. These effects should stop at similar distances - $\sim 4 \times 10^{17}$ cm. With this data in mind, we can give a first look at the evolution of the fractional abundance with Figure 5.9.

With the fractional abundance of species, we can easily identify some important steps in the evolution of the chemical content. Firstly, and coinciding with the beginning of the Ion-Neutral drift, we have an increase of a factor of 2.5 in the abundance of CH_3OH* at $\sim 2 \times 10^{16}$ cm. This increase is directly followed by a total desorption of the CH_3OH molecules at $\sim 6 \times 10^{16}$. This abrupt desorption also characterizes a huge increase in the abundance of CH_3OH by a factor of 3×10^8 which is also the enhancement factor in C-type shocks for this shock model. We have to remark that even if the increase of CH_3OH is of the same order as the number of desorbed molecules, it is still significantly below. At $\sim 1 \times 10^{17}$ cm, we observe another abrupt increase in the fractional abundance of an order of $\sim 7 \times 10^5$ for the CH_5O^+ ion. This increase is followed by other ones for CH_3OH^+ and H_3CO^+. All the fractional abundance of gas phase species tends to begin to decrease from $\sim 4 \times 10^{17}$ cm which is also the moment where the temperature and the Ion-Neutral drift come back to normal. After the shock, all fractional abundance are closer to the abundance from the preshock region. Nevertheless, even if it will be of the

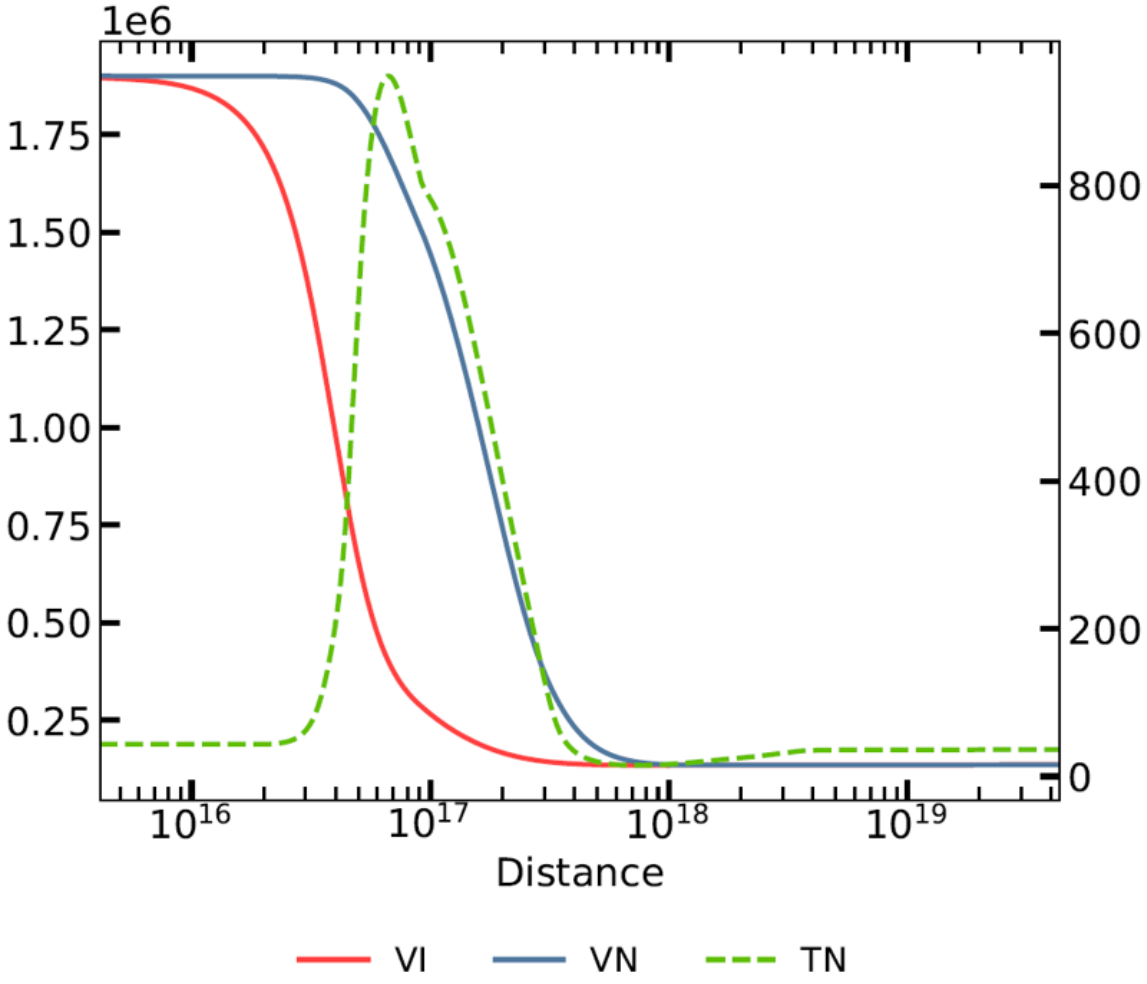

Figure 5.8: Evolution of the physical parameters through a C-type shock. The x-axis represents the distance along the shock in cm. The left y-axis plots the velocities of the ionic (VI) and neutral (VN) fluxes in cm s^{-1}. The right y-axis plots the temperature of neutrals (TN) in K.

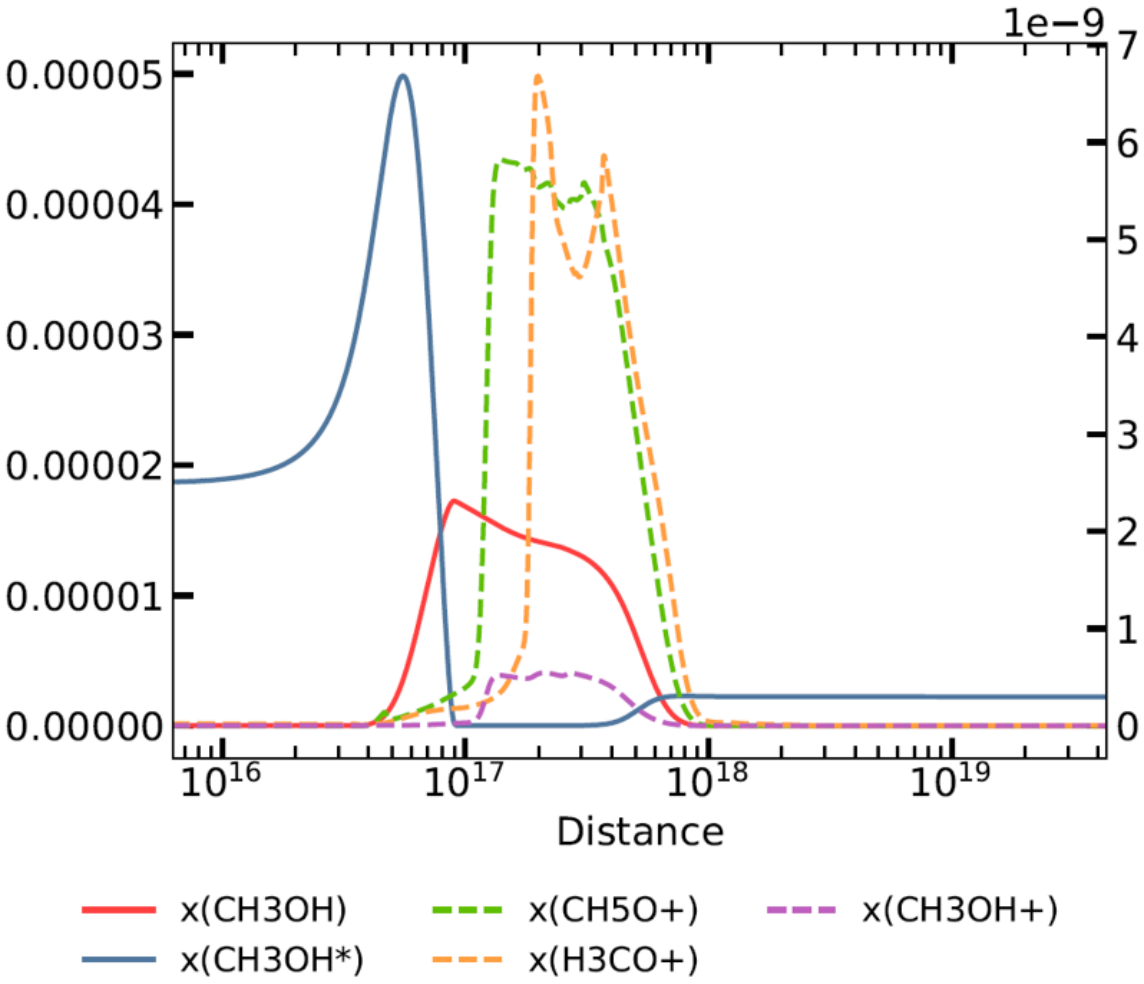

Figure 5.9: Evolution of the fractional abundance through a C-type shock for our molecules of interest. The x-axis represents the distance along the shock in cm. The left y-axis plots the fractional abundance of neutral species. The right y-axis plots the fractional abundance of ionic species.

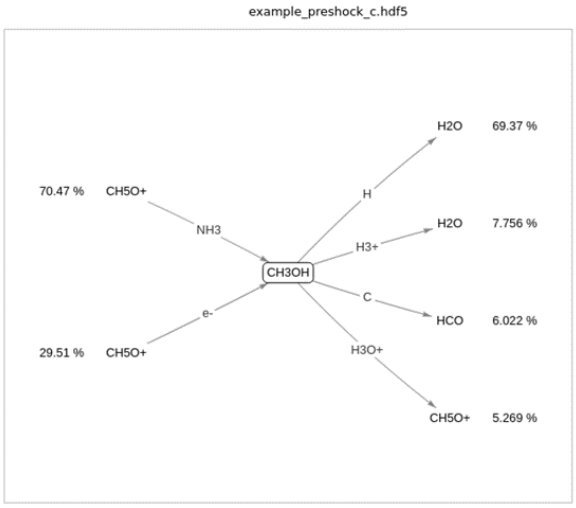

Formation of CH3OH — Total formation rate 1.51e-17 cm-3 s-1

A + B → C + D	n(A) (cm-3)	n(B) (cm-3)	k	rate (cm-3 s-1)	proportion
$CH_5O^+ + NH_3 \rightarrow NH_4^+ + CH_3OH$	5.16e-7	2.06e-2	1.00e-9	1.06e-17	70.47 %
$CH_5O^+ + e^- \rightarrow CH_3OH + H$	5.16e-7	6.02e-4	1.44e-8	4.46e-18	29.51 %

Destruction of CH3OH — Total destruction rate 1.08e-13 cm-3 s-1

A + B → C + D	n(A) (cm-3)	n(B) (cm-3)	k	rate (cm-3 s-1)	proportion
$CH_3OH + H \rightarrow CH_3 + H_2O$	2.21e-2	4.17e-1	8.13e-12	7.51e-14	69.37 %
$H_3^+ + CH_3OH \rightarrow CH_3^+ + H_2O + H_2$	3.40e-4	2.21e-2	1.11e-9	8.40e-15	7.756 %
$CH_3OH + C \rightarrow HCO + CH_3$	2.21e-2	9.82e-4	3.00e-10	6.52e-15	6.022 %
$H_3O^+ + CH_3OH \rightarrow CH_5O^+ + H_2O$	2.19e-4	2.21e-2	1.18e-9	5.70e-15	5.269 %

Figure 5.10: Chemistry of CH_3OH during the postshock phase in C-type shocks at a distance of $\sim 1 \times 10^{17}$ cm.

same order of magnitude, we never retrieve the initial level of adsorption of dust grains for CH_3OH.

Even if we can already guess the influence of the Ion-Neutral drift and the temperature, it is still useful to take a closer look at the chemistry of these elements. We plotted the major chemical reactions in Figures 5.10, 5.11, 5.12, 5.13 and 5.14. As we already know that the behavior of dust grains will have an impact on the chemistry, we plotted their evolution in Figure 5.15. This enables us to retrieve a possible idea of the evolution of the chemistry throughout a C-type shock with the Paris-Durham Shock code. In fact, the research was made top-down in the sense that we tried to understand what were the causes of the last mechanisms of the shock until we go back to its beginning. But, for the sake of clarity, we will show our results in the good sense. The evolution of CH_3OH in a C-type shock can thus be described as:

1. At the beginning of the shock – at $\sim 1 \times 10^{16}$ cm, the Ion-Neutral drift appears and begins to grow. CH_3OH is still in the reservoir of CH_3OH* and is not impacted. Instead of this, the ionic and neutral fluxes enhance the collisions between charged species and dust grains. Due to a good sticking coefficient for electrons, grains become negatively charged. The reaction $G + e^- \rightarrow G^- +$ photon is the only way to negatively charge grains in our chemical network (see the decrease in the abundance of neutral grains and the beginning of the increase in negatively charged grains in Figure 5.15).

2. As grains become charged with time, they enter the ionic flux and begin to encounter more and more neutral species such as CH_3OH. This will a little bit increase the adsorption rate even if it is here limited by the very low abundance of gas phase species. Concerning the dynamic of grains, there is a high concentration as we come closer to the shock front increasing the abundance of grains and thus of grain phase species such as CH_3OH*. This explains the high increase for grains in Figure 5.15

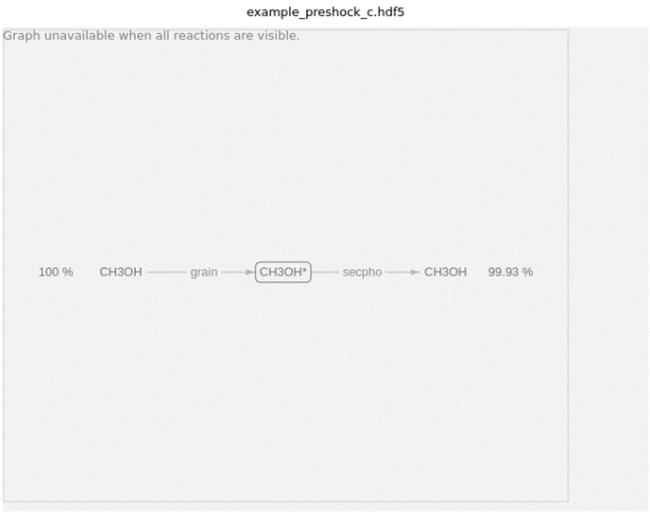

Formation of CH3OH*			Total formation rate 3.17e-16 cm-3 s-1		
A + B → C + D	n(A) (cm-3)	n(B) (cm-3)	k	rate (cm-3 s-1)	proportion
CH_3OH + grain → CH_3OH*	6.12e-3		5.17e-14	3.17e-16	100 %

Destruction of CH3OH*				Total destruction rate 8.15e-19 cm-3 s-1	
A + B → C + D	n(A) (cm-3)	n(B) (cm-3)	k	rate (cm-3 s-1)	proportion
CH_3OH^* + secpho → CH_3OH + grain	5.18e-2		1.57e-17	8.13e-19	99.82 %
CH_3OH^* + He → CH_3OH + He + grain	5.18e-2	1.08e+2	1.36e-22	7.64e-22	0.09381 %
CH_3OH^* + H_2 → CH_3OH + H_2 + grain	5.18e-2	5.41e+2	2.40e-23	6.73e-22	0.0826 %
CH_3OH^* + H → CH_3OH + H + grain	5.18e-2	3.15e-1	1.36e-23	2.22e-25	2.719e-05 %
CH_3OH^* + crp → CH_3OH + grain	5.18e-2		1.96e-33	1.02e-34	1.249e-14 %
CH_3OH^* + voisin → CH_3OH + grain	5.18e-2		4.40e-99	2.28e-100	2.799e-80 %
CH_3OH^* + photon → CH_3OH + grain	5.18e-2		0.00e+0	0.00e+0	0 %

Figure 5.11: Chemistry of CH_3OH^* during the postshock phase in C-type shocks at a distance of $\sim 6 \times 10^{16}$ cm.

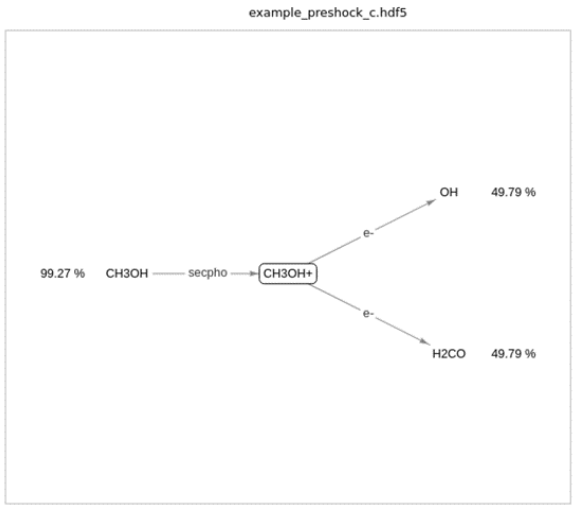

Formation of CH3OH+			Total formation rate 2.97e-17 cm-3 s-1		
A + B → C + D	n(A) (cm-3)	n(B) (cm-3)	k	rate (cm-3 s-1)	proportion
CH_3OH + secpho → CH_3OH^+ + e^-	8.15e-3		3.61e-15	2.95e-17	99.27 %

Destruction of CH3OH+				Total destruction rate 2.13e-18 cm-3 s-1	
A + B → C + D	n(A) (cm-3)	n(B) (cm-3)	k	rate (cm-3 s-1)	proportion
CH_3OH^+ + e^- → CH_3 + OH	7.23e-9	8.68e-4	1.69e-7	1.06e-18	49.79 %
CH_3OH^+ + e^- → H_2CO + H_2	7.23e-9	8.68e-4	1.69e-7	1.06e-18	49.79 %

Figure 5.12: Chemistry of CH_3OH^+ during the postshock phase in C-type shocks at a distance of $\sim 6 \times 10^{16}$ cm.

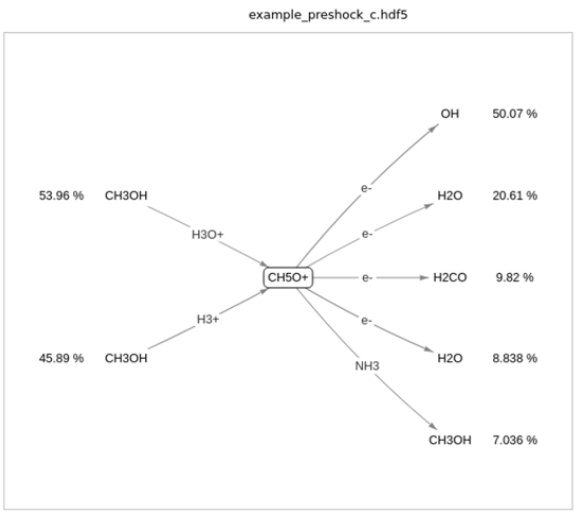

Formation of CH5O+ — Total formation rate 1.06e-14 cm-3 s-1

A + B → C + D	n(A) (cm-3)	n(B) (cm-3)	k	rate (cm-3 s-1)	proportion
$H_3O^+ + CH_3OH \rightarrow CH_5O^+ + H_2O$	2.19e-4	2.21e-2	1.18e-9	5.70e-15	53.96 %
$H_3^+ + CH_3OH \rightarrow CH_5O^+ + H_2$	3.40e-4	2.21e-2	6.44e-10	4.85e-15	45.89 %

Destruction of CH5O+ — Total destruction rate 1.51e-16 cm-3 s-1

A + B → C + D	n(A) (cm-3)	n(B) (cm-3)	k	rate (cm-3 s-1)	proportion
$CH_5O^+ + e^- \rightarrow CH_3 + OH + H$	5.16e-7	6.02e-4	2.44e-7	7.58e-17	50.07 %
$CH_5O^+ + e^- \rightarrow CH_2 + H_2O + H$	5.16e-7	6.02e-4	1.01e-7	3.12e-17	20.61 %
$CH_5O^+ + e^- \rightarrow H_2CO + H_2 + H$	5.16e-7	6.02e-4	4.79e-8	1.49e-17	9.82 %
$CH_5O^+ + e^- \rightarrow CH_3 + H_2O$	5.16e-7	6.02e-4	4.31e-8	1.34e-17	8.838 %
$CH_5O^+ + NH_3 \rightarrow NH_4^+ + CH_3OH$	5.16e-7	2.06e-2	1.00e-9	1.06e-17	7.036 %

Figure 5.13: Chemistry of CH_5O^+ during the postshock phase in C-type shocks at a distance of $\sim 1 \times 10^{17}$ cm.

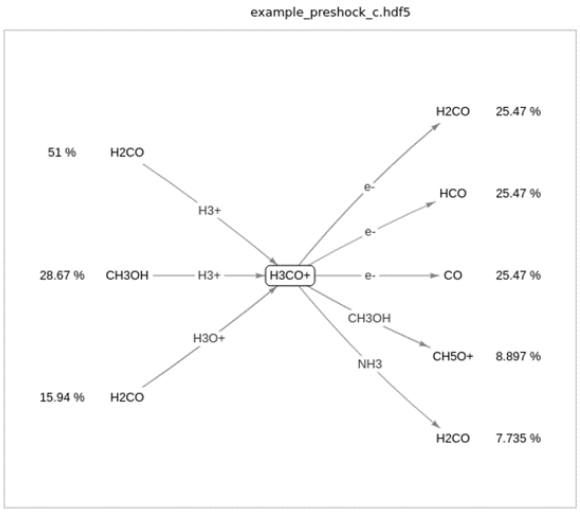

Formation of H3CO+ — Total formation rate 1.82e-14 cm-3 s-1

A + B → C + D	n(A) (cm-3)	n(B) (cm-3)	k	rate (cm-3 s-1)	proportion
$H_3^+ + H_2CO \rightarrow H_3CO^+ + H_2$	3.40e-4	7.84e-3	3.48e-9	9.29e-15	51 %
$H_3^+ + CH_3OH \rightarrow H_3CO^+ + H_2 + H_2$	3.40e-4	2.21e-2	6.94e-10	5.22e-15	28.67 %
$H_3O^+ + H_2CO \rightarrow H_3CO^+ + H_2O$	2.19e-4	7.84e-3	1.69e-9	2.90e-15	15.94 %

Destruction of H3CO+ — Total destruction rate 7.23e-17 cm-3 s-1

A + B → C + D	n(A) (cm-3)	n(B) (cm-3)	k	rate (cm-3 s-1)	proportion
$H_3CO^+ + e^- \rightarrow H_2CO + H$	2.47e-7	6.02e-4	1.24e-7	1.84e-17	25.47 %
$H_3CO^+ + e^- \rightarrow HCO + H + H$	2.47e-7	6.02e-4	1.24e-7	1.84e-17	25.47 %
$H_3CO^+ + e^- \rightarrow CO + H_2 + H$	2.47e-7	6.02e-4	1.24e-7	1.84e-17	25.47 %
$H_3CO^+ + CH_3OH \rightarrow CH_5O^+ + H_2CO$	2.47e-7	2.21e-2	1.18e-9	6.43e-18	8.897 %
$H_3CO^+ + NH_3 \rightarrow NH_4^+ + H_2CO$	2.47e-7	2.06e-2	1.10e-9	5.59e-18	7.735 %

Figure 5.14: Chemistry of H_3CO^+ during the postshock phase in C-type shocks at a distance of $\sim 1 \times 10^{17}$ cm.

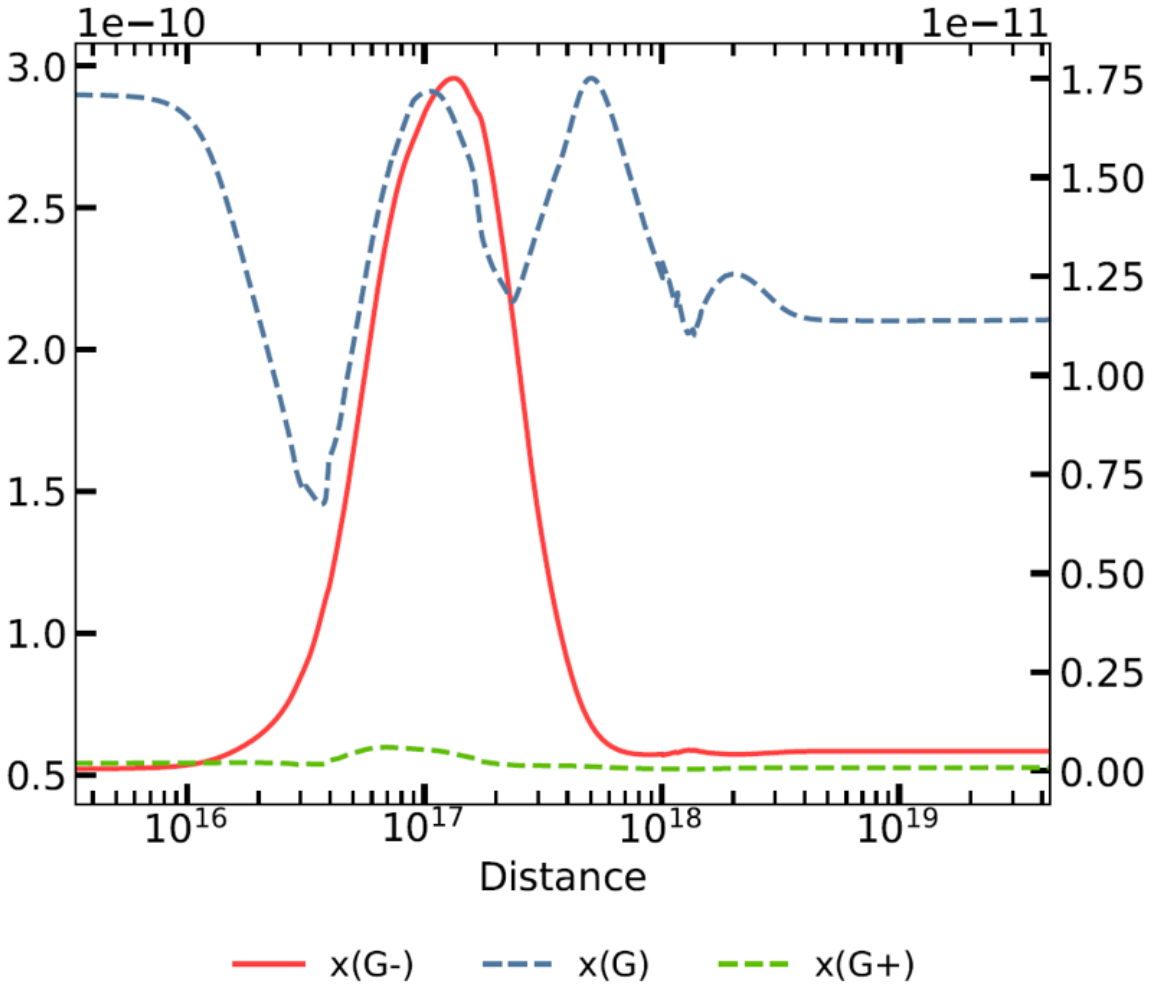

Figure 5.15: Evolution of the fractional abundance through a C-type shock for dust grains. The x-axis represents the distance along the shock in cm. The left y-axis plots the fractional abundance of negatively charged grains. The right y-axis plots the fractional abundance of neutral and positively charged grains.

and the high increase for CH_3OH^* in Figure 5.9.

3. At $\sim 5 \times 10^{16}$ cm, the Ion-Neutral drift is close to its maximum and the temperature is enhanced to 600 K (knowing that it was about ~ 50 K before the shock). These two aspects will enhance collisions between grains and neutral species such as He, H_2, and H and will provoke via sputtering the release of CH_3OH into the gas phase. In parallel, we see that the increase in CH_3OH in the gas phase is totally proportional to the decrease in its grain phase homologue (see Figure 5.9).

4. The abrupt increase in CH_3OH is partially counterbalanced by the enhancement of destructive processes (see Figure 5.10). This explains why the number of released CH_3OH^* is not exactly equal to the number of arriving CH_3OH. In every case, the increase in CH_3OH will now activate all the reactions where it is a reactant in the chemical network (Figure 5.4). This explains the following increase of CH_5O^+, CH_3OH^+, and H_3CO^+ with some delay compared to the apparition of CH_3OH.

5. The formation of CH_5O^+ will be the first to be activated. The reason is that it is formed by collisions between CH_3OH with cations (see Figure 5.13). These reactions are now highly enhanced by the Ion-Neutral drift. It is followed by the formation of H_3CO^+ that will also be enhanced by the Ion-Neutral drift (see Figure 5.14). Nevertheless, H_3CO^+ seems to take an important part of the chemical network of H_2CO and its understanding is thus out of the scope of this discussion. We will thus from now focus on the other molecules. The formation of the cation CH_3OH^+ will be the last one to be activated. This is because it is only formed by photoionization (see Figure 5.12). It is enhanced by the huge amount of CH_3OH, but does not benefit from the Ion-Neutral drift as the other cations.

6. At $\sim 1 \times 10^{17}$ cm, as the efficiency of destructive reactions increases with the abundance of reactants, we reach a plateau where the chemistry of CH_3OH and CH_5O^+ is mostly equilibrated. The destruction of CH_3OH is now greater than formation processes but is still very attenuated. We now have a very good coupling between CH_3OH and CH_5O^+ (Figures 5.10 and 5.13) that will form each other, justifying the kind of plateau. (The quantity of CH_5O^+ formed is proportional to the abundance of CH_3OH.) From other measures, we also know that the transformation of CH_5O^+ into CH_3OH will be enhanced by a huge increase in the amount of NH_3 in the medium as we go through the shock front. This reinforces the connection between them.

7. At $\sim 4 \times 10^{17}$ cm, the Ion-Neutral drift and the enhancement by the temperature stop. The destruction processes begin to take the lead and we notice a slow decrease of the gas phase molecules (see Figure 5.9). A small part of the CH_3OH molecules will be saved on dust grains knowing that sputtering processes have been deactivated. But it will not retrieve the same values as before due to the strength of the destructive processes. We can also see in Figure 5.15 that the grain densities come back to normal even if we finish with a small enhancement of negatively charged grains. Even if it is not directly visible due to the different scales, we retrieve similar

quantities of grains. This was expected as destructive processes such as grain-grain collisions are not included in the Paris-Durham Shock code (but are not very efficient at these relatively low densities). Nevertheless, all of this part is out of the postshock region and does not account for the enhancement and comparison factors.

This story concludes the behavior of our main molecular tracer in C-type shocks. But three main points have to be emphasized:

- The chemistry is highly activated by the increase of some species in the gas phase and the temperature. This increase is mainly due to the release in two steps (charging of grains and sputtering) of grain phase species with the help of the Ion-Neutral drift. The Ion-Neutral drift is thus fundamental to the chemistry of C-type shocks. As it is dependent on the velocity, we can expect that the differences between C-type and J-type shocks will grow with the shock velocity.

- The behavior of CH_3OH is very well coupled with CH_5O^+. This is not the case with its ionic homologue CH_3OH^+. The reason is that the ionization is highly dependent on processes with photons that are not enhanced by the Ion-Neutral drift. Other reactions are difficult to imagine as collisions with other species often lead to fragmentation. CH_3OH and CH_5O^+ benefits from a good interplay enhanced by the Ion-Neutral drift.

- The rise of the temperature over a long distance tends to enhance the chemical kinetics and thus the presence of a plateau – a first equilibrium between formation and destruction reactions.

Of course, even if this story takes into account and explains each element represented in our graphics, it does not go into all the details of the chemistry of interstellar shocks. At this level (meaning with this method), it is not possible to be fully exhaustive and some points can be slightly different in reality. Nevertheless, we have to be honest by specifying that there exists a specific dark spot in our explanations. Point 2. talks about a higher concentration of dust grains leading to an increase in the fractional abundance of CH_3OH^*. Even if this interpretation is plausible, we are not sure that it does not come from a specificity of the Paris-Durham Shock code while it interprets the evolution of the icy mantles. Better methods with detailed grain dynamics in shocks should be able to decide on a solution. But in every case, even if it is a "dark spot" of our theory, it is not very relevant. The increase in grain abundance only multiplies the abundance of CH_3OH^* by a factor of 2.5. The release of grain phase species should thus lead to a number of CH_3OH molecules in the gas phase of the same order of magnitude as before. In short, even if we are not sure about the physical meaning of Point 2, it does not change the following reasoning.

5.2.3 The postshock region in J-type shocks

We will now attack the behavior of CH_3OH in J-type shocks. This type of shock is characterized by a low magnetic field and thus a very good coupling between the ionic

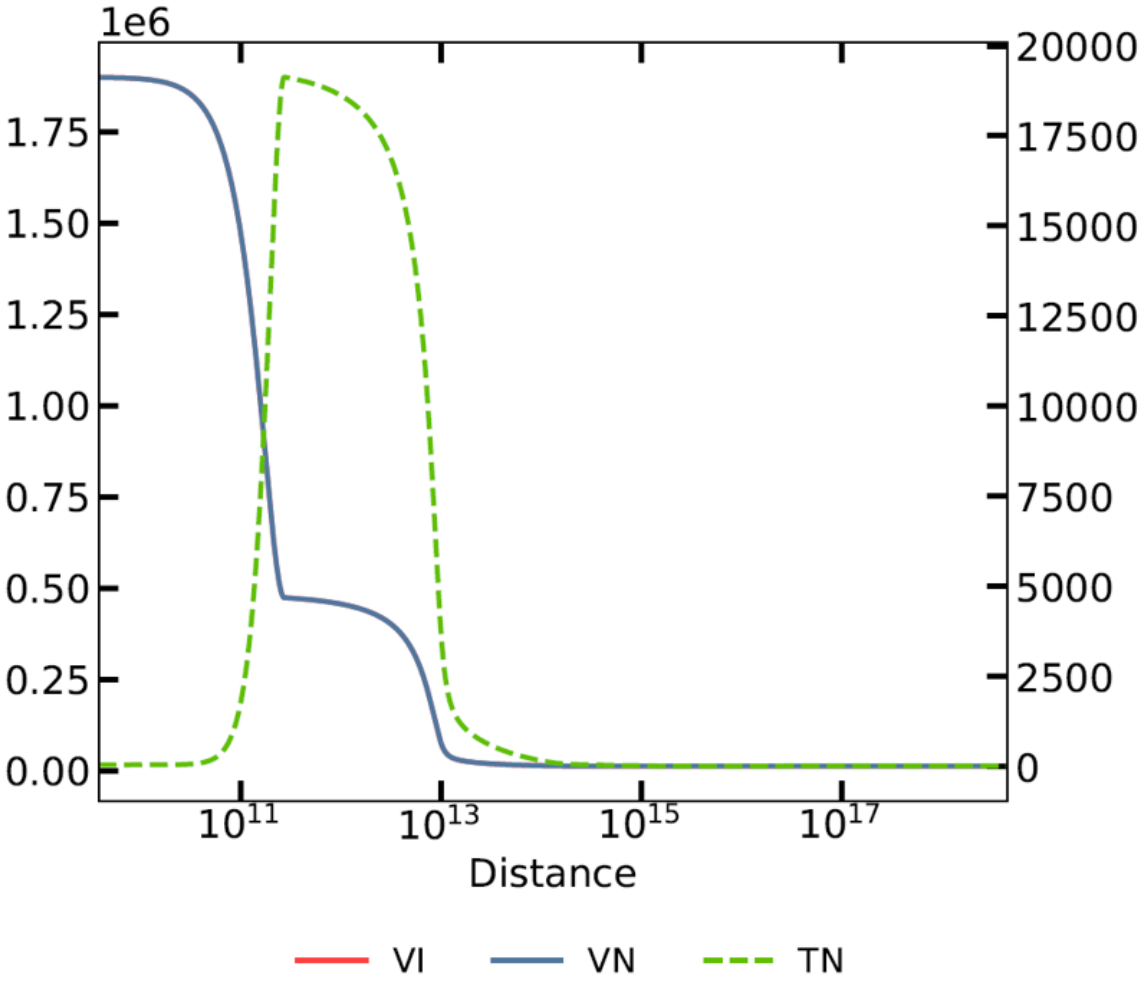

Figure 5.16: Evolution of the physical parameters through a J-type shock. The x-axis represents the distance along the shock in cm. The left y-axis plots the velocities of the ionic and neutral fluxes in cm s^{-1}. The right y-axis plots the temperature in K.

and the neutral species. (Computationally, we only consider one fluid when we simulate J-type shocks.) Again, our reasoning will be based on the physical and chemical evolution of the properties of the shock (Figure 5.16), the abundance of our molecules of interest (Figures 5.17 and 5.18), their chemistry (Figures 5.19, 5.20, 5.21, and 5.22), and the dust grains (Figure 5.23). Again, we analyze of shock at $nH = 10^3$ cm^{-3} and $Vs = 19$ km s^{-1}.

As expected, the physics of J-type shocks is simpler than for C-type shocks (Figure 5.16). There is no differentiation between the velocities and there is thus no Ion-Neutral drift through the shock. The only notable element is the huge increase in temperature at $\sim 1 \times 10^{11}$ cm to ~ 18000 K which will be stopped at $\sim 1 \times 10^{13}$ cm. The length scale is thus much smaller than the one used for C-type shocks. Concerning the evolution of the fractional abundance, no real disturbance is predicted for the grain phase with CH_3OH* (Figure 5.17). The gas phase still benefits from an increase in the abundance at $\sim 1 \times 10^{12}$ cm for neutrals and $\sim 1 \times 10^{13}$ cm for ions (Figure 5.18). However, this increase is only of

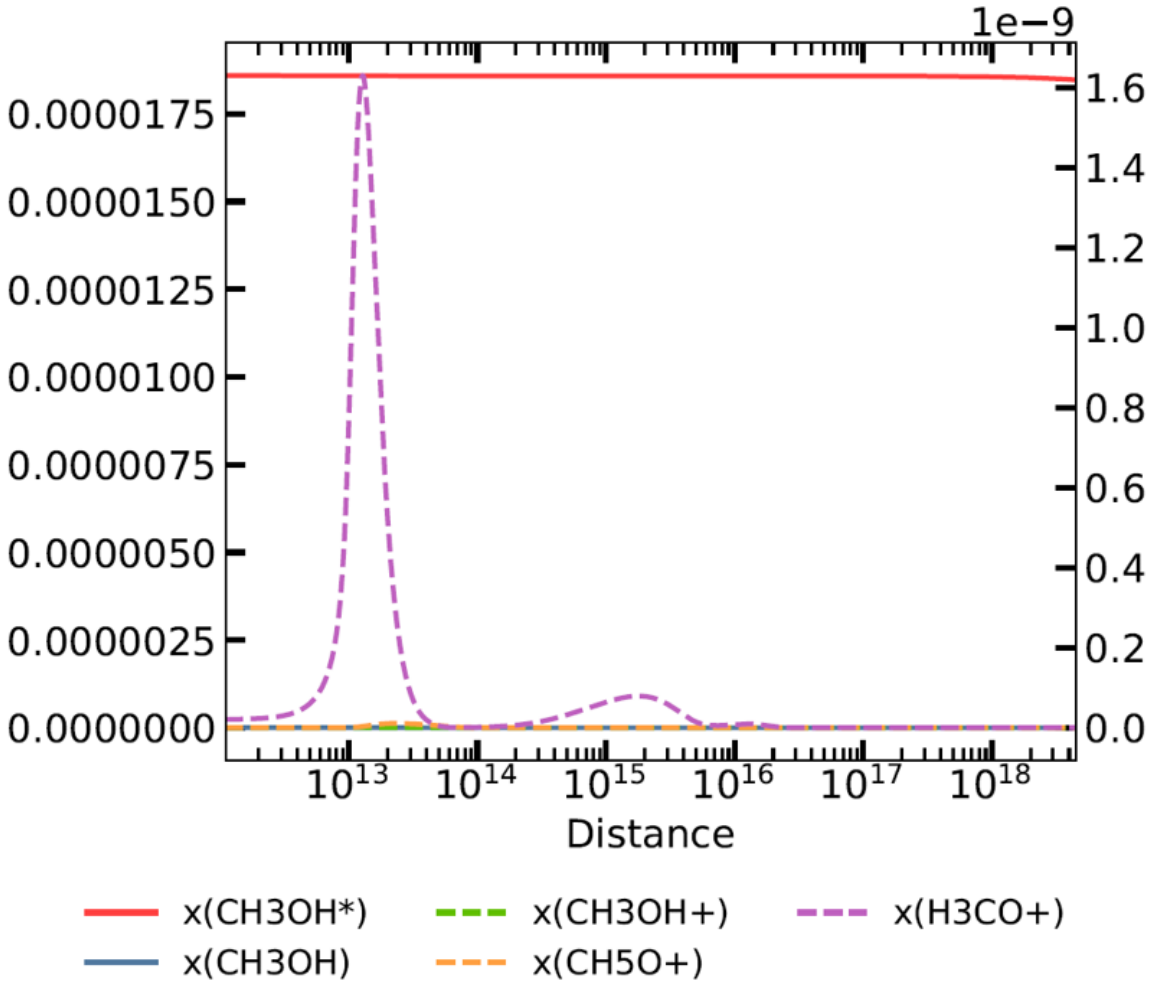

Figure 5.17: Evolution of the fractional abundance through a J-type shock for our molecules of interest. The x-axis represents the distance along the shock in cm. The left y-axis plots the fractional abundance of neutral species. The right y-axis plots the fractional abundance of ionic species.

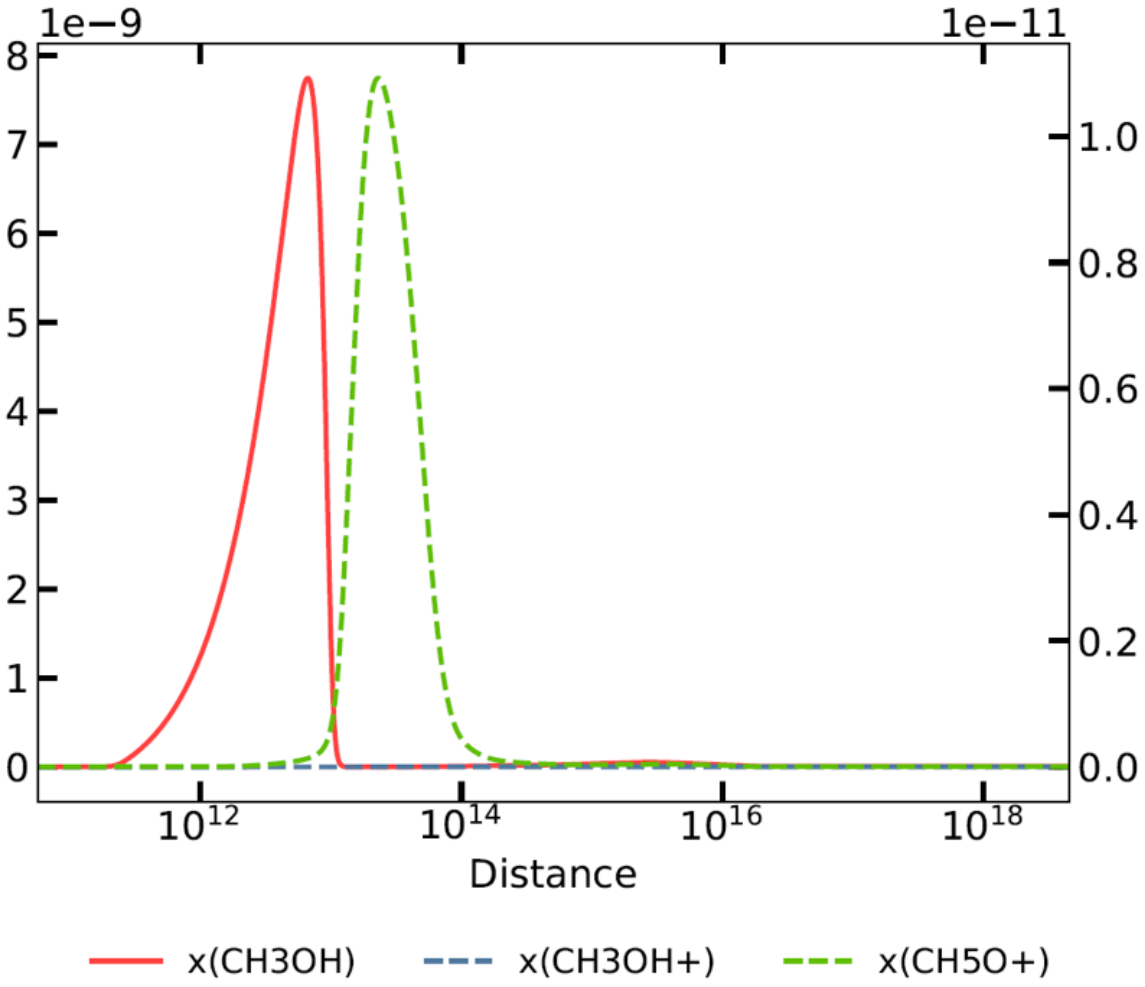

Figure 5.18: Evolution of the fractional abundance through a J-type shock for our molecules of interest. The x-axis represents the distance along the shock in cm. The left y-axis plots the fractional abundance of neutral species. The right y-axis plots the fractional abundance of ionic species. Compared to before, the graphic is now focused on the evolution of CH_3OH and CH_5O^+ - the two most interesting molecules of the previous discussion. Even if it is not visible here, CH_3OH^+ also benefits from an increase during the shock.

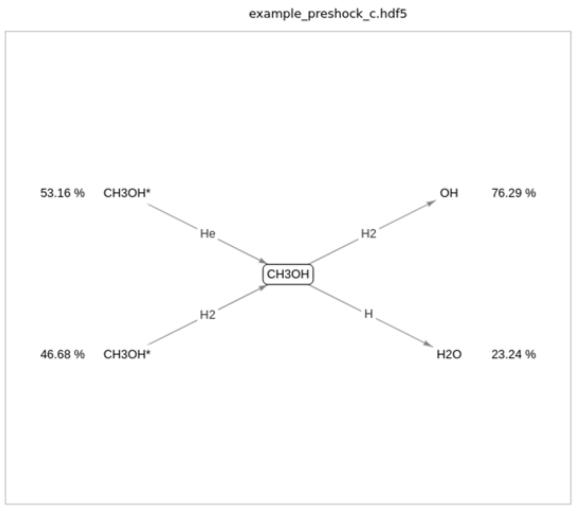

Formation of CH3OH — Total formation rate 3.10e-12 cm-3 s-1

A + B → C + D	n(A) (cm-3)	n(B) (cm-3)	k	rate (cm-3 s-1)	proportion
CH_3OH^* + He → CH_3OH + He + grain	7.72e-2	4.15e+2	5.15e-14	1.65e-12	53.16 %
CH_3OH^* + H_2 → CH_3OH + H_2 + grain	7.72e-2	2.07e+3	9.06e-15	1.45e-12	46.68 %

Destruction of CH3OH — Total destruction rate 7.76e-14 cm-3 s-1

A + B → C + D	n(A) (cm-3)	n(B) (cm-3)	k	rate (cm-3 s-1)	proportion
CH_3OH + H_2 → CH_3 + OH + H_2	5.17e-6	2.07e+3	5.53e-12	5.92e-14	76.29 %
CH_3OH + H → CH_3 + H_2O	5.17e-6	1.23e+1	2.84e-10	1.80e-14	23.24 %

Figure 5.19: Chemistry of CH_3OH during the postshock phase in J-type shocks at a distance of $\sim 1 \times 10^{12}$ cm.

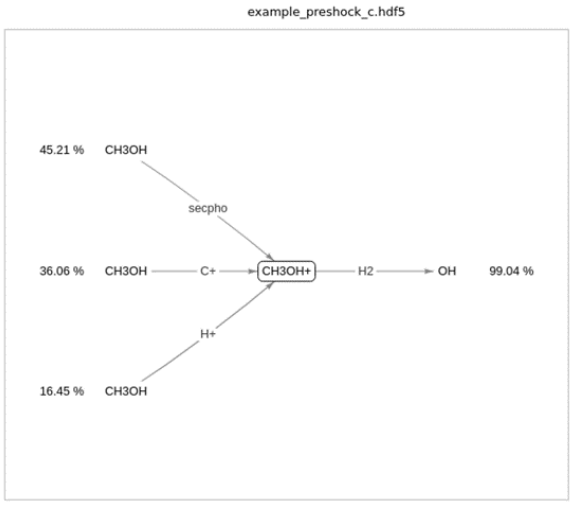

Formation of CH3OH+ — Total formation rate 1.22e-19 cm-3 s-1

A + B → C + D	n(A) (cm-3)	n(B) (cm-3)	k	rate (cm-3 s-1)	proportion
CH_3OH + secpho → CH_3OH^+ + e^-	5.17e-6		1.06e-14	5.50e-20	45.21 %
C^+ + CH_3OH → CH_3OH^+ + C	8.16e-5	5.17e-6	1.04e-10	4.39e-20	36.06 %
H^+ + CH_3OH → CH_3OH^+ + H	5.17e-5	5.17e-6	7.49e-11	2.00e-20	16.45 %

Destruction of CH3OH+ — Total destruction rate 3.46e-21 cm-3 s-1

A + B → C + D	n(A) (cm-3)	n(B) (cm-3)	k	rate (cm-3 s-1)	proportion
CH_3OH^+ + H_2 → CH_3^+ + OH + H_2	1.51e-13	2.07e+3	1.10e-11	3.43e-21	99.04 %

Figure 5.20: Chemistry of CH_3OH^+ during the postshock phase in J-type shocks at a distance of $\sim 1 \times 10^{12}$ cm.

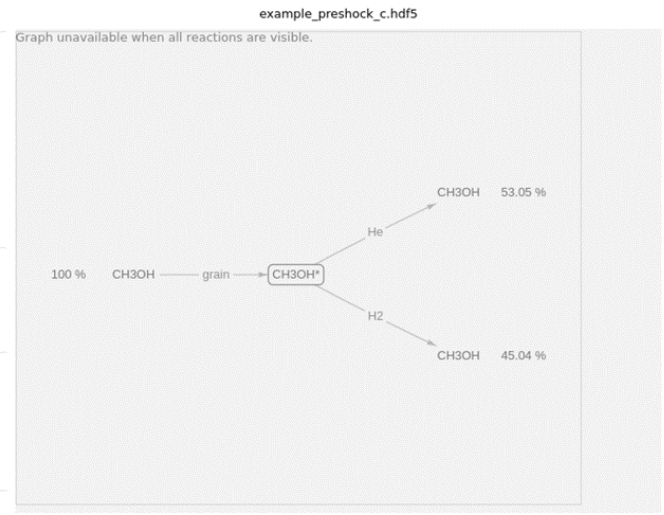

Formation of CH3OH* — Total formation rate 5.92e-21 cm-3 s-1

A + B → C + D	n(A) (cm-3)	n(B) (cm-3)	k	rate (cm-3 s-1)	proportion
CH_3OH + grain → CH_3OH*	5.17e-6		1.14e-15	5.92e-21	100 %

Destruction of CH3OH* — Total destruction rate 3.10e-12 cm-3 s-1

A + B → C + D	n(A) (cm-3)	n(B) (cm-3)	k	rate (cm-3 s-1)	proportion
CH_3OH^* + He → CH_3OH + He + grain	7.72e-2	4.15e+2	5.15e-14	1.65e-12	53.16 %
CH_3OH^* + H_2 → CH_3OH + H_2 + grain	7.72e-2	2.07e+3	9.06e-15	1.45e-12	46.68 %
CH_3OH^* + H → CH_3OH + H + grain	7.72e-2	1.23e+1	5.13e-15	4.86e-15	0.1566 %
CH_3OH^* + secpho → CH_3OH + grain	7.72e-2		3.85e-17	2.97e-18	9.571e-05 %
CH_3OH^* + crp → CH_3OH + grain	7.72e-2		1.62e-33	1.25e-34	4.041e-21 %
CH_3OH^* + voisin → CH_3OH + grain	7.72e-2		7.30e-93	5.64e-94	1.815e-80 %
CH_3OH^* + photon → CH_3OH + grain	7.72e-2		0.00e+0	0.00e+0	0 %

Figure 5.21: Chemistry of CH_3OH^* during the postshock phase in J-type shocks at a distance of $\sim 1 \times 10^{12}$ cm.

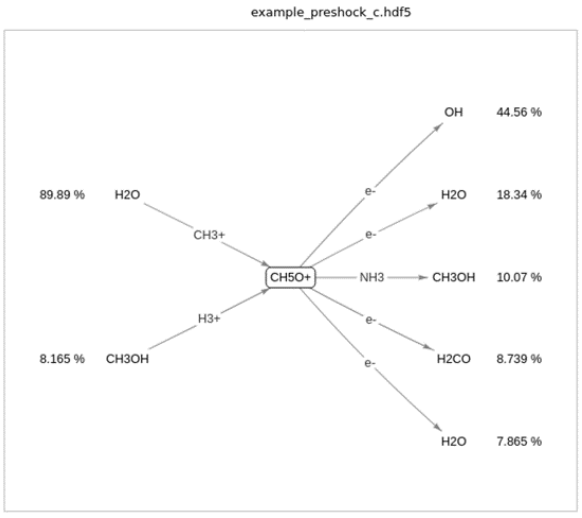

Formation of CH5O+ — Total formation rate 7.88e-16 cm-3 s-1

A + B → C + D	n(A) (cm-3)	n(B) (cm-3)	k	rate (cm-3 s-1)	proportion
CH_3^+ + H_2O → CH_5O^+ + photon	3.65e-4	9.71e-1	2.00e-12	7.08e-16	89.89 %
H_3^+ + CH_3OH → CH_5O^+ + H_2	5.87e-3	3.77e-5	2.91e-10	6.43e-17	8.165 %

Destruction of CH5O+ — Total destruction rate 2.10e-17 cm-3 s-1

A + B → C + D	n(A) (cm-3)	n(B) (cm-3)	k	rate (cm-3 s-1)	proportion
CH_5O^+ + e^- → CH_3 + OH + H	1.45e-8	7.68e-3	8.42e-8	9.37e-18	44.56 %
CH_5O^+ + e^- → CH_2 + H_2O + H	1.45e-8	7.68e-3	3.46e-8	3.86e-18	18.34 %
CH_5O^+ + NH_3 → NH_4^+ + CH_3OH	1.45e-8	1.46e-1	1.00e-9	2.12e-18	10.07 %
CH_5O^+ + e^- → H_2CO + H_2 + H	1.45e-8	7.68e-3	1.65e-8	1.84e-18	8.739 %
CH_5O^+ + e^- → CH_3 + H_2O	1.45e-8	7.68e-3	1.49e-8	1.65e-18	7.865 %

Figure 5.22: Chemistry of CH_5O^+ during the postshock phase in J-type shocks at a distance of $\sim 1 \times 10^{13}$ cm.

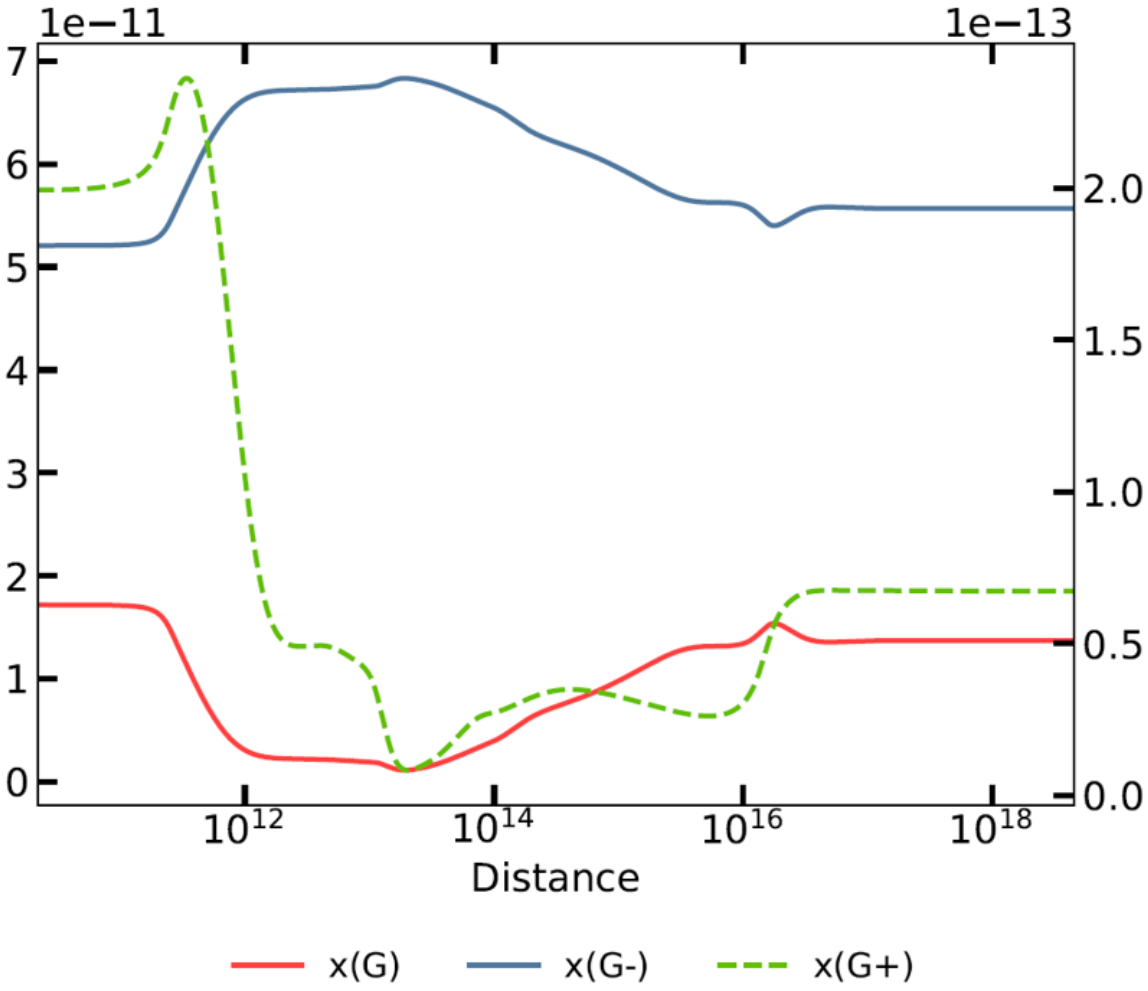

Figure 5.23: Evolution of the fractional abundance through a C-type shock for dust grains. The x-axis represents the distance along the shock in cm. The left y-axis plots the fractional abundance of negatively charged grains and neutral grains. The right y-axis plots the fractional abundance of positively charged grains.

the order of 10^5 for CH_3OH which is not comparable with the results for C-type shocks. One could notice that this number is greater than the enhancement factor for this shock model. This is simply because the enhancement factor is based on an average value and not a maximum. As before, it is possible to read all our graphics to track down the story of CH_3OH in J-type shocks:

1. The first step is thus the high increase in the temperature at $\sim 1\times10^{11}$ cm due to the normal evolution of shocks. The increase in thermal energy will affect the number of collisions between grains and electrons and it will lead to a rise of negatively charged grains (Figure 5.23). Due to the efficiency of the process and the lack of external photons, these electrons will take advantage compared to positive ions. As we are mainly determined by the temperature, we could expect this behavior as the mean speed for particles is proportional to $m^{-1/2}$ where m is the mass. It is thus clear that light particles such as the electrons move faster than the positive ions.

2. Despite the charge of grains, we do not have any Ion-Neutral drift as the fluids are coupled, and the sputtering of grains is only fed by thermally agitated He, H, and H_2 (see Figure 5.21). This will lead to a gradual rise of CH_3OH molecules in the gas phase (see Figure 5.18). The increase is not comparable to C-type shocks but will be the main way to extract CH_3OH from the grain phase reservoir. We note that as the processes take a certain amount of time, we observe a delay between the increase in temperature and the increase in CH_3OH in the gas phase.

3. The release of CH_3OH is small but is the only way to create CH_3OH^+ (see Figure 5.20). Knowing that the high temperature also enhances destructive processes for CH_3OH (see Figure 5.19), the increase will never be comparable to its homologue CH_5O^+. Concerning this last molecule, even if it is a little bit influenced by the release of CH_3OH, its apparition mainly comes from the enhanced formation reactions from H_2O with CH_3^+ but the destructive processes are also enhanced. Again, let's remark on the importance of electrons in dissociative electron recombination that is justified by the small mass of the electron. We thus only have a small increase in the abundance (see Figure 5.22). An interesting point is the presence of a delay between the formation of neutrals from the release of grain phase species in the first step and the formation of ions from these neutrals in the second step. In conclusion, we never reach a good coupling between CH_3OH and CH_5O^+.

4. At a distance of $\sim 1\times10^{13}$ cm, the shock stops and the temperature drops to its initial value. Formation processes are not enhanced anymore while destructive processes are still active due to the high density of the reactants. The abundance will thus drop to the normal. Again, we have a delay between the destruction of ions and neutrals which is the expected consequence of a delay in their formation. The medium goes back to its normal.

This was thus the story of CH_3OH in J-type shocks. The main difference with C-type shocks is the absence of the Ion-Neutral drift that will, in fine, prevent a good release of the neutral species trapped in the grain phase. The only processes of desorption are

due to the thermal agitation of particles. Given that and the high temperature, we still have an enhancement of the chemistry. But even if we have a high temperature, it is over a small distance and we thus do not retrieve an efficiency as in C-type shocks. One can argue that we should still have thermal desorption. Unfortunately (or fortunately for the relevance of our shock models), the grains stay at low temperatures and the binding energy of CH_3OH is at 3820 K in our chemical network. Even if we take into account the work of Miura et al. 2017, we can only have at maximum a desorption ratio at $\sim 1 \times 10^{-2}$. Even if it will change all our quantitative results for J-type shocks, it is still negligible compared to the desorption ratio in C-type shocks which is very close to 1 in our shock models. In conclusion, for these velocities, C-type shocks are way better than J-type shocks in enhancing the chemistry of CH_3OH.

5.2.4 A final look into the comparison factor

Before finishing the discussion of this master's thesis, we can take advantage of these last pages to discuss one more time the look of the comparison factor – Figure 7.7 (and the enhancement factors – Figures 7.8 and 7.9) of CH_3OH. Indeed, even if we now understand the chemistry for shocks with a velocity greater than 12 km s^{-1}, the left part of the graphic is still intriguing. Let's analyze that:

- **Why do we have a barrier at 12 km s^{-1}?** The answer directly comes from Figure 5.3. The effective temperature needed to activate the sputtering reactions between the grains and atoms of helium or molecules of H_2 is directly proportional to Vs^2. When we pass the barrier of 12 km s^{-1}, the effective temperature becomes largely greater than the adsorption energy (3820 K). Given that, the sputtering is now active, and C-type shocks can differentiate from J-type shocks.

- **Why do we have an increase in the comparison factor when we increase the shock velocity in the left part of Figure 7.7?** Before the frontier of 12 km s^{-1}, C-type shocks essentially act as J-type shocks as the determining factor is the ratio of desorbed species. Nevertheless, there is still a differentiation because of the thermal agitation of particles. This thermal agitation increases with the temperature and the temperature increases much faster in J-type shocks than in C-type shocks. Even if the scales of distance are not the same, the very high temperature in J-type shocks compensates.

- **Why do we have an increase in the comparison factor when we increase the density in the left part of Figure 7.7?** The answer is close to the previous one. The best way to release species from the grain phase comes from collisions with gas phase species. These collisions are enhanced by the temperature, and by the density. The answer should thus stand in the fact that a dense gas will be better for sputtering at high temperatures than at low temperatures. This is why the increase of efficiency in J-type shocks with the velocity is better at high densities than at low densities.

This finishes explaining the behavior of CH_3OH in low-velocity interstellar shocks.

One purpose of this chapter was to understand the chemistry of these shocks, another was also to justify or not the relevance of CH_3OH as a molecular tracer (it was the most impacting one in the previous discussion). Can we thus consider CH_3OH to be reliable? The answer should be yes as the basics of the chemical theory of interstellar shocks succeed in consistently explaining its evolution. We also proved that the main limitation of our grain treatment was not mainly impacting the behavior of CH_3OH due to the importance of non-thermal desorption processes. We can conclude that chemical considerations enable judging a shock model's consistency. Of course, writing the evolution of a shock from an astrochemical perspective also enabled us to deeply understand how shocks influence the chemical behavior of the medium (through the temperature, but also with the ion-neutral drift, the sputtering, ...)

Chapter 6

Conclusion

6.1 A summary

Being at the frontier of chemistry and astrophysics, astrochemistry is still a new field of study compared to the giants it combines. The chemical point of view is not often taken to observe and analyze astrophysical environments such as star births, planetary formation, or, in our case, interstellar shocks. However, the influence of physical conditions and the evolution of these physical conditions leave a signature in the abundance of chemical species that can be very enlightening information for astronomers. Astrochemistry enables us to make and understand the links between these physical conditions and chemical evolution. In this way, astrochemists create a chemical identity card to characterize the studied environments. From another point of view, astronomers tend to increase the number of methods to analyze and apprehend the multitude of astrophysical objects given the diversity of processes occurring in outer space. Astrochemistry is thus in perfect adequacy with this trend of modern astronomy.

This Master's thesis is part of this 'astrochemistry' objective, as a way of looking at space with fresh eyes – more specifically to look at interstellar shocks. Indeed, the physics of shocks is known to be diversified given the number of physical processes taking place in them (we have seen the effects of the velocity, the density, the magnetic field, the presence of ions and neutrals, ...). Knowing that, it is clear that scientists should find it useful to have observational constraints that are dependent on the physical conditions to characterize these shocks. The chemistry of shocks was thus the red thread of this Master's thesis. Taking advantage of the format of a master's thesis, we began our investigation with a quite large review of the basic knowledge of what is the interstellar medium and of what are the components of astrochemistry in **Chapter 1**. We have built the bases by defining the two research questions that have guided our research:

- How can we make use of astrochemistry to characterize interstellar shocks?
- How do shocks influence the overall chemistry of the interstellar medium?

To undertake this research, we described in **Chapter 2** the physics of interstellar shocks and the Paris-Durham shock code that was the main tool used in all our work. As this master's thesis wanted to move away from previous research that parametrized the physics of shocks to study the chemistry in them, we have chosen a code that computed the physics and the chemistry in parallel. In this way, it became possible to incorporate in our simulations the interplay that exists between the physical and chemical evolution of the medium such as the cooling processes for example. This dynamic point of view was made possible given the recent updates (May 2022) brought to the Paris-Durham Shock code. With this tool, we simulated a complete set of interstellar shocks with different densities, shock velocities, and types. The parameters of these simulations were discussed in **Chapter 3**. In that chapter, we also defined the main mathematical objects we needed to compare computations and observations: the enhancement and comparison factors. These factors made the ratio between the abundance in a shocked and in a quiescent region for each chemical element in our chemical network. With this data at our disposal, the first point was that shocks were very strongly associated with changes in the chemical conditions of the medium.

All our results were discussed in **Chapters 4 and 5**. **Chapter 4** discussed our first research question on the possibility of using astrochemistry as a way to analyze interstellar shocks. To be in the continuity of current scientific research, we began this chapter with a deep description of previous works (to know what was already known) and we enlightened the differences between their results and ours. The answer was there were profound and contradictory differences in the results we achieved. We argued that they were mainly due to the treatment of grains in our code and put limitations on what has been done in their and our works. After that, and to answer our first research question, we analyzed the real case of L1157 B2 – a shocked region near a protostar and identified the possible parameters able to define at best the physics in it. We found as in previous research that it was a low-velocity shock with – when we put the scientific efforts in common – a C-type shock behavior. We also found that CH_3OH, H_2S, and CN were good molecular tracers in this context with a big preference for CH_3OH Nevertheless, this did not exclude the possibility of a multi-component shocked region and we did not determine the density of the medium. With the purpose of understanding and justifying the relevance of our methods, we analyzed and described the physical processes able to influence the chemistry of shocks in **Chapter 5**. Basing our discussion on our best molecular tracer CH_3OH, we told the story of the evolution of this molecule through C-type and J-type shocks to emphasize the differences. This enabled us at the same time to clearly understand the various patterns we predict from comparison factors. Indeed, we discovered that methanol was mainly trapped in dust surfaces and all the chemical differences between these two shock types mainly reside in the efficiency of C-type shocks to release molecules in the gas phase through the sputtering enhanced by the ion-neutral drift. This explains why we have a huge increase in the abundance of C-type shocks when the velocity exceeds 12 km s^{-1} as the sputtering is now activated by a sufficient effective temperature. By doing so, we answered our second research question.

And now, in this final **Chapter 6** concluding our master's thesis, we will address the last interesting points of our research and will bring some ideas and remarks about the

future of astrochemistry as a way to investigate space.

6.2 The research questions

Even if we already answered our research questions through Chapters 4 and 5. The answers were quite diffused in the main text and, after more than one hundred pages, it can be useful to summarize what were the main conclusions we achieved in our two discussions. Of course, we invite the reader to go back to the discussion chapters to have a complete answer to our research questions.

How can we make use of astrochemistry to characterize interstellar shocks? Through our discussion in Chapter 4, we defined a method to characterize the main parameters of interstellar shocks using astrochemistry: the shock velocity, the preshock density, and the shock type. Based on a complete set of simulations where dynamic and chemical equations were coupled and computed, we found the enhancement factor (Eq. 3.1) (ratio between the abundance in postshock and preshock regions) for each species in our chemical network. By comparing these enhancement factors with available data, we created a derivate of the geometric standard deviation (Eq. 4.6) and some criteria to choose which molecules have to be used for the comparison (See the second attempt.). The minima of our reduced geometric standard deviation told us the best shock model to reproduce the reality and thus best values for the shock parameters.

We applied our method to the real case of L1157 B2 and found that methanol CH_3OH, H_2S, and CN were good molecular tracers in this context. Good means that we have data for these molecules and that they show good contrast between each shock model. It enabled us to identify a low-velocity shock with if put in comparison with previous studies, a C-type shock behavior. (It did not exclude the possibility of a multi-component shock.) Unfortunately, we did not find these tracers to be able to probe the preshock density efficiently. By doing this, we proved that the astrochemical point of view can be useful to characterize interstellar shocks and gave a complete method to do so. (We nevertheless have to remind that the reliability of the results should be studied through an analysis of the most important identified molecular tracers.)

How do shocks influence the overall chemistry of the interstellar medium? In Chapter 5, we listed the different physical properties of shock impacting the chemistry of the medium. We analyzed them insisting on the differences between C-type and J-type shocks and used them to recreate the journey of methanol in these shocks through the prism of our shock models. We discovered that shocks tend to enhance the chemical reactions by an increase in the temperature. This increase is greater in J-type shocks when the maximum temperature is evaluated, but the friction between the ions and neutrals (heating the gas) means that this increase lasts longer in C-type shocks. The next points differed a lot from C-type shocks to J-type shocks: The Ion-Neutral Drift and the sputtering. The Ion-Neutral Drift (or the enhancement of the collisions between ions and neutrals due to their relative velocities) enhanced the ion-neutral reactions, and the sputtering processes including charged grains and neutrals. As molecules were trapped on the dust surfaces, the Ion-Neutral drift in C-type shocks was necessary to release them in the gas phase and

feed the overall chemistry.

In the case of methanol, we found that its chemistry in C-type shocks began with the charging of dust grains and the sputtering of trapped species through the neutral ion drift. During its release, it began to be destroyed more efficiently until an equilibrium between formation and destruction was reached. Meanwhile, through its chemical network reactions (Fig. 5.4), it allowed the creation of CH_5O^+ and CH_3OH^+. We therefore saw a sharp increase in the abundance of our molecules in the post-shock region until the temperature began to return to its normal value and destructive processes took over, reducing the abundance. We understood that this was the case for C-type shocks with a sufficiently high speed to activate sputtering. In type J shocks, we only benefited from the increase in temperature, and the chemistry remained blocked by the low release of species from the dust phase. The special case of methanol was necessary to clearly understand all the impacts of the shocks on the chemistry and the profile of the comparison factor, and to validate the answer of our first research question.

6.3 What was brought by this master's thesis?

It is now time to look back on our master's thesis to emphasize why and how our work can be useful in the current context. Again, many topics have been addressed in the previous chapters and it is useful to stress some of the main interesting points that could have been drowned in the fifties pages of discussion:

- **A method to characterize shocked systems using astrochemistry:** The use of astrochemistry and the enhancement factors to probe the characteristics of a shock is not new and the comparison factor profiles already existed in previous studies (James et al. 2020). However, papers studying shocks based on a great set of molecular tracers are rare and they did not define a complete method to choose the best shock model. Our master's thesis complements what has already been done (comparison factor profiles for numerous molecules) by testing and defining a complete method to increase the contrast between the shock models (by a good choice of molecular tracers) and to find the best fitting with real values. As our method was made to be general, it should be useful for all shocked systems (such as L1157 B2) for astronomers having a good astrochemical code such as the Paris-Durham Shock code.

- **A complete study of the methanol chemistry in shocks:** More than just accepting the results of the Paris-Durham shock code, we deeply analyzed the behavior of our main molecular tracer – CH_3OH through its chemical network (Fig. 5.4). Understanding changes in abundance is often limited to temporal profiles of fractional abundance without looking in detail at the chemical reactions and therefore the chemical network (or at least, this is not presented in the articles except rarely as in the work by Pineau des Forêts (Pineau des Forets, Roueff, et al. 1993). We thus did it for methanol by retrieving all the relevant information in the thousands of graphs given by our astrochemical code and can expect our analysis to be quite new in the scientific literature. Methanol is interesting for its high variability concerning the

shock velocity and the shock type, and the fact that it is a basic organic molecule.

- **A confrontation with the literature:** A very interesting point of our master's thesis is also that it directly confronts the current literature in the domain. In one of the last papers on the subject (James et al. 2020), published in 2020 and peer-reviewed, the authors concluded that the most impacting factors were not the shock type or the shock velocity, but the preshock density. By saying that the chemistry is mostly dependent on the preshock density and not the shock parameters, they decreased the ability of astrochemical simulations to probe shocked systems. However, their results suffered from a bad treatment of the grain temperature and thus thermal desorption. But we have found that desorption was the main process influencing the abundance of species. Their abundance is thus the same in J-type and C-type shocks as molecules efficiently desorb in all their shocks and the differences between shock types vanish. As we found in Chapter 4, grains do not heat that much in shocks and the release of grain-phase species is thus highly dependent on non-thermal processes such as the sputtering. This master's thesis thus indicates that contrary to what we thought, abundance is influenced by the shock type and the shock velocity. We thus encourage astronomers to use astrochemistry to probe the shock properties. The strength of the difference between previous studies and our master's thesis can be particularly appreciated when we compare the comparison factor profiles in Figures 4.5 and 7.7.

6.4 Future perspectives

Science tends to improve itself through the years thanks to the efforts of the scientific community. More specifically, all set of points in our master's thesis can be criticized and put in perspective with the future advances we hope to see coming in astrophysics and astrochemistry. It is already our mission to define these spots of improvement to lead the mind of the scientist on all we still have to do. In the context of this master's thesis, we identified some weak spots in our reasoning and methods. Even if they are justified by the constraints imposed by the context – the lack of time, resources, computational methods, ... - they have been enumerated during our research and will be exposed in the following paragraphs:

- **Leaving the too-simple model of plane-parallel shock:** An approximation often made to simulate shocks is that these shocks have a very simple geometry. In the Paris-Durham Shock code, but also others including chemistry, we mainly consider plane-parallel shocks where the magnetic field is perpendicular to the flow. The geometry of these unidimensional shocks is a very strong constraint that does not well represent the diversity of configurations present in space. Typically, how can we retrieve multi-component shocks with our drastic assumptions? Simulations of more complex models such as 3D bow shocks already exist (Gustafsson et al. 2010). However, a complexification of the model induces an increase in the computational cost and these models are often not sufficiently coupled to astrochemical networks. Some methods such as the superposition of 1D shocks to simulate bow shocks (Tram et al. 2018) begin to appear and are a good first step in the improve-

ment of the geometry of shocks in astrochemical studies. We can only encourage the development of techniques to simulate complex structures from simpler ones or an improvement of the computational and algorithmic techniques to maximize the complexity of the simulations.

- **Revealing time-dependent patterns by avoiding the steady-state approximation:** Our second drastic assumption was that shocks were at a steady state. Even if this approximation makes sense if the characteristic dynamic time of shocks is way greater than the time needed for chemistry to reach equilibrium (which is supposed to be acceptable due to the high temperature in the important regions), it does not allow us to study and analyze the variability of shocks as a function of time. However, this information is important to every scientist wanting to write with assurance the chemical journey of a shock. Again, time-dependent astrochemistry already began to appear as is the case with the Astrochem code (Maret and Bergin 2015). However, the computation of the reaction rate equations is computationally costly, and astrochemical codes that do not assume the steady-state approximation only describe the simplest physical situations (in a parametrized way). It should be useful to successfully couple dynamical and chemical equations in a time-dependent way to analyze more complex dynamical environments from an astrochemical point of view. In this way, we can simulate more temporary astrophysical events where the steady-state assumption is not valid anymore.

- **Grains are more than a reservoir of hydrogenated species**: Concerning the chemical assumptions, the treatment of grains and their chemical properties was a very drastic assumption in the Paris-Durham Shock code. To remind the reader, grains only serve in the code to store atoms and molecules to hydrogenate them. However, the chemistry in the grain phase is very diversified. Grains are even the best way to create (as they serve as a third body taking away the energy) more and more complex molecules. If we do not include real grain chemistry in our chemical network, we choose to avoid the possibility of creating and evaluating the presence of more complex molecules and we limit ourselves to the basic ones. Even if we can guess that the more complex molecules, due to the very low abundance, will not have great feedback on the medium, it is impossible with this assumption to answer many questions of astrobiological interests. The evaluation of molecules such as amino acids requires a better treatment of the grain chemistry. Efforts were already made to simulate grains from one part (Garrod 2013) and to add reactions in the overall chemical network with branching ratios (Cordiner and Charnley 2012) to take into account the efficiency of the reactions on grains. But again, this is computationally costly and must wait to get the advancements in computational techniques to be used in complex systems. We also need to remember that thermal desorption is not well taken into account as it strongly depends on the presence of deviation in the binding energy that is not described in many current codes.

- **For the inclusion of grains in dynamic processes:** Shocks passing through a medium tend to shock the molecular material. If it is particularly easy to write, it is not that easy to simulate specifically when we are talking about grains. The

Paris-Durham Shock code does not take into account grain-grain interactions for the moment, limiting us to low-density shocks where we can neglect them. However, if we want to simulate denser environments (such as very dense clouds or protostellar regions), the coagulation and the shattering of grains will deeply affect the size distribution of grains and their chemistry, and the release of species trapped in dust grains. Some improvements begin to appear and should be incorporated into the Paris-Durham Shock code in the future (Guillet, Pineau Des Forêts, and Jones 2007). These advances will enable us to extend the domain of environments that are possible to study.

- **More, more, and more chemical reactions:** Obviously, chemical simulations are highly dependent on the set of chemical reactions put in them. One recurrent problem encountered in chemical studies with computational methods is the incompleteness of the chemical network leading to an overestimated (underestimated) abundance of our chemical species. Viewing the chemical network we made for CH_3OH, even the question of our completeness is worth asking. But in our case, the main destruction processes were well described. Only the formation of more complex species was not described, but at this level of complexity, it is negligible in the gas phase. To continue on the perspectives, it should always be kept in mind that the evolution of astrochemical simulations should evolve in parallel with the computation (or evaluation) of the reaction rates of a maximum of reactions. They are fundamental to ensure the relevance of the results, and they are mandatory for astrochemists wanting to improve the chemical complexity in their models.

These points summarize the path astrochemistry can take soon as they are all sources of improvements. We can also add the inclusion of new but important physical processes as a better treatment of irradiation. But new challenges have been recently beaten in this domain even for the Paris-Durham Shock code (Godard et al. 2019). The non-inclusion of irradiated shocks in this master's thesis was more a question of computational time and the fact that we always have to limit the context of our studies at one moment. In all cases, writing this master's thesis was already enlightening for us as it enabled us to deeply study the domain of astrochemistry and interstellar shocks and to prove the validity of astrochemistry as an essential point of view to analyze astrophysical environments. Science is an interconnected whole and astrochemistry is one of the best manifestations of this verity.

Chapter 7

Appendix

7.1 A brief introduction to chemical kinetics

Chemical kinetics is the study of reaction rates (Atkins, de Paula, and Keeler 2018) and thus the speed at which a reaction occurs. This discipline is essential in astrochemistry as it enables the computation of the chemistry of the system. In this brief introduction, we will introduce the essential concepts to understand chemical kinetics and the associated discussions in our master's thesis. We will thus explain the concepts of elementary reactions, rate constants, and activation barriers as written in Visart de Bocarmé, T. 2022.

7.1.1 The elementary reactions

In chemistry, reactions such as (Visart de Bocarmé, T. 2022)

$$2\,O_3 \rightarrow 3\,O_2 \tag{7.1}$$

are not necessarily straightforward and the computation of the speed at which they occur can be complicated. This is a consequence that usual reactions can often be decomposed into more elementary processes: the elementary reactions. For Re. 7.1, we can decompose it into:

$$O_3 \rightleftharpoons O_2 + O^{\cdot} \tag{7.2}$$

$$O^{\cdot} + O_3 \rightarrow 2\,O_2 \tag{7.3}$$

These reactions are elementary in the sense that they are one-step reactions. It is now easier to compute their kinetics as we know these reactions only need their reactants

to meet and do not hide any more complex mechanisms. This will enable us to compute the reaction rate of the reaction.

7.1.2 The reaction rate

Let's analyze a basic equation of the form:

$$A + B \rightarrow C + D \tag{7.4}$$

and let's try to define the speed $r = -\frac{d[A]}{dt}$ at which the reaction occurs. The reaction needs the encounter of molecule A with molecule B. We can thus write the frequency of collisions per unit of volume:

$$Z_{AB} = n_A n_B \pi \sigma_{AB}^2 \sqrt{\frac{8 k_B T}{\pi \mu_{AB}}} \tag{7.5}$$

where n_X is the abundance of X molecules (cm^{-3}), $\pi\sigma_{AB}^2$ represents the cross-section as illustrated in Figure 7.1, and $\sqrt{\frac{8k_BT}{\pi\mu_{AB}}}$ is the mean relative speed between A and B molecules where μ_{AB} is their reduced mass.

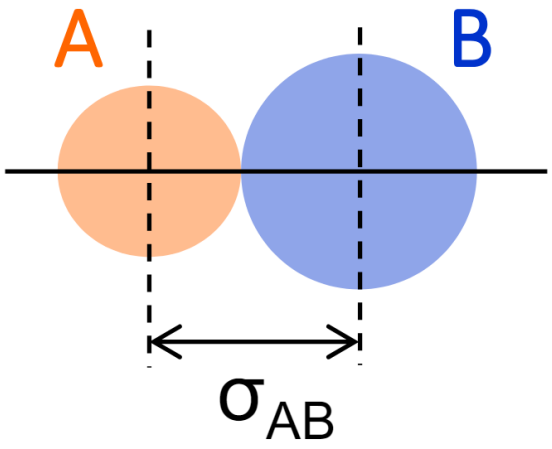

Figure 7.1: The cross-section $\pi\sigma_{AB}^2$ gives the disk area where molecule B should stand to collide with molecule A. The figure comes from Visart de Bocarmé, T. 2022.

As we will detail later, collisions between molecules are insufficient to ensure chemical reactions. They also need to have enough energy for the reaction to occur. This minimum energy is called E_a and enables us to define the frequency of effective collisions. As we assume a Maxwellian distribution:

$$Z_e = n_A n_B \pi \sigma_{AB}^2 \sqrt{\frac{8 k_B T}{\pi \mu_{AB}}} \cdot e^{-\frac{E_a}{k_B T}} \tag{7.6}$$

We can multiply this frequency of effective collisions by a steric factor P to ensure that molecule A collides with molecule B with a good orientation to obtain the speed of the reaction r:

$$r = P \cdot Z_e \tag{7.7}$$

If we compare it to the ODEs that astrochemical codes have to solve (Eq. 1.2), we can identify the part taken by the constant k, called the rate constant. As described in the introduction, it is well a function of the temperature. (As we are not considering reactions with light or cosmic rays here, it does not depend on other parameters.)

$$k(T) = P \pi \sigma_{AB}^2 \sqrt{\frac{8 k_B T}{\pi \mu_{AB}}} \cdot e^{-\frac{E_a}{k_B T}} \tag{7.8}$$

This is essentially the same form as the rate function in Table 1.6 for A + B $\rightarrow$ C + D reactions. The only difference is that we have a factor T^{α} instead of a factor $T^{1/2}$. This comes from the fact that different theories (such as the transition state theory) exist and will change the dependence on the temperature. Now that we have the rate constant, we can technically compute the density evolution for each species. Nevertheless, let's take a special look at the parameter E_a.

7.1.3 The activation energy

From thermodynamics, we know that during a chemical reaction, the energy will change from the reactants to the products and the reaction will release (or require) energy. This energy difference represents the blue domain in Figure 7.2. However, reactions are not a smooth journey from A to B but consist of travel on a potential energy surface (PES) as the reaction progresses. This movement on the PES often consists of reaching a maximum of energy before going back down to the energy of the product. The difference between this maximum and the initial energy (the pink domain in Figure 7.2) needs to be crossed and is called the activation energy E_a. As we can expect and this will be one of the main points in our discussions, this activation energy is a barrier against the reaction. We will thus require a sufficient temperature to enable the reaction to occur.

Elementary reactions, rate constants, and activation energy were thus the main concepts to understand all the chemistry present in this master's thesis.

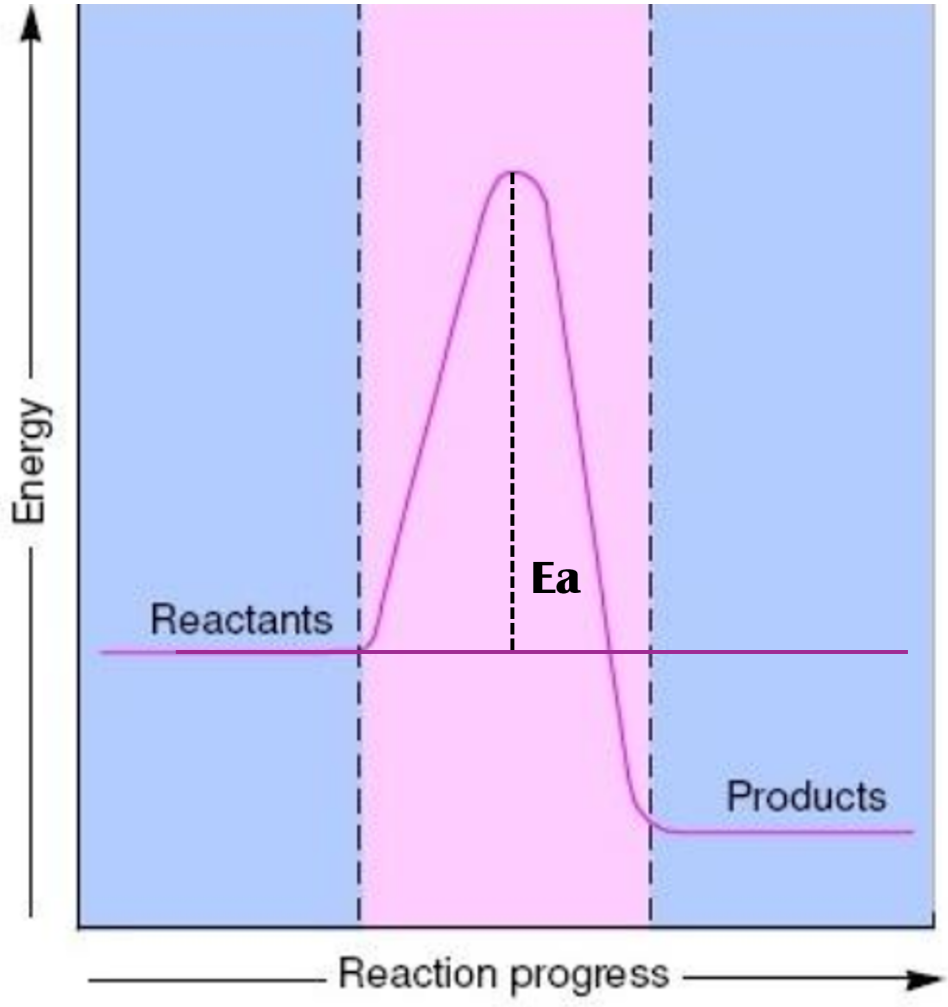

Figure 7.2: A reaction pathway is characterized by an activation barrier as present in the pink domain (giving the activation energy) that will lead to the speed of the reaction depending on the available energy. The figure is inspired by Visart de Bocarmé, T. 2022.

7.2 The exploration of the parameter space - The graphics

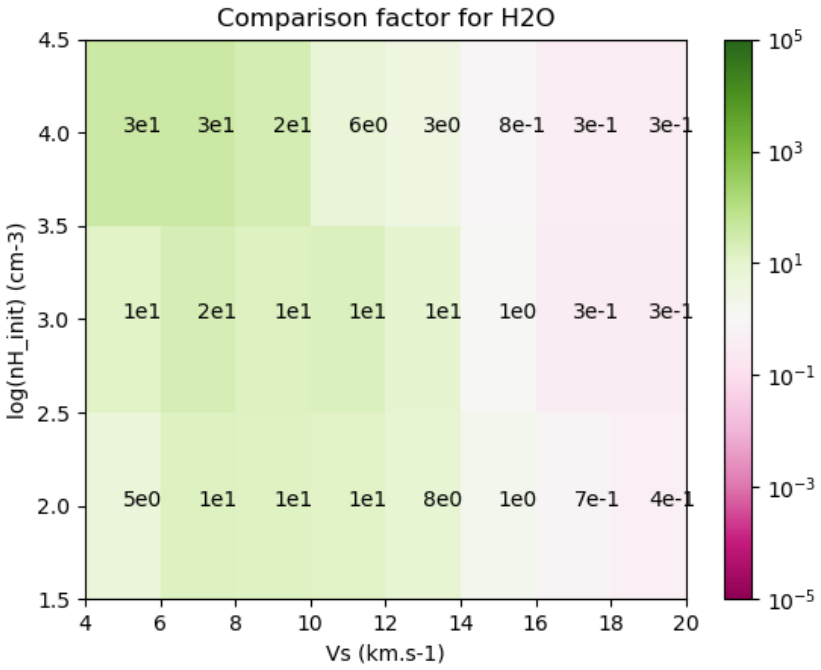

Figure 7.3: Comparison factors in our simulations for the H_2O molecule.

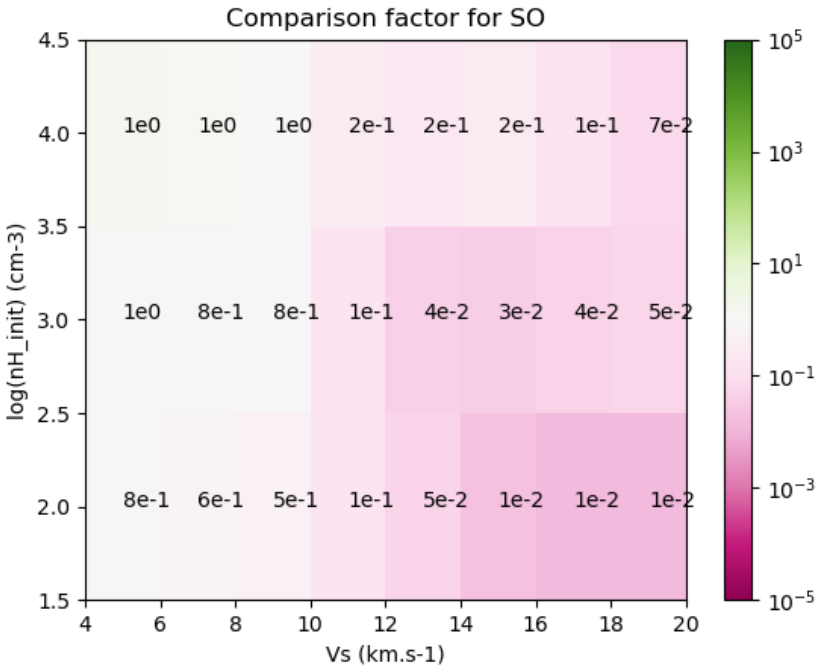

Figure 7.4: Comparison factors in our simulations for the SO molecule.

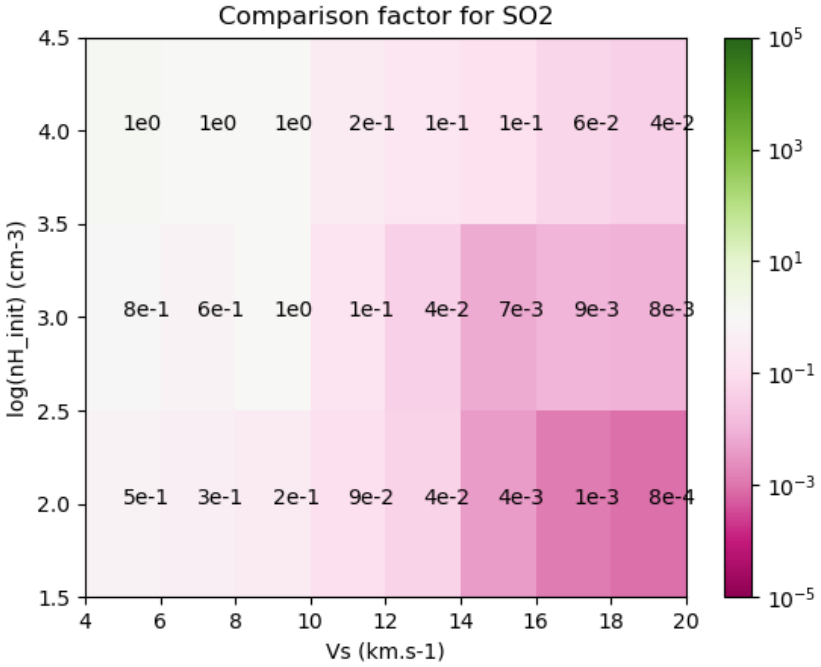

Figure 7.5: Comparison factors in our simulations for the SO_2 molecule.

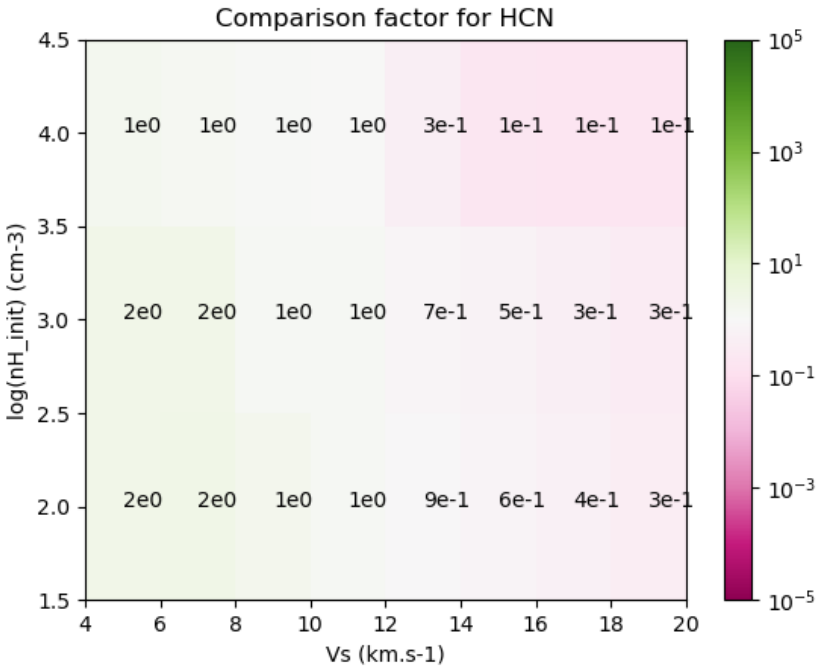

Figure 7.6: Comparison factors in our simulations for the HCN molecule.

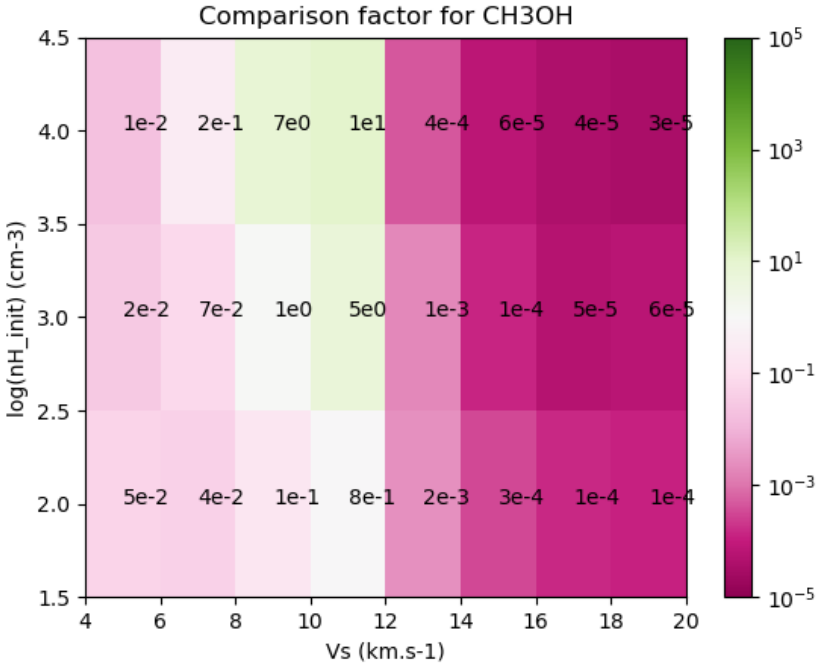

Figure 7.7: Comparison factors in our simulations for the CH_3OH molecule.

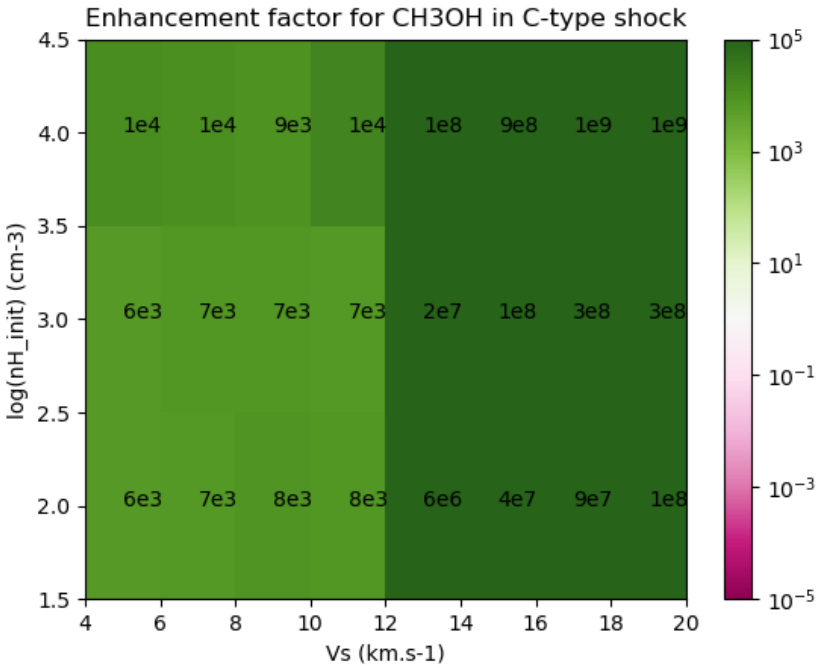

Figure 7.8: Enhancement factors in C-type shocks in our simulations for the CH_3OH molecule.

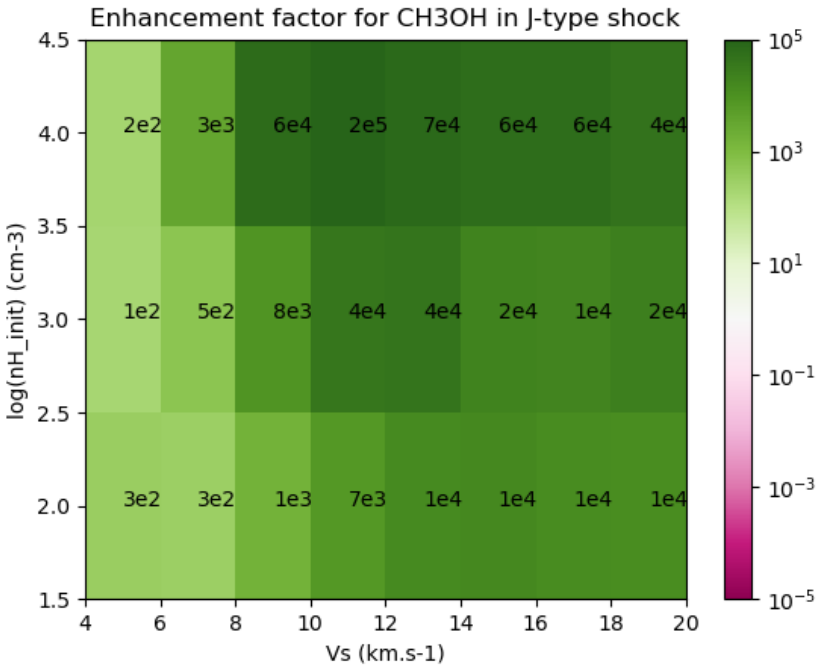

Figure 7.9: Enhancement factors in J-type shocks in our simulations for the CH_3OH molecule.

7.3 Geometric Standard Deviations

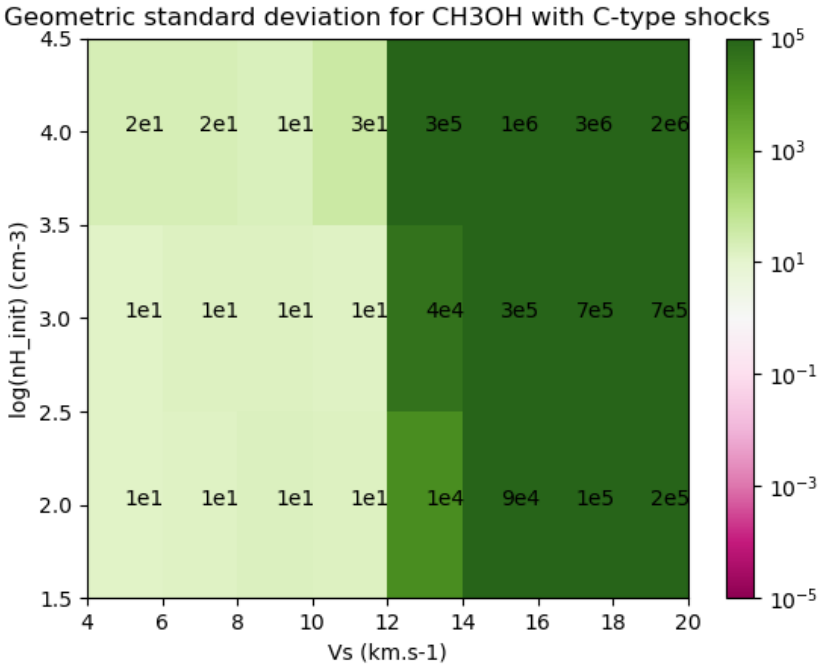

Figure 7.10: Geometric standard deviations (Eq. 4.6) for CH_3OH in C-type shocks.

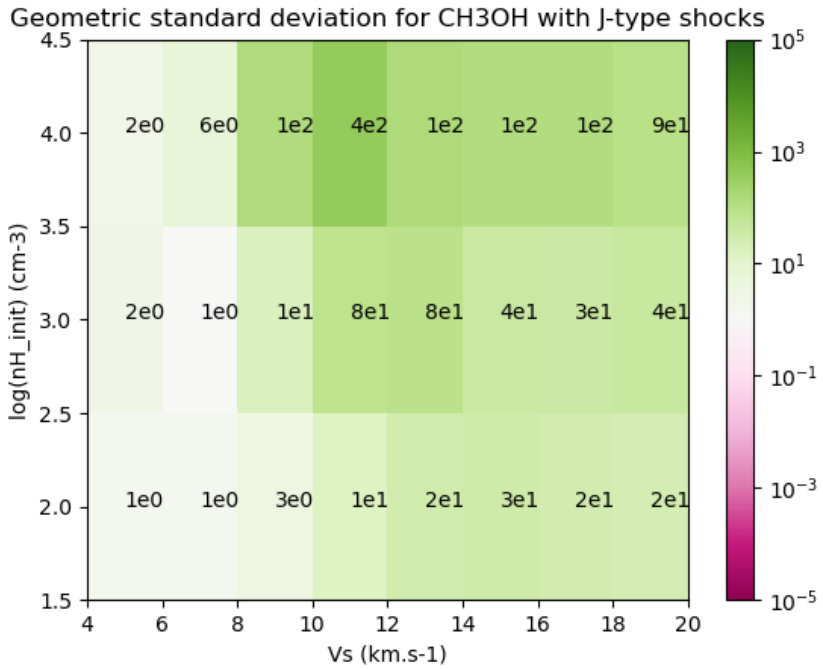

Figure 7.11: Geometric standard deviations (Eq. 4.6) for CH_3OH in J-type shocks.

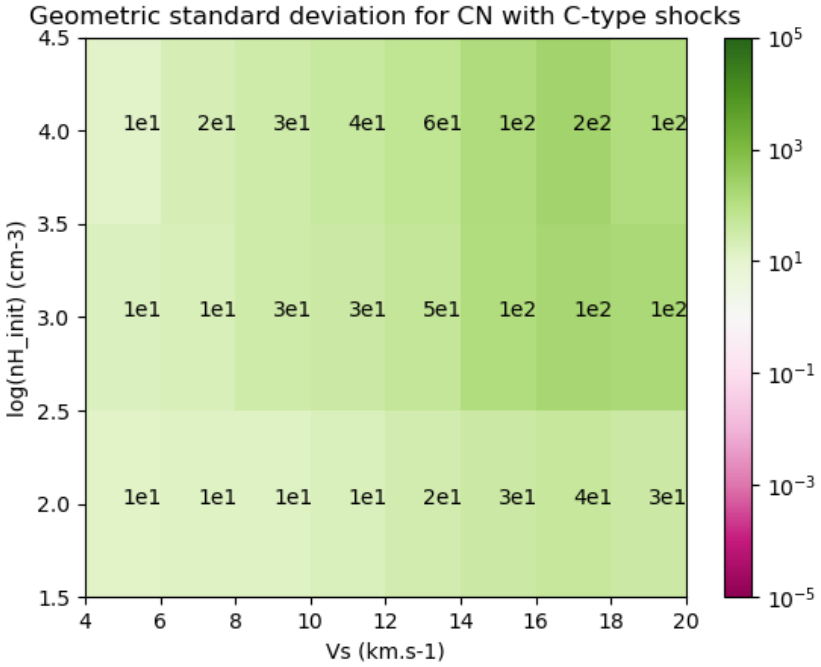

Figure 7.12: Geometric standard deviations (Eq. 4.6) for CN in C-type shocks.

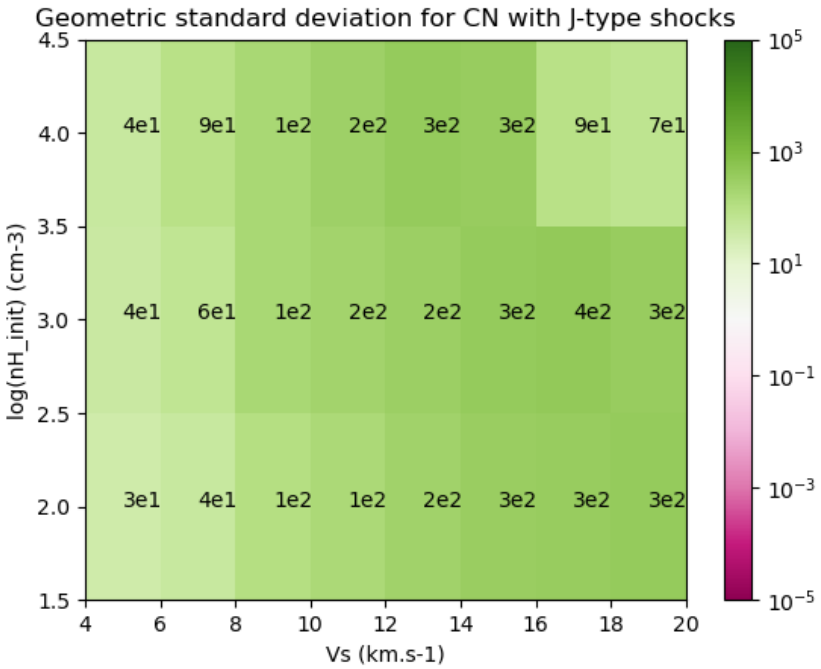

Figure 7.13: Geometric standard deviations (Eq. 4.6) for CN in J-type shocks.

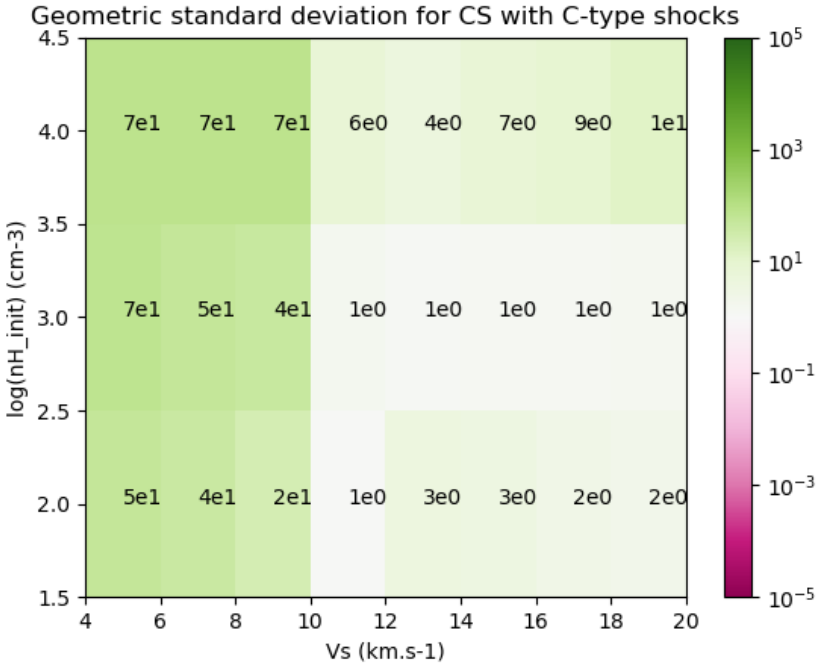

Figure 7.14: Geometric standard deviations (Eq. 4.6) for CS in C-type shocks.

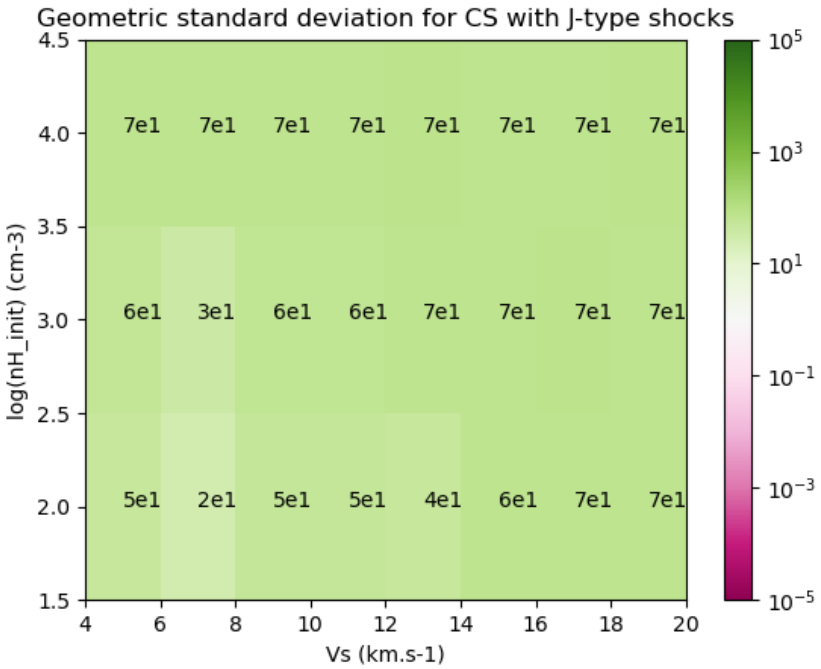

Figure 7.15: Geometric standard deviations (Eq. 4.6) for CS in J-type shocks.

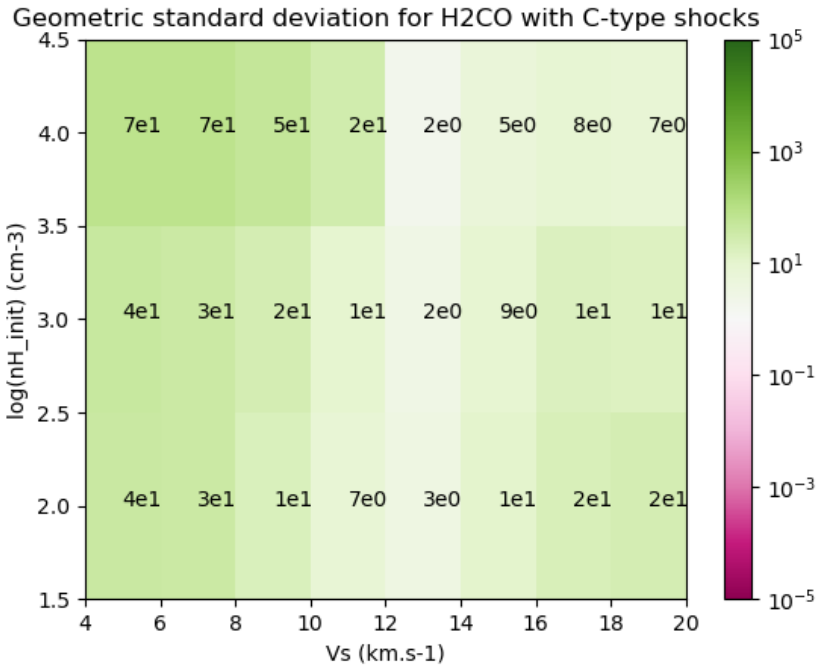

Figure 7.16: Geometric standard deviations (Eq. 4.6) for H_2CO in C-type shocks.

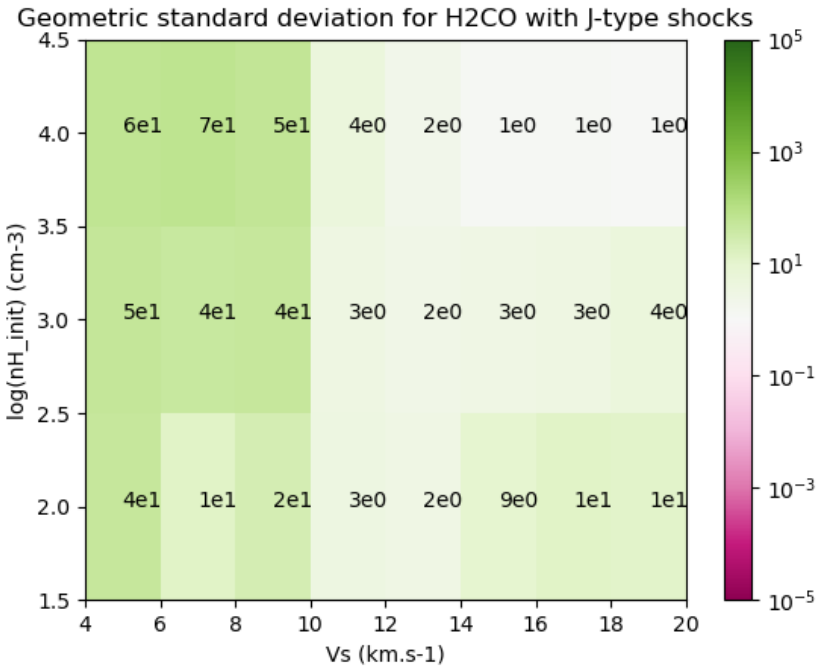

Figure 7.17: Geometric standard deviations (Eq. 4.6) for H_2CO in J-type shocks.

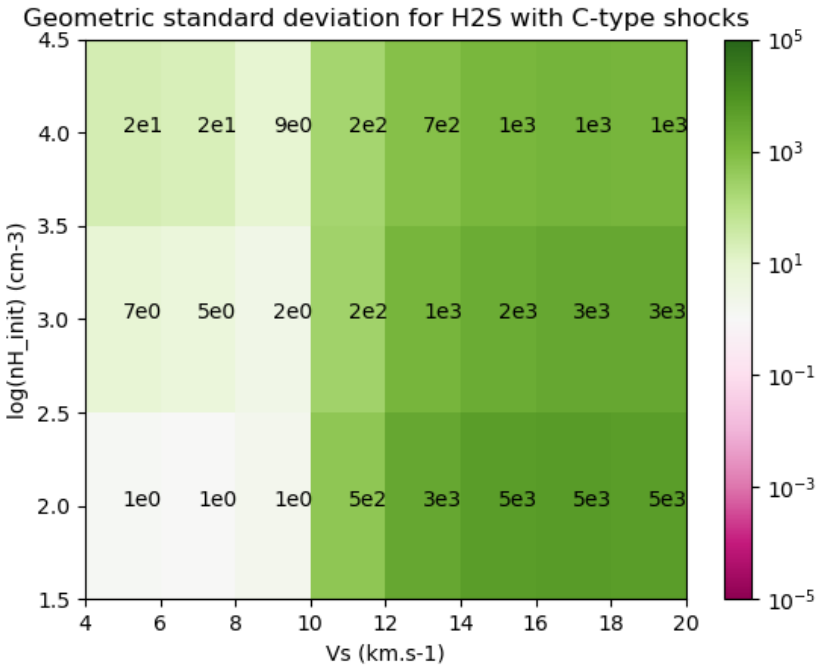

Figure 7.18: Geometric standard deviations (Eq. 4.6) for H_2S in C-type shocks.

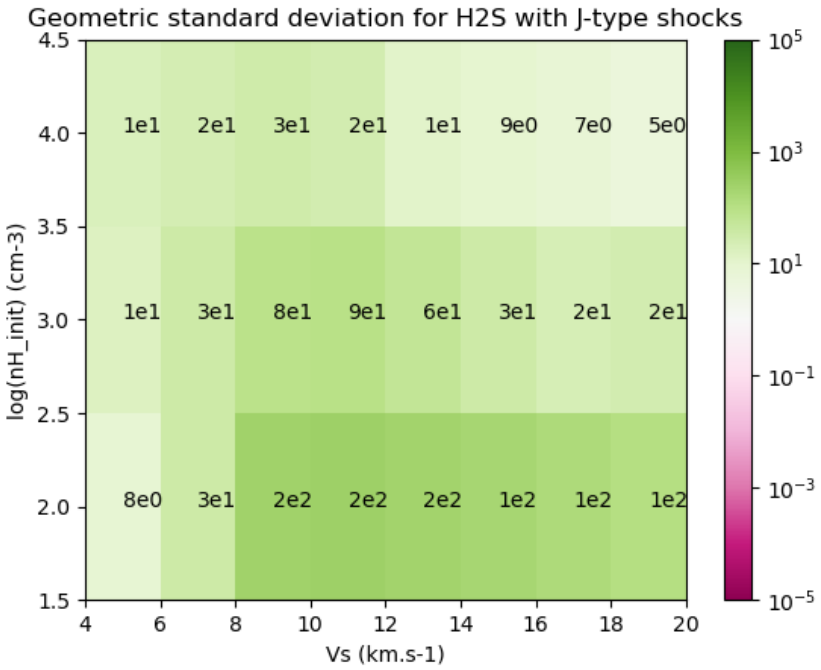

Figure 7.19: Geometric standard deviations (Eq. 4.6) for H_2S in J-type shocks.

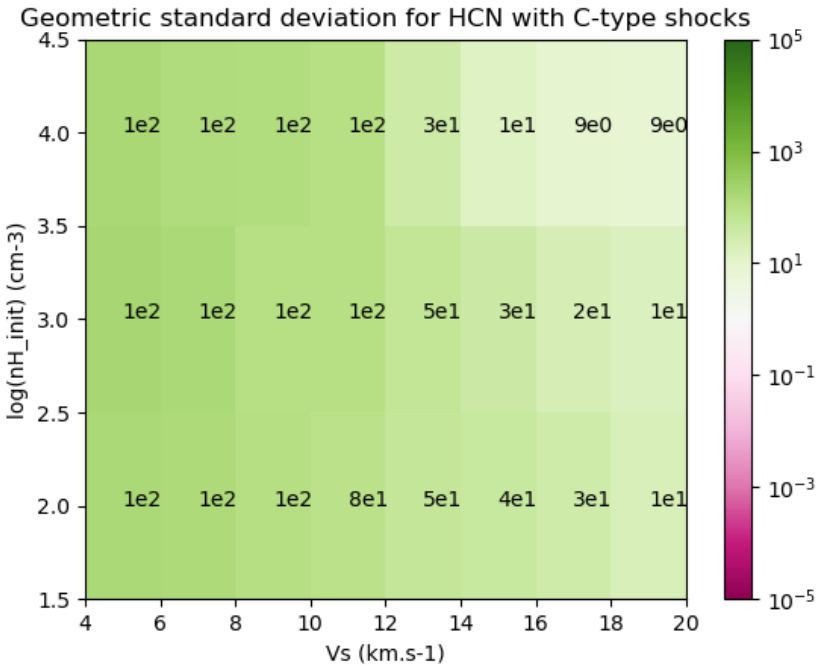

Figure 7.20: Geometric standard deviations (Eq. 4.6) for HCN in C-type shocks.

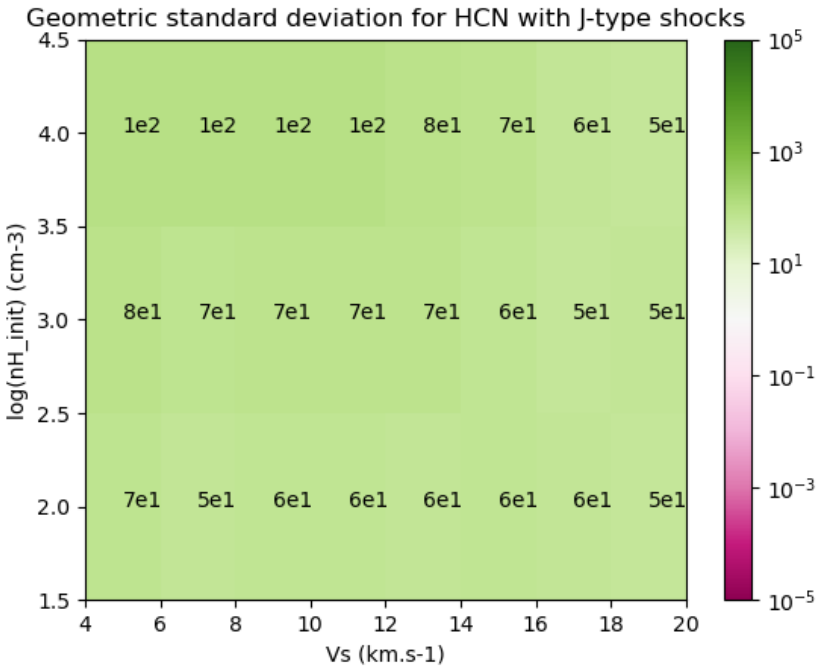

Figure 7.21: Geometric standard deviations (Eq. 4.6) for HCN in J-type shocks.

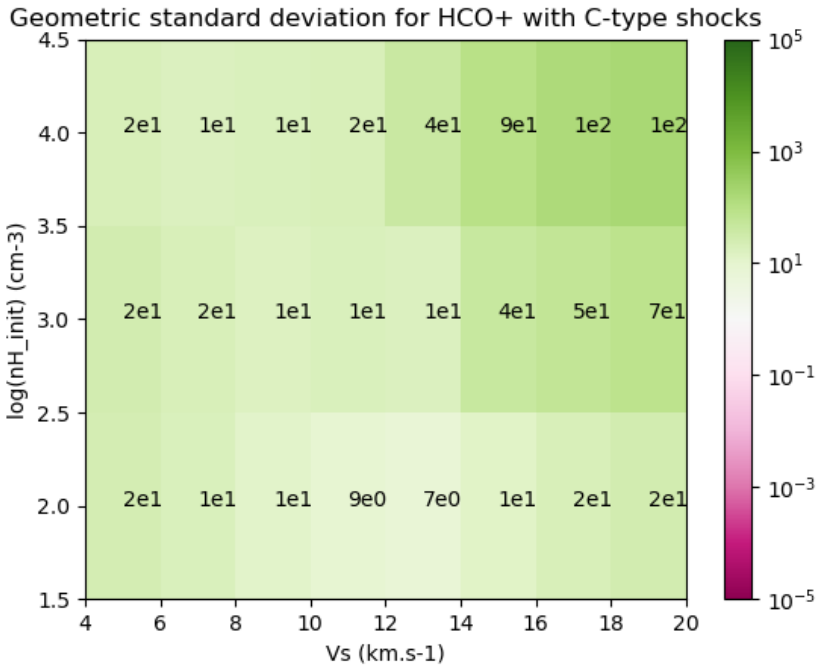

Figure 7.22: Geometric standard deviations (Eq. 4.6) for HCO^+ in C-type shocks.

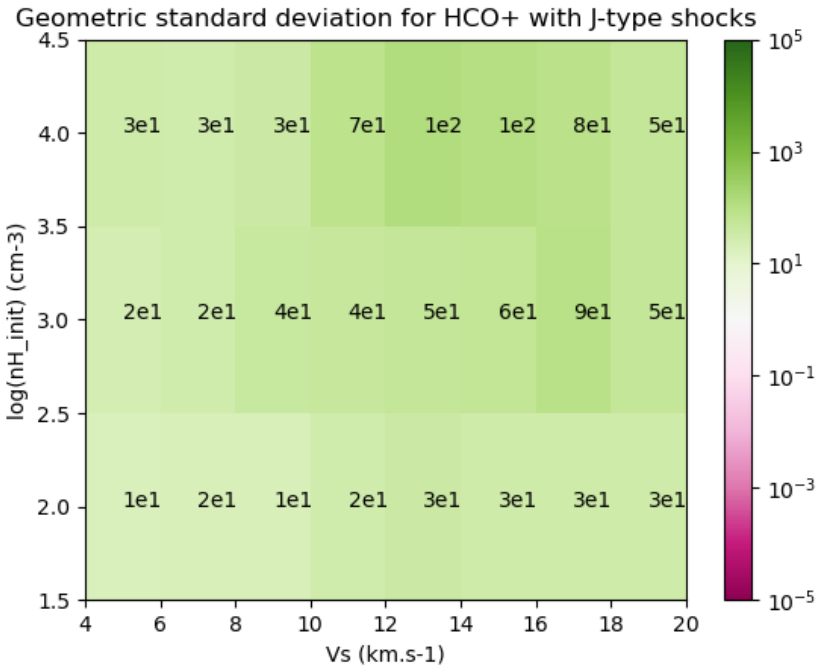

Figure 7.23: Geometric standard deviations (Eq. 4.6) for HCO^+ in J-type shocks.

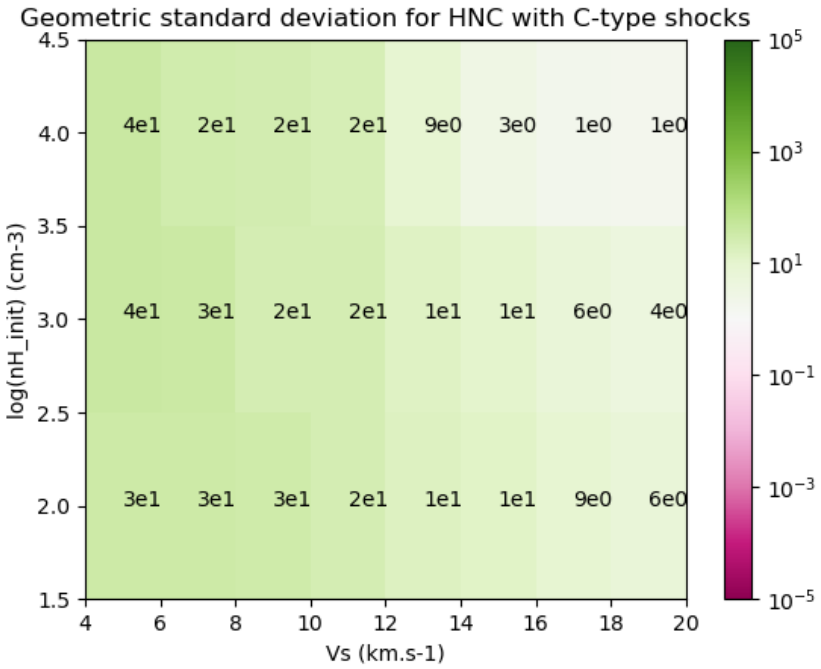

Figure 7.24: Geometric standard deviations (Eq. 4.6) for HNC in C-type shocks.

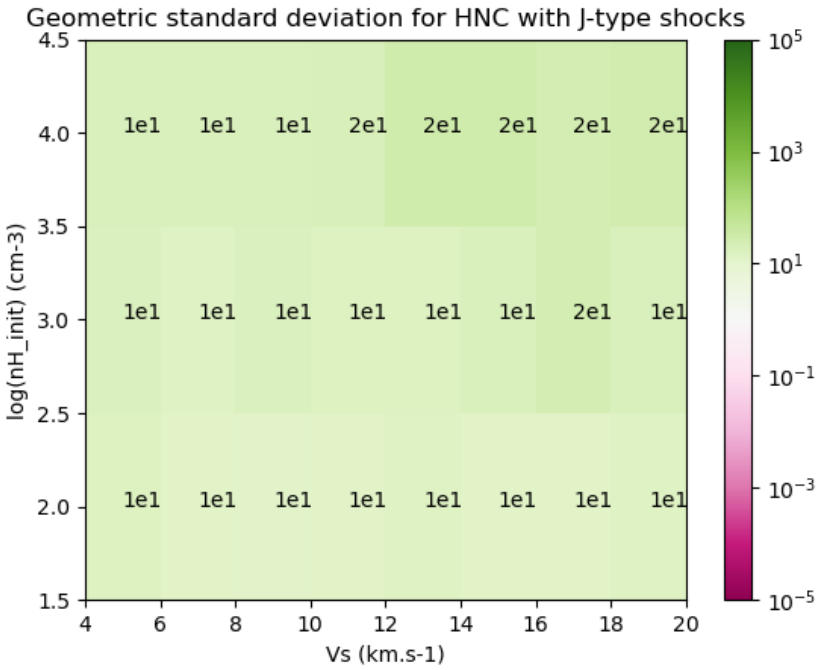

Figure 7.25: Geometric standard deviations (Eq. 4.6) for HNC in J-type shocks.

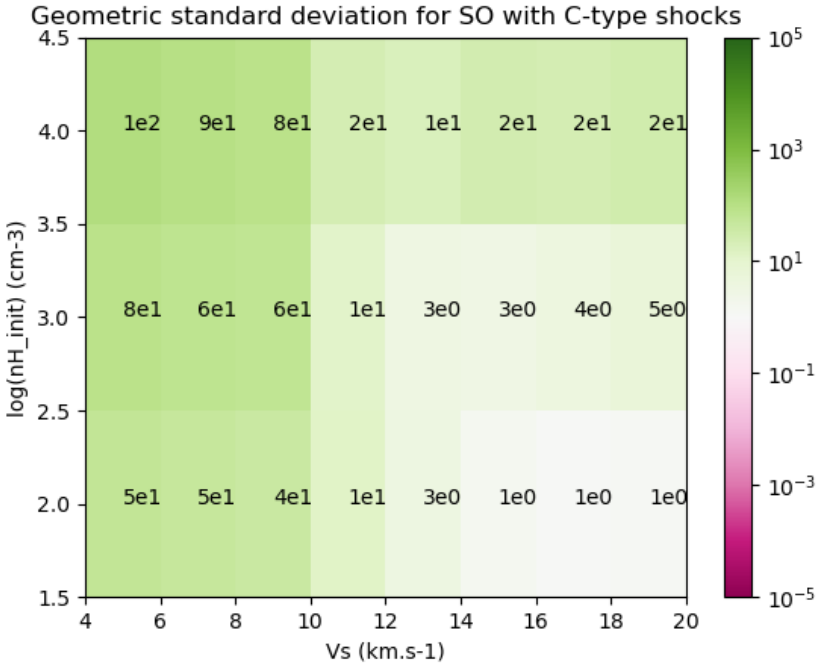

Figure 7.26: Geometric standard deviations (Eq. 4.6) for SO in C-type shocks.

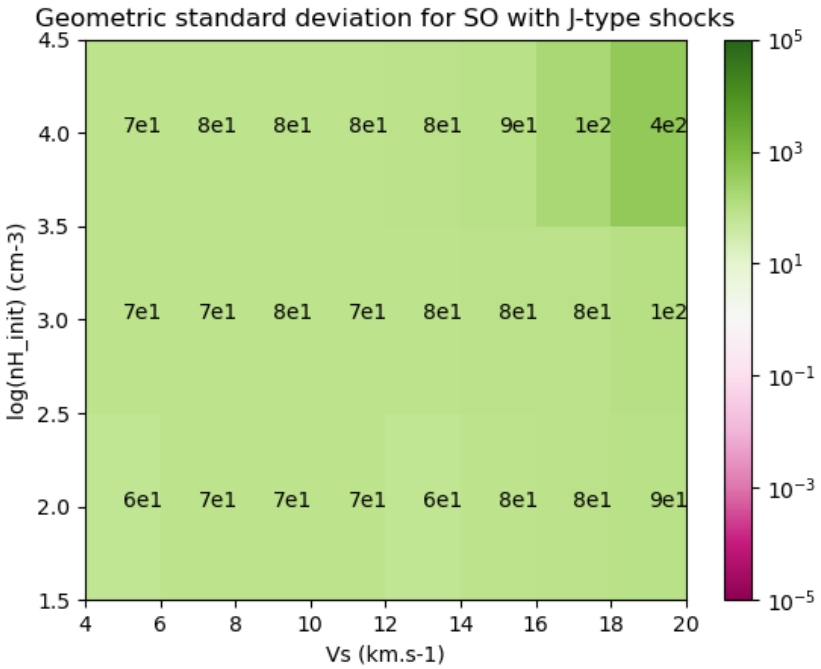

Figure 7.27: Geometric standard deviations (Eq. 4.6) for SO in J-type shocks.

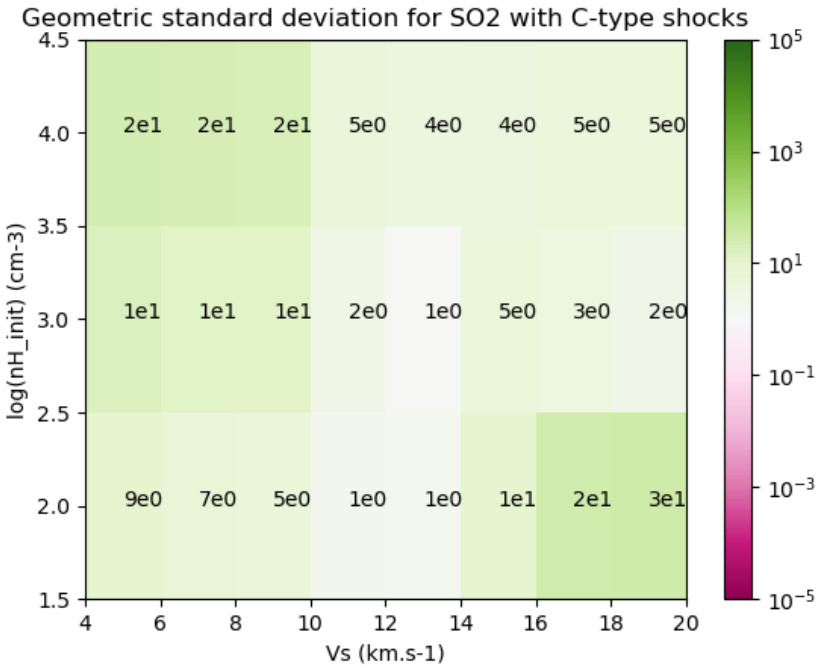

Figure 7.28: Geometric standard deviations (Eq. 4.6) for SO_2 in C-type shocks.

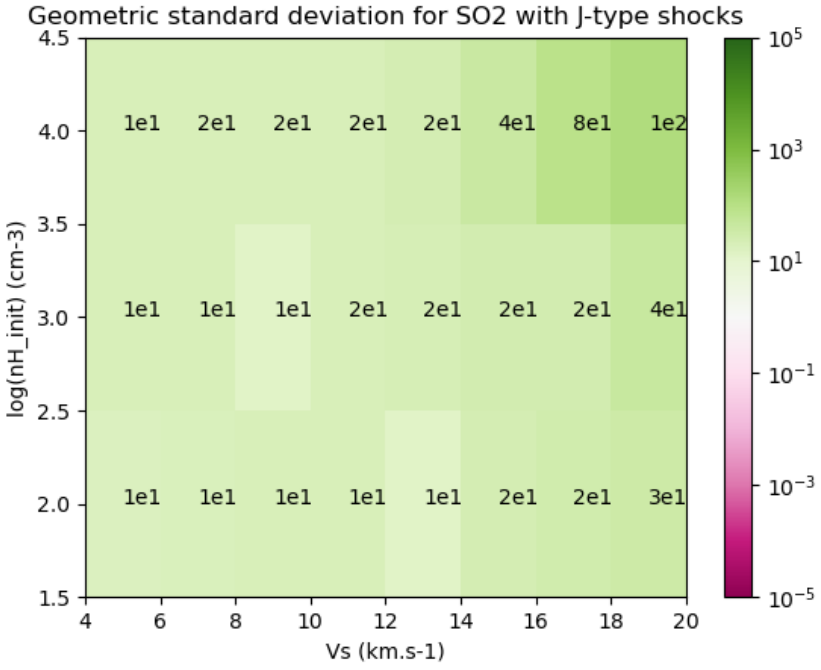

Figure 7.29: Geometric standard deviations (Eq. 4.6) for SO_2 in J-type shocks.

Bibliography

1. Héctor G. Arce et al. "Complex Molecules in the L1157 Molecular Outflow". In: *ApJ* 681.1 (July 2008), p. L21. DOI: 10.1086/590110. arXiv: 0805.2550 [astro-ph].

2. Peter Atkins, Julio de Paula, and James" Keeler. *Physical Chemistry*. Oxford University Press, 2018.

3. R. Bachiller and M. Pérez Gutiérrez. "Shock Chemistry in the Young Bipolar Outflow L1157". In: *ApJ* 487.1 (Sept. 1997), pp. L93–L96. DOI: 10.1086/310877.

4. Giovanni Carraro. *Astrophysics of the Interstellar Medium*. 2021. DOI: 10.1007/978-3-030-75293-4.

5. M. A. Cordiner and S. B. Charnley. "Gas-Grain Models for Interstellar Anion Chemistry". In: *ApJ* 749.2, 120 (Apr. 2012), p. 120. DOI: 10.1088/0004-637X/749/2/120. arXiv: 1202.2872 [astro-ph.GA].

6. De Becker, M. *Astrochemistry, SPAT0020-2, lecture notes*. 2021.

7. De Becker, M. *Interstellar medium, SPAT0008-1, lecture notes (first part)*. 2023.

8. B. T. Draine. "Interstellar shock waves with magnetic precursors". In: *ApJ* 241 (Nov. 1980), pp. 1021–1038. DOI: 10.1086/158416.

9. B. T. Draine, W. G. Roberge, and A. Dalgarno. "Magnetohydrodynamic shock waves in molecular clouds." In: *ApJ* 264 (Jan. 1983), pp. 485–507. DOI: 10.1086/160617.

10. Bruce T. Draine. *Physics of the Interstellar and Intergalactic Medium*. 2011.

11. L. Oc. Drury. "REVIEW ARTICLE: An introduction to the theory of diffusive shock acceleration of energetic particles in tenuous plasmas". In: *Reports on Progress in Physics* 46.8 (Aug. 1983), pp. 973–1027. DOI: 10.1088/0034-4885/46/8/002.

12. D. Field et al. "Sputtering of the refractory cores of interstellar grains". In: *MNRAS* 285.4 (Mar. 1997), pp. 839–846. DOI: 10.1093/mnras/285.4.839.

13. D. R. Flower and G. Pineau des Forets. "Grain / Mantle Erosion in Magnetohydrodynamic Shocks". In: *MNRAS* 268 (June 1994), p. 724. DOI: 10.1093/mnras/268.3.724.

14. D. R. Flower, G. Pineau des Forets, and T. W. Hartquist. "Theoretical studies of interstellar molecular shocks. I - General formulation and effects of the ion-molecule chemistry". In: *MNRAS* 216 (Oct. 1985), pp. 775–794. DOI: 10.1093/mnras/216.4.775.

15. D. R. Flower and G. Pineau des Forêts. "The influence of grains on the propagation and structure of C-type shock waves in interstellar molecular clouds". In: *MNRAS* 343.2 (Aug. 2003), pp. 390–400. DOI: 10.1046/j.1365-8711.2003.06716.x.

16. D. R. Flower and G. Pineau des Forêts. "The influence of grains on the propagation and structure of C-type shock waves in interstellar molecular clouds". In: *MNRAS* 343.2 (Aug. 2003), pp. 390–400. DOI: 10.1046/j.1365-8711.2003.06716.x.

17. D. R. Flower and G. Pineau des Forêts. "Interpreting observations of molecular outflow sources: the MHD shock code mhd_vode". In: *A&A* 578, A63 (June 2015), A63. DOI: 10.1051/0004-6361/201525740.

18. D. R. Flower, G. Pineau-Des-Forets, and T. W. Hartquist. "Theoretical studies of interstellar molecular shocks. II - Molecular hydrogen cooling and rotational level populations". In: *MNRAS* 218 (Feb. 1986), pp. 729–741. DOI: 10.1093/mnras/218.4.729.

19. Robin T. Garrod. "Three-dimensional, Off-lattice Monte Carlo Kinetics Simulations of Interstellar Grain Chemistry and Ice Structure". In: *ApJ* 778.2, 158 (Dec. 2013), p. 158. DOI: 10.1088/0004-637X/778/2/158. arXiv: 1310.2512 [astro-ph.IM].

20. B. Godard et al. "Models of irradiated molecular shocks". In: *A&A* 622, A100 (Feb. 2019), A100. DOI: 10.1051/0004-6361/201834248. arXiv: 1901.04273 [astro-ph.GA].

21. A. I. Gómez-Ruiz et al. "Diagnosing shock temperature with NH_3 and H_2O profiles". In: *MNRAS* 462.2 (Oct. 2016), pp. 2203–2217. DOI: 10.1093/mnras/stw1811. arXiv: 1607.05343 [astro-ph.GA].

22. Michel Guélin and Jose Cernicharo. "Organic Molecules in Interstellar Space: Latest Advances". In: *Frontiers in Astronomy and Space Sciences* 9, 787567 (Mar. 2022), p. 787567. DOI: 10.3389/fspas.2022.787567. arXiv: 2201.06106 [astro-ph.GA].

23. V. Guillet, G. Pineau Des Forêts, and A. P. Jones. "Shocks in dense clouds. I. Dust dynamics". In: *A&A* 476.1 (Dec. 2007), pp. 263–277. DOI: 10.1051/0004-6361:20078094.

24. M. Gustafsson et al. "3D model of bow shocks". In: *A&A* 513, A5 (Apr. 2010), A5. DOI: 10.1051/0004-6361/200912977.

25. J. Holdship et al. "UCLCHEM: A Gas-grain Chemical Code for Clouds, Cores, and C-Shocks". In: *AJ* 154.1, 38 (July 2017), p. 38. DOI: 10.3847/1538-3881/aa773f. arXiv: 1705.10677 [astro-ph.GA].

26. *Interstellar Medium Services Platform*. https://ism.obspm.fr/tools.html. Accessed: 2023-11-12.

27. T. A. James et al. "Tracing shock type with chemical diagnostics. An application to L1157". In: *A&A* 634, A17 (Feb. 2020), A17. DOI: 10.1051/0004-6361/201936536. arXiv: 1912.03721 [astro-ph.SR].

28. P. Lesaffre et al. "Low-velocity shocks: signatures of turbulent dissipation in diffuse irradiated gas". In: *A&A* 550, A106 (Feb. 2013), A106. DOI: 10.1051/0004-6361/201219928. arXiv: 1301.7598 [astro-ph.GA].

29. Leslie W. Looney, John J. Tobin, and Woojin Kwon. "A Flattened Protostellar Envelope in Absorption around L1157". In: *ApJ* 670.2 (Dec. 2007), pp. L131–L134. DOI: 10.1086/524361. arXiv: 0710.2314 [astro-ph].

30. Leslie W. Looney, John J. Tobin, and Woojin Kwon. "A Flattened Protostellar Envelope in Absorption around L1157". In: *ApJ* 670.2 (Dec. 2007), pp. L131–L134. DOI: 10.1086/524361. arXiv: 0710.2314 [astro-ph].

31. Sébastien Maret and Edwin A. Bergin. *Astrochem: Abundances of chemical species in the interstellar medium*. Astrophysics Source Code Library, record ascl:1507.010. July 2015.

32. Hitoshi Miura et al. "Comprehensive Study of Thermal Desorption of Grain-surface Species by Accretion Shocks around Protostars". In: *ApJ* 839.1, 47 (Apr. 2017), p. 47. DOI: 10.3847/1538-4357/aa67df.

33. Antonio Parravano, David Hollenbach, and Christopher F. McKee. "The FUV Radiation Field and the Two phase Structure of the Interstellar Medium". In: *Cosmic Evolution and Galaxy Formation: Structure, Interactions, and Feedback*. Ed. by José Franco et al. Vol. 215. Astronomical Society of the Pacific Conference Series. Jan. 2000, p. 87.

34. Jessica Perrero et al. "Binding Energies of Interstellar Relevant S-bearing Species on Water Ice Mantles: A Quantum Mechanical Investigation". In: *ApJ* 938.2, 158 (Oct. 2022), p. 158. DOI: 10.3847/1538-4357/ac9278. arXiv: 2209.07255 [astro-ph.GA].

35. G. Pineau des Forets, D. R. Flower, et al. “Theoretical studies of interstellar molecular shocks - III. The formation of CH+ in diffuse clouds.” In: *MNRAS* 220 (June 1986), pp. 801–824. DOI: 10.1093/mnras/220.4.801.

36. G. Pineau des Forets, E. Roueff, et al. “Sulphur-bearing molecules as tracers of shocks in interstellar clouds”. In: *MNRAS* 262.4 (June 1993), pp. 915–928. DOI: 10.1093/mnras/262.4.915.

37. Pinto, C. *The composition of the interstellar medium in the Galaxy as seen through X-rays*. 2013.

38. L. Podio et al. “First image of the L1157 molecular jet by the CALYPSO IRAM-PdBI survey”. In: *A&A* 593, L4 (Sept. 2016), p. L4. DOI: 10.1051/0004-6361/201628876. arXiv: 1608.05026 [astro-ph.GA].

39. Marc. Séguin and Benoît Villeneuve. *Astronomie et astrophysique Cinq grandes idées pour explorer et comprendre l’Univers*. 2002.

40. *Setups—Laboratory for Astrophysics—Leiden Observatory*. https://home.strw.leidenuniv.nl/~linnartz/setups.html. Accessed: 2023-10-03.

41. P. Swings and L. Rosenfeld. “Considerations Regarding Interstellar Molecules”. In: *ApJ* 86 (Nov. 1937), pp. 483–486. DOI: 10.1086/143880.

42. M. Tafalla and R. Bachiller. “Ammonia Emission from Bow Shocks in the L1157 Outflow”. In: *ApJ* 443 (Apr. 1995), p. L37. DOI: 10.1086/187830.

43. The ISM Team of Paris Observatory. *Documentation Shock code*. ISMServices. 2020.

44. The ISM Team of Paris Observatory. *Hands-on session with the Paris-Durham shock code: How to run a shock model*. ISMServices. 2022.

45. L. N. Tram et al. “Bow-shock chemistry in the interstellar medium”. In: *arXiv e-prints*, arXiv:1808.01439 (Aug. 2018), arXiv:1808.01439. DOI: 10.48550/arXiv.1808.01439. arXiv: 1808.01439 [astro-ph.SR].

46. Ewine F. van Dishoeck, Eric Herbst, and David A. Neufeld. “Interstellar Water Chemistry: From Laboratory to Observations”. In: *Chemical Reviews* 113.12 (Dec. 2013), pp. 9043–9085. DOI: 10.1021/cr4003177. arXiv: 1312.4684 [astro-ph.GA].

47. Van Grootel, V. *Interstellar medium, SPAT0008-1, lecture notes (second part)*. 2023.

48. M. Vasta et al. “Water emission from the chemically rich outflow L1157”. In: *A&A* 537, A98 (Jan. 2012), A98. DOI: 10.1051/0004-6361/201118201. arXiv: 1111.0461 [astro-ph.GA].

49. Visart de Bocarmé, T. *CHIM-F320 - Cinétique chimique*. 2022.

50. S. Viti et al. "L1157-B1: Water and Ammonia as Diagnostics of Shock Temperature". In: *ApJ* 740.1, L3 (Oct. 2011), p. L3. DOI: 10.1088/2041-8205/740/1/L3. arXiv: 1108.2892 [astro-ph.GA].

51. D. A. Williams et al. *Dynamical Astrochemistry*. Royal Society of Chemistry, 2018.

52. David A. Williams and Cecchi. *The chemistry of cosmic dust*. 2016.

53. David A. Williams and Serena Viti. *Observational Molecular Astronomy*. 2014.

List of Figures

List of Tables